University of Miami
Scholarly Repository

Open Access Dissertations | Electronic Theses and Dissertations

2011-05-05

Age-Related Structural and Functional Changes of the Mouse Eye: Role of Intraocular Pressure and Genotype

Tsung-Han Chou
University of Miami, kikonline@yahoo.com

Follow this and additional works at: https://scholarlyrepository.miami.edu/oa_dissertations

Recommended Citation
Chou, Tsung-Han, "Age-Related Structural and Functional Changes of the Mouse Eye: Role of Intraocular Pressure and Genotype" (2011). *Open Access Dissertations*. 532.
https://scholarlyrepository.miami.edu/oa_dissertations/532

This Embargoed is brought to you for free and open access by the Electronic Theses and Dissertations at Scholarly Repository. It has been accepted for inclusion in Open Access Dissertations by an authorized administrator of Scholarly Repository. For more information, please contact repository.library@miami.edu.

www.manaraa.com

UNIVERSITY OF MIAMI

AGE-RELATED STRUCTURAL AND FUNCTIONAL CHANGES OF THE MOUSE EYE: ROLE OF INTRAOCULAR PRESSURE AND GENOTYPE

By

Tsung-Han Chou

A DISSERTATION

Submitted to the Faculty
of the University of Miami
in partial fulfillment of the requirements for
the degree of Doctor of Philosophy

Coral Gables, Florida

May 2011

www.manaraa.com

©2011
Tsung-Han Chou
All Rights Reserved

www.manaraa.com

UNIVERSITY OF MIAMI

A dissertation submitted in partial fulfillment of
the requirements for the degree of
Doctor of Philosophy

AGE-RELATED STRUCTURAL AND FUNCTIONAL CHANGES OF THE MOUSE EYE: ROLE OF INTRAOCULAR PRESSURE AND GENOTYPE

Tsung-Han Chou

Approved:

_____ Vittorio Porciatti, Ph.D. Professor of Ophthalmology and Biomedical Engineering	_____ Terri A. Scandura, Ph.D. Dean of the Graduate School
_____ Fabrice Manns, Ph.D. Associate Professor of Biomedical Engineering and Ophthalmology	_____ Douglas R. Anderson, M.D. Professor of Ophthalmology
_____ Jorge E. Bohórquez, Ph.D. Assistant Professor of Professional Practice of Biomedical Engineering	_____ Jean-Marie Parel, Ph.D. Research Professor of Ophthalmology and Biomedical Engineering

www.manaraa.com

CHOU, TSUNG-HAN (Ph.D., Biomedical Engineering)

Age-Related Structural and Functional Changes of the Mouse Eye: Role of Intraocular Pressure and Genotype (May 2011)

Abstract of a dissertation at the University of Miami.

Dissertation supervised by Professor Vittorio Porciatti and Fabrice Manns.
No. of pages in text. (94)

The murine eye naturally undergoes post-natal changes in eye size. This dissertation quantifies longitudinal structural and functional changes in control mice (C57BL/6J (B6), D2-Gpnmb+/SjJ) and in DBA/2J (D2) mice, which spontaneously develop elevated intraocular pressure (IOP). IOP elevation results in abnormal eye elongation, retinal nerve fiber layer (RNFL) thickness thinning and retinal ganglion cell (RGC) dysfunction and demise resembling human glaucoma. I measured structural changes with Optical Coherence Tomography (OCT), and RGC function with Pattern Electroretinogram (PERG). I also developed and refined provocation approaches (IOP elevation with changes in body posture; metabolic load with flickering light) to probe susceptibility of RGC function in D2 mice prone to glaucoma. Finally, I developed a novel system for recording, simultaneously but independently, the PERG from both eyes using asynchronous visual stimuli and deconvolution analysis. Simultaneous PERG recording from each eye was hitherto impossible due to the interocular cross-talk of the PERG signal.
Altogether, the combination of these measures (OCT, PERG) and provocative conditions may represent powerful tools for glaucoma research using mouse models.

www.manaraa.com

This dissertation is dedicated to my mother, Yen-Hsiu Liu and my father, Mao-Shen Chou.

www.manaraa.com

Acknowledgement

I would like acknowledge my mentor, Vittorio Porciatti, Ph.D., for his patience, guidance, wisdom, and tireless dedication. Also, I thank my BME advisor, Fabrice Manns, Ph.D., for guiding me through my Ph.D. study and helping me through my life in Miami during Ph.D. study. I am also grateful to Billy Lee, Izuru Nose, Derek Nankivil, Jean-Marie Parel, Ph.D. from the Ophthalmic Biophysics Center for their support to build up the mechanical part of PERG system. Marco Ruggeri, Omer Kocaoglu Ph.D., and David Borja, Ph.D. helped me on the experiment of ocular dimension measurement by time-domain OCT. Jonathon Anthony, Toft-Nielsen and Dr. Bohorquez help me on the engineering part of LED pattern stimulation. My Ph.D. project would be difficult to achieve the goal if without their help. I would like to thank Douglas R. Anderson, M.D. for his input of the IOP related project. John R. Guy, M.D. and Sanjoy K. Bhattacharya, Ph.D. provided some animal models to test our designed PERG tool to achieve the measurement of retinal dysfunction. Lori M. Ventura, M.D. and Vittorio Porciatti, Ph.D. were very kind and supported me all the time during my Ph.D. study. It is also a beautiful place to study in Florida, the sunshine state. I really enjoyed my life with friends in school and in Miami. The BME program at the University of Miami is really a great academic environment and I appreciate the financial support that was extended to me. Finally, I thank my parents who have prayed for me and supported me during these past five years.

www.manaraa.com

Table Of Contents

www.manaraa.com

www.manaraa.com

List of Figures

www.manaraa.com

www.manaraa.com

www.manaraa.com

www.manaraa.com

www.manaraa.com

www.manaraa.com

List of Tables

www.manaraa.com

List of Abbreviations

AC: Anterior chamber.

AL: axial length.

B6: C57BL/6J mouse.

CT: corneal thickness.

D2: DBA/2J mouse.

D2-Gpnmb+: DBA/2J-Gpnmb+/SjJ.

FERG: Flash Electroretingram.

Gpnmb: glycosylated protein nmb.

IPL: Inner plexiform layer.

IOP: Intraocular pressure.

ISCEV: International Society for Clinical Electrophysiology of Vision.

LT: lens thickness.

PDS: Pigment dispersion syndrome.

PERG: Pattern Electroretinogram.

RT: retinal thickness.

RGC: Retinal Ganglion Cell.

RNFL: Retinal Nerve Fiber Layer.

SD-OCT: Spectral domain optical coherence tomography.

Tyrp1: tyrosinase-related protein 1.

TD-OCT: Time domain optical coherence tomography.

VCD: vitreous chamber depth.

www.manaraa.com

Publication Note

The following are peer-reviewed articles, and conference presentations that resulted from this dissertation:

Peer-Reviewed Publications:

Tsung-Han Chou, Omer Kocaoglu, David Borja, Marco Ruggeri, Stephen R. Uhlhorn, Fabrice Manns, Vittorio Porciatti. Postnatal elongation of eye size in DBA/2J mice compared with C57BL/6J mice: In-vivo analysis with whole-eye OCT. Investigative Ophthalmology and Visual Science 2011, In press.

Mabel Enriquez-Algeciras, D. Ding, **Tsung-Han Chou**, J. Wang, K.R. Padgett, V. Porciatti, Bhattacharya SK. Evaluation of a transgenic mice model of multiple sclerosis with non invasive methods. Investigative Ophthalmology and Visual Science 2011 January 12; 10: 6425-.

Vittorio Porciatti, **Tsung-Han Chou**, Feuer WJ. C57BL/6J, DBA/2J, and DBA/2J.Gpnmb+ mice have different visual signal processing in the inner retina, Molecular vision. 2010, December 31; 16: 2939-2947.

Rajeshwari D. Koilkonda, **Tsung-Han Chou**, Vittorio Porciatti, William W. Hauswirth, John Guy, Induction of rapid and highly efficient expression of the human ND4 complex I subunit in the mouse visual system by self-complementary adeno-associated virus, Archives of Ophthalmology. 2010 July; 128(7):876-883.

John Guy, Xiaoping Qi, Rajeshwari D. Koilkonda, Tania Arguello, **Tsung-Han Chou,** Marco Ruggeri, Vittorio Porciatti, Alfred S. Lewin, and William W. Hauswirth , Efficiency and safety of AAV-mediated gene delivery of the human ND4 complex I subunit in the mouse visual system, Investigative Ophthalmology and Visual Science. 2009; 50: 4205-4214.

Conference Presentations:

Tsung-Han Chou, V. Porciatti (2011), The bioelectric field of the Pattern Electroretinogram (PERG) in the mouse: Differences with the Flash Electroretinogram (FERG), ARVO Conference paper.

Vittorio Porciatti, **Tsung-Han Chou** (2011), Adaptive changes in the Pattern Electroretinogram (PERG) induced by flickering light in the mouse, ARVO Conference paper.

Tsung-Han Chou, W. Lee, I. Nose, J.-M. Parel, V. Porciatti (2010). "Susceptibility of retinal ganglion cell function to acute IOP modulation in DBA/2J Glaucoma." ARVO meeting abstracts 51(5): 5484.

Tsung-Han Chou, Omer Kocaoglu, David Borja, Marco Ruggeri, Stephen R. Uhlhorn, Fabrice Manns, Vittorio Porciatti. (2009). "Postnatal growth of eye size in DBA/2J mice compared with C57BL/6J mice: In-vivo analysis with OCT." Investigative Ophthalmology and Visual Science. 50(5): 2776-.

www.manaraa.com

Chapter 1. Aims Of The Study

Glaucoma is the second most common cause of blindness in the United States. Glaucoma refers to a group of diseases that affect the optic nerve and involves a loss of retinal ganglion cells in a characteristic pattern. Raised intraocular pressure is a significant risk factor for developing glaucoma (above 22 mmHg or 2.9 kPa).

The goal of this dissertation is to better understand the relationship between IOP, RNFL thickness, RGC function, and growth of eye size in glaucoma mice model.

The specific aims are listed as the below section:

1.1 Characterize the postnatal changes of the main variables of the DBA/2J mouse model. We will measure the postnatal changes of eye size, IOP, RGC function, and RNFL thickness in D2 and B6 mice between 2.5 to 18 month old ages.

1.2 Characterize the changes in the main variables induced by artificial IOP modulation.

In mouse models of glaucoma, artificial induction of IOP elevation/lowering may provide key information on susceptibility of retinal ganglion cells to IOP insult. IOP can be changed in a number of ways and body tilt is one of the simple and noninvasive ways. We will demonstrate how we achieve the body tilt in the chapter 5.

1.3 Model the relationship between age-related IOP elevation and 1) Eye size, 2) RGC function, 3) RNFL thickness.

Our previous published data(Chou, Borja et al. 2009) implies that eye size grows up with increase of IOP and with age in DBA/2J model; RNFL thickness and RGC function decrease with age(Porciatti 2007; Saleh, Nagaraju et al. 2007). By contrast, B6 mice display spontaneous growth of eye size with age while the IOP does not change. We will

www.manaraa.com

also measure how the RGC structure and function change with age in B6 mice. However, there was a study that presented a mouse strain with Gpnmb and Tyrp1 genes of normal function and with a D2 genetic background. These mice did not develop elevated IOP or glaucoma. Figure 1 shows the expected relationships between the relevant variables based on the results in Chapter 5. In the upper part of figure 1, we can see that IOP grows more with age in D2 than in B6. We assume that eye size should also grow more with age in D2 than in B6 mice because of the different eye pressure growth rates as shown in middle plot of figure 1. D2 mice are expected to have a reduced RNFL thickness and reduced RGC function compared to B6 as shown in the lower plot of figure 1.

We will combine all these measurement and try to understand the relationship between these variables and IOP elevation during glaucoma development.

www.manaraa.com

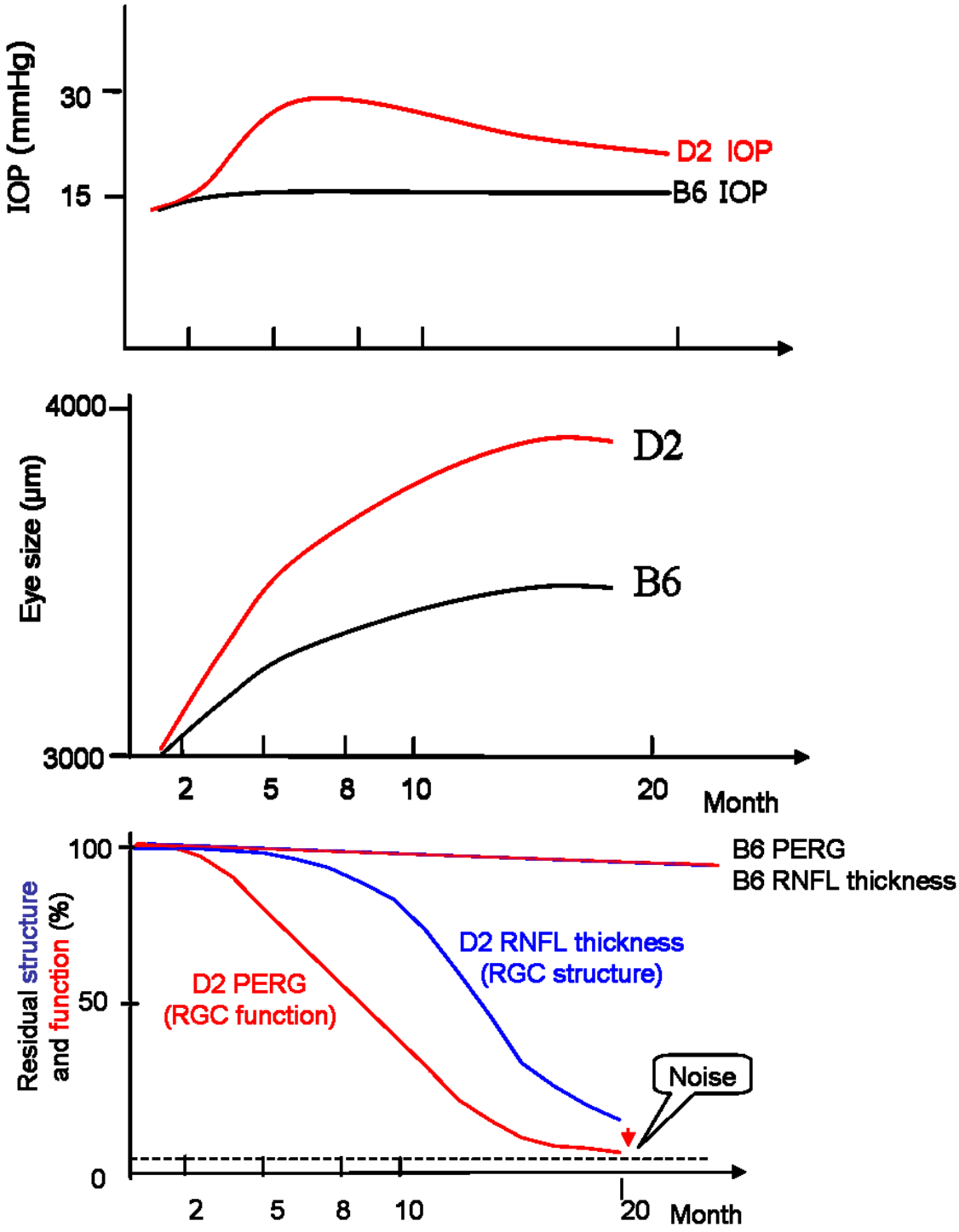

Figure.1. Expected age-related changes of IOP, RGC function, RNFL thickness, and eye size in D2 mice in comparison with B6 mice.

www.manaraa.com

1.4 Characterize the PERG phenotype in DBA/2J mice and non-glaucomatous control strains C57BL/6J and DBA/2J-Gpnmb+ by changing spatial frequency and contrast.

In the published paper (Howell, Libby et al. 2008), some scientists tried to understand how genetic background affects susceptibility of retinal ganglion cells (RGC) to IOP-related stress. We will use the PERG to systematically investigate the spatial-contrast characteristics of RGC response in young B6 and D2 mice before development of iris disease and IOP elevation in D2 mice.(Chou, Lee et al. 2010) We will also investigate DBA/2J mice homozygous for wild-type versions of Gpnmb (D2-Gpnmb+) that develop mild iris disease and modest IOP elevation but not glaucomatous nerve damage.(Howell, Libby et al. 2007)

1.5 Characterize the change of retinal function induced by metabolic adaptation in response to 10 Hz flicker.

Illumination of the eye with flicker light is known to increase the metabolic demand of the inner retina.(Bill and Sperber 1990; Bill and Sperber 1990) (Falsini, Riva et al. 2002; Falsini, Riva et al. 2002) An increased blood flow in the retina secondary to flicker light stimulation, measured in monkeys using labeled microspheres, was first reported by Bill and Sperber.(Bill and Sperber 1990) Furthermore, the flicker frequency of 12.5 Hz is known to increase retinal blood flow

(Riva, Logean et al. 2005) Thus, we will characterize the PERG change in amplitude and latency by applying 10 Hz flicker (know to increase metabolic demand in inner retina) in D2 compared with B6 and D2-Gpnmb+ mice. [ARVO 2011]

www.manaraa.com

1.6 Characterize the bioelectrical field of the PERG in comparison with Flash-ERG, and measure the cross-talk of PERG signal between the two eyes.

We discovered the phenomena of cross-talk during PERG recording but not during FERG recording in mice. [ARVO, 2011] Neural processing in the retina generates an electric field throughout the eye and surrounding tissue. As PERG and FERG have different retinal generators, the PERG responses are from inner retina and the FERG responses are from outer retina, we will investigate differences in the bioelectric fields of the PERG and FERG in the mouse model.

1.7 Design of a new system for binocular PERG recording that eliminates the problem of cross-talk by means of de-synchronized LED pattern stimuli and acquisition/analysis of deconvolved retinal signals.

We will record PERG in both eyes simultaneously, but independently, by eliminating the interocular cross-talk by triggering the pattern stimuli delivered to each eye with a newly designed asynchronous sequence. In order to get good and consistent PERG in a short period of recording time, the new measurement device for PERG recording will measure simultaneously and independently both eyes at average of 1116 sweeps (see methods in 4.2). This achievement will reduce PERG recording time from both eyes by half, and will allow comparing the response of the two eyes simultaneously. This will be especially useful for experiments in which one eyes is experimental and the other serves as a control. For manipulating IOP during PERG recording in two eyes, we will combine the custom-made body-tilt apparatus with the PERG acquisition system to achieve the goal of understanding the relationship between induced IOP change and RGC function. In order to induce metabolism change in the retina during PERG recording, flicker at 10 Hz will

www.manaraa.com

be applied in this system to make comparison at different strain mice (D2, B6, D2-Gpnmb+) and compared to flicker at 100 Hz (at which retina is unresponsive, beyond temporal resolution of mouse cone ERG) (See method in 4.2).

The hypotheses to be tested are:

A.) The eye grows differently in all ocular dimensions with age both in glaucomatous DBA/2J and non-glaucomatous C57BL/6J mice. (Exam tool: Time-domain OCT)

B.) IOP increases with age in DBA/2J but does not change with age in C57BL/6J. (Exam tool: Tonometer) The eye growth rate with age is greater in D2 than in B6 mice because of the IOP elevation.

C.) PERG amplitudes decrease with age in DBA/2J but do not change with age in C57BL/6J. (Exam tool: PERG acquisition instrument)

D.) Retinal thickness decreases with age in DBA/2J because of glaucoma development, but it remains almost the same thickness with age in C57BL/6J. (Exam tool: Spectral domain OCT)

E.) Experimental-induced IOP change can be proved by body-tilt; reducing IOP can improve altered RGC function.

To evaluate those hypotheses, the following steps are taken:

www.manaraa.com

Steps	
1.	**Optimization of experimental tools**
	a. Device for IOP modulation by means body-tilting (prototype)
	b. Independently operated LED pattern stimuli for PERG recording from both eyes
	c. Device for simultaneous PERG acquisition and processing from both eyes
	d. Device for delivering flickering light at 10 Hz and 100 Hz
	e. Combination of all devices in one single instrument prototype
2.	**Evaluation of longitudinal changes in eye structure and function with different strains of mice.**
	a. Measurement of IOP in DBA/2J mice and C57BL/6J mice aged 2-20 month old
	b. Measurement of eye size in DBA/2J and C57BL/6J mice aged 2-20 month old **c. Measurement of PERG in DBA/2J and DBA/2J-Gpnmb+ mice aged 2-20 month old**
3.	**Induced IOP change.**
	a. Modulation of IOP by means sequential changes of body posture with a customized tilting apparatus: effect on PERG of D2 and B6 mice.

www.manaraa.com

Chapter 2. Review Of DBA/2J Glaucoma Mouse Model

2.1 Background of glaucoma model DBA/2J mice and significance

Glaucoma is a leading cause of blindness affecting at least 66 million people worldwide. Vision loss in glaucoma is caused by the dysfunction and death of retinal ganglion cells (RGCs).(Thylefors and Negrel 1994; Quigley 1996) Lowering intraocular pressure (IOP) frequently slows or arrests the development as well as the progression of glaucoma.(Kass, Heuer et al. 2002) Thus, IOP is considered to be the major risk factor in the glaucoma disease.(Quigley, Hohman et al. 1983; Hernandez 2000; Nagaraju, Saleh et al. 2007) All current glaucoma treatments in clinic aim to manipulate this factor (Yanoff M. 2004), so it is important to understand the relationship between glaucoma and IOP.

Glaucoma associated with elevated IOP is not unique to humans. Pigment dispersion syndrome (PDS) is a common condition that results in the dispersion of iris pigment into the anterior chamber (AC). The dispersed pigment accumulates within the ocular drainage structures (figure 2), resulting in IOP elevation and glaucoma.

www.manaraa.com

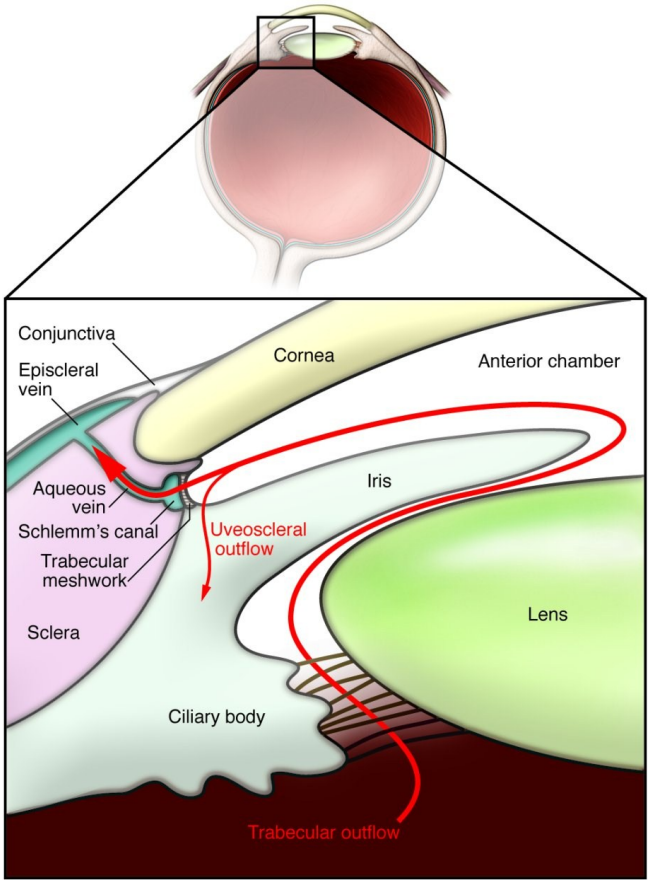

Figure 2. Schematic diagram of eye structures involved in aqueous humor dynamics in human. Aqueous humor is produced by the ciliary body and passes from the posterior chamber through the pupil into the anterior chamber into the trabecular meshwork, Schlemm's canal, and finally into the episcleral venous system. The unconventional path is the "uveoscleral outflow" that drains fluid through the ciliary muscle into the supraciliary and suprachoroidal spaces and then out of the eye through the sclera. Approximately 80% of aqueous humor is removed by the conventional trabecular meshwork pathway, and the remainder is removed by the uveoscleral pathway. Elevated IOP in glaucoma is caused by alterations to the conventional trabecular meshwork pathway. (Bao Jian Fan, Janey L. Wiggs, J Clin Invest. 2010; 120(9):3064–3072).

DBA/2J (D2) mice, and some related substrains, develop a form of glaucoma characterized by a pigment-dispersing iris disease that aberrantly deposits pigment throughout the AC, including the drainage structures of the eye. Endothelialization of anterior chamber angle occurs in mice of the DBA/2J and AKXD-28/Ty strains, both of which develop progressive angle closure glaucoma (figure 3c.d.f).(Richard S. Smith

www.manaraa.com

2002) As a consequence, IOP becomes elevated and glaucomatous RGC degeneration ensues.(Anderson, Smith et al. 2002; Anderson, Libby et al. 2005; Zhou, Li et al. 2005)

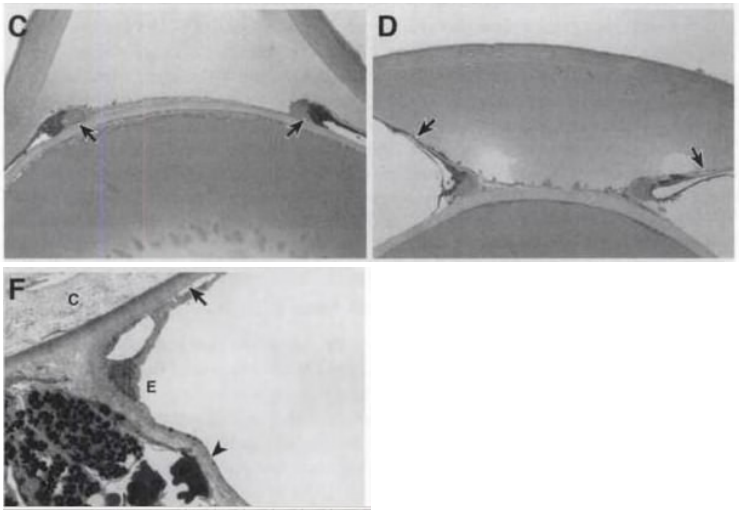

Figure 3c. In AKXD-28/Ty mouse, posterior synechiae have firmly attached the iris to the lens in this. An subcapsular cataract is present. Figure 3d. If the posterior synechias completely surround the pupil, aqueous will be trapped in the posterior chamber, causing the iris to balloon forward- an iris bombe. An eosinophilic exudate fills the anterior chamber. The iris leaflets are indicated by arrows. Figure 3f. In a 9.5- month- old DBA/2J mouse, Descemet's membrane (arrow) and the corneal endothelium cover the posterior corneal (C) surface. An endothelial cell (E) lies on the iris surface and newly formed Descemet's membrane- like material (arrowhead) continues across the iris surface.(Richard S. Smith, Simon W. M. John, Pasty M. Nishina, John P. Sundberg. Systematic evaluation of the mouse eye. Anatomy, Pathology and Biomethods. Page.135, Figure 8.18)

In the past few years, the DBA/2J mouse has been described as an animal model of human pigmentary glaucoma. This mouse strain presents several hallmarks of the human pigmentary glaucoma including iris atrophy, pigment dispersion, peripheral anterior synechiae that are associated with development of elevated IOP, retinal ganglion cell loss, and optic nerve head excavation.(Chang, Smith et al. 1999; John 2005) DBA/2J mouse provides a tractable model of inherited glaucoma and allows us to change the

www.manaraa.com

genotype which cannot be done in human. At the age of about 6 months (figure 4D.E), the D2 mice develop iris disease that is caused by recessive mutations in two genes, glycosylated protein nmb (*Gpnmb*; NCBI GeneID 93695) and tyrosinase-related protein 1 (*Tyrp1*; NCBI GeneID 22178)(Libby, Anderson et al. 2005) , involved in melanin synthesis and melanocyte structure.(Chang, Smith et al. 1999; Anderson, Smith et al. 2002) The resulting pathology to the iris leads to damage of the trabecular meshwork. By 8 to 9 months of age (figure 4G.H), these mice generally show elevated IOPs in the high 20 to low 30 mmHg ranges. By 10 to12 months (figure 4J.K), these mice have developed an optic neuropathy with retinal ganglion cell loss.(Danias 2004; Libby, Anderson et al. 2005; Filippopoulos, Danias et al. 2006; Schlamp, Li et al. 2006)

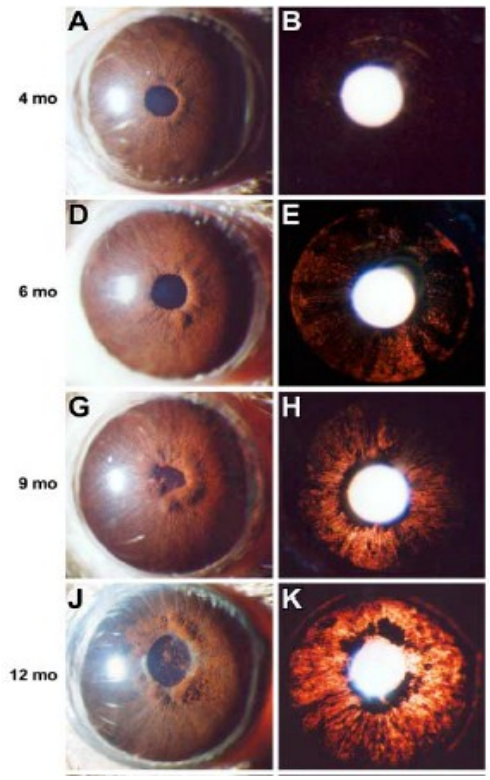

Figure.4. In D2 mice, the iris disease involves iris stromal atrophy and progressive depigmentation with abnormal dispersion of iris pigment causing transillumination defects. Pigment granules liberated into the anterior chamber cause pigmentary glaucoma. (Libby, Anderson et al. 2005)

www.manaraa.com

The IOP elevation is subsequent to an iris disease that deposits pigment in the ocular drainage structures. Previous studies characterized how eye size, eye weight, lens weight, and body weight grows with age in different strains of mice by several methods.(Schmucker and Schaeffel 2004; Brown 2005; Puk, Dalke et al. 2006; Calkins, Horner et al. 2008) Other studies also investigated about genes related eye size development in D2 and B6 mice.(Zhou and Williams 1999) However, how elevated IOP causes RGC death remains unclear. The goal of this study is to determine how the IOP plays a role and interacts with eye size, optics, RGC structure and function during the glaucoma disease progression comparing with B6 mice by designed engineering tool.

Eye size, RNFL thickness, and RGC function can also be affected by IOP elevation. In order to show the effects, we will measure these four relevant variables that list in table 1.

Relevant variables	**Tool**
Ocular dimension	Time domain OCT
IOP	Rebound tonometer (TonoLab)
RGC function	PERG
RNFL thickness	Spectral domain OCT

Table1. Relevant variables measured and the tools those need to be used.

2.2 Age-related RGC function and IOP changes of the mouse eyes

By means of PERG and tonometer, previous studies have been able to noninvasively characterize the natural history of RGC dysfunction and its association with IOP in a 12-month longitudinal study of DBA/2J mice with the animal resting in a horizontal position.(Saleh, Nagaraju et al. 2007; Saleh, Nagaraju et al. 2007) Longitudinal changes

www.manaraa.com

in PERG and FERG amplitude and IOP are summarized in Figure 5. The major feature of Figure 5 is that, on average, PERG amplitude progressively decreases with age until it reaches the upper limit of the noise range at approximately 11 months of age. The preliminary result indicates age-related PERG amplitude changes are highly significant. Results also indicate that the cone-flash ERG, including both the positive and negative components, is not much affected in this glaucoma model. Age-related PERG changes may be largely explained by changes occurring in the inner retina. We can compare the D2 mice with B6 mice (control group) to understand the relationship between IOP changes with ages and RGC function.

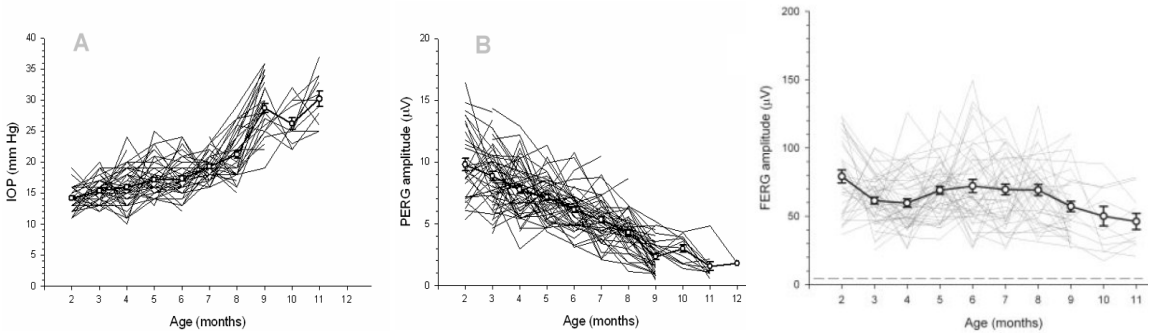

Figure.5. A. IOP increases with age. B. PERG amplitude decreases with age. Note the close association between IOP increase and PERG amplitude decrease with age. C. FERG amplitude does not significantly change with age (n= 64 eyes). (Nagaraju, M., M. Saleh, Vittorio Porciatti, IOVS, October 2007, 48 (10): 4564-4572)

2.3 Age-related structural changes of the mouse eyes by histology

One previous published study (Libby, Anderson et al. 2005) compares average PERG amplitude changes with average RNFL thicknesses (both eyes) on a normalized scale (Figure 6). Previous cross-sectional data (Anderson, Libby et al. 2005; Libby, Porciatti et

www.manaraa.com

al. 2006) in mice of different ages have been combined and included to make a comparison between PERG, RNFL thickness at end point, and axon counts of optic nerves (Figure 6). The RNFL thickness at end point was measured by histology and the data was published recently by our group.(Porciatti, Saleh et al. 2007) (Figure 7) The previous reports show that relative changes in RNFL thickness in DBA/2J mice of different ages are in good agreement with corresponding changes of optic nerve axons.(Anderson, Libby et al. 2005; Libby, Anderson et al. 2005) An approximate axon count evaluation was possible, because Libby et al.(Libby, Porciatti et al. 2006) graded severity of optic nerve damage in a large population of D2 mice, and Anderson et al.(Anderson, Libby et al. 2005) reported the mean axon count for each severity grade. Note that progressive loss of RGC axons lags behind progressive loss of PERG amplitude by approximately 3 months. Also note that relative changes in RNFL thickness are in agreement with corresponding changes in RGC axons.

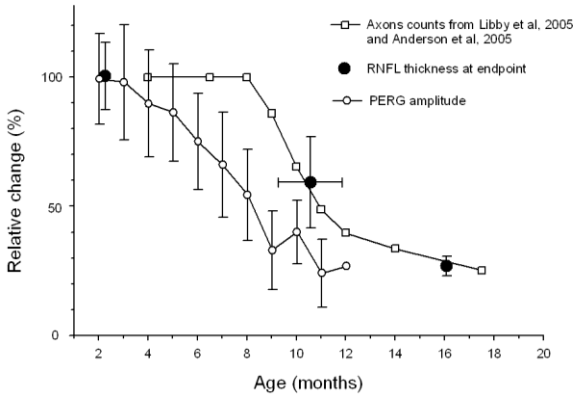

Figure.6. Average PERG amplitude (n= 32 eyes), RNFL thickness (n= 20 eyes), and axon count for both eyes as a function of age in D2 mice. Data are plotted on a normalized scale. Open circles: PERG amplitude; open squares: axon counts; filled circles: RNFL thickness. Error bars represent the standard deviation (SD). (Nagaraju, M., M. Saleh, Vittorio Porciatti, IOVS, 2007, 48 (10): 4573-9)

www.manaraa.com

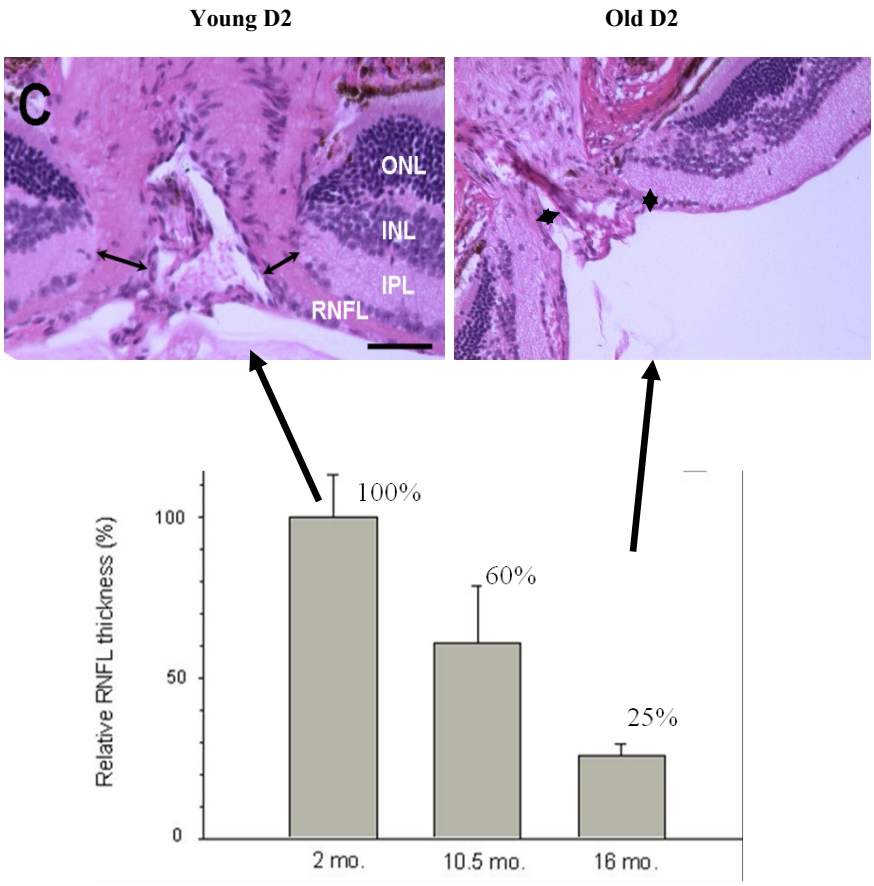

Figure.7. RNFL thickness was measured in axial section through the optic nerve head of the D2 mice at the age groups 2-3 month (n=5 eyes), 9-11 month (n=20 eyes)and 16-18 month (n= 5 eyes) old. (Nagaraju, M., M. Saleh, Vittorio Porciatti, IOVS, 2007, 48 (10): 4573-9)

2.4 Acute induced IOP elevation by head-down body-tilt and RGC function

In order to investigate the association between IOP elevation and PERG reduction, posture-induced IOP elevation has been done by head-down (60 deg) position for 30 minutes and then back to horizontal position for at least 20 minutes (recovery period).(Nagaraju, Saleh et al. 2007) Average PERG amplitudes recorded in horizontal position (baseline), 10-30 minutes after head-down position (60 deg tilted), and 10-30

www.manaraa.com

minutes after repositioning mice in horizontal position (recovery) are displayed together with corresponding IOP in figure 8.

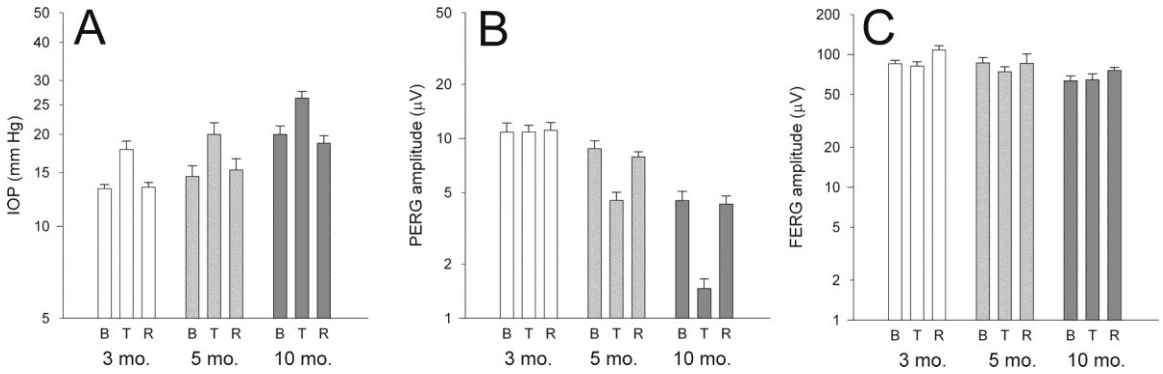

Figure 8. Average (±SEM) values for IOP (A), PERG amplitude (B) in DBA/2J mice of different ages measured in horizontal baseline condition (B), during head-down body tilting (T), and during recovery (R) in horizontal position. (C) FERG amplitude. Data are plotted on log scales to normalize relative changes. (n= 21 eyes) (Nagaraju, M., M. Saleh, Vittorio Porciatti, IOVS, 2007, 48 (10): 4573-9)

This study has shown that it is possible to induce transient and consistent elevations of IOP in Ketamine-Xylazine anesthetized DBA/2J mice of different age by positioning the animals 60 deg head-down. Mean PERG amplitudes recorded in baseline and tilted positions have been plotted against corresponding mean IOP values, and data fitted with linear regressions (Figure 11). The IOP reduction experiment was also done by intraperitoneal injection of mannitol 25% (2.5 g/Kg; Hospira, Inc. Lake Forest, USA). Mannitol treatment consistently reduced the IOP to a relatively stable average value of 16.3 ± 2.8 mm Hg (−38%) ($P<0.001$) over the next 20-60 minutes. After mannitol treatment the PERG amplitude improved by about 83% ($P<0.01$) (Figure 9).

IOP lowering has also been done by head-up position (60 deg) position for 30 minutes and then repositioned horizontally for at least 20 minutes (recovery period).(Porciatti,

www.manaraa.com

Nagaraju et al. 2008) The preliminary result is in figure 9. The magnitude and time course of IOP change is approximately similar for head-down and head-up tilt, and is rather independent of age.

In our previous study, body tilts (60°) induce acute IOP elevation of ~ 5mm Hg in head-down.(Nagaraju, Saleh et al. 2007) From figure 10, we can tell that tilt-induced IOP elevation is associated with reduction of PERG amplitude especially in older D2 mice (10-12 month).

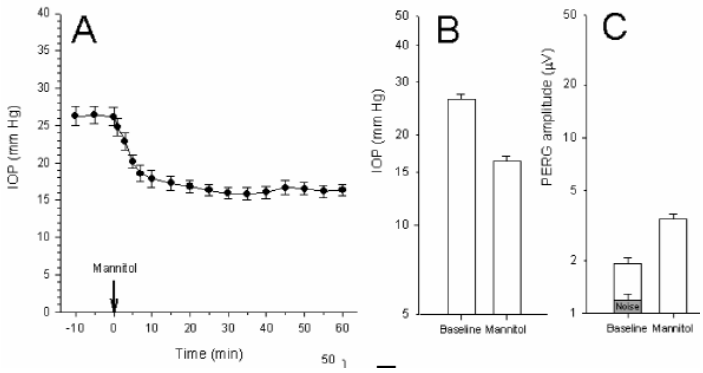

Figure 9. Effect of mannitol treatment on IOP and PERG in 11 month-old DBA/2J mice. (n=8 mice) (Nagaraju, M., M. Saleh, Vittorio Porciatti, IOVS, 2007, 48 (10): 4573-9)

www.manaraa.com

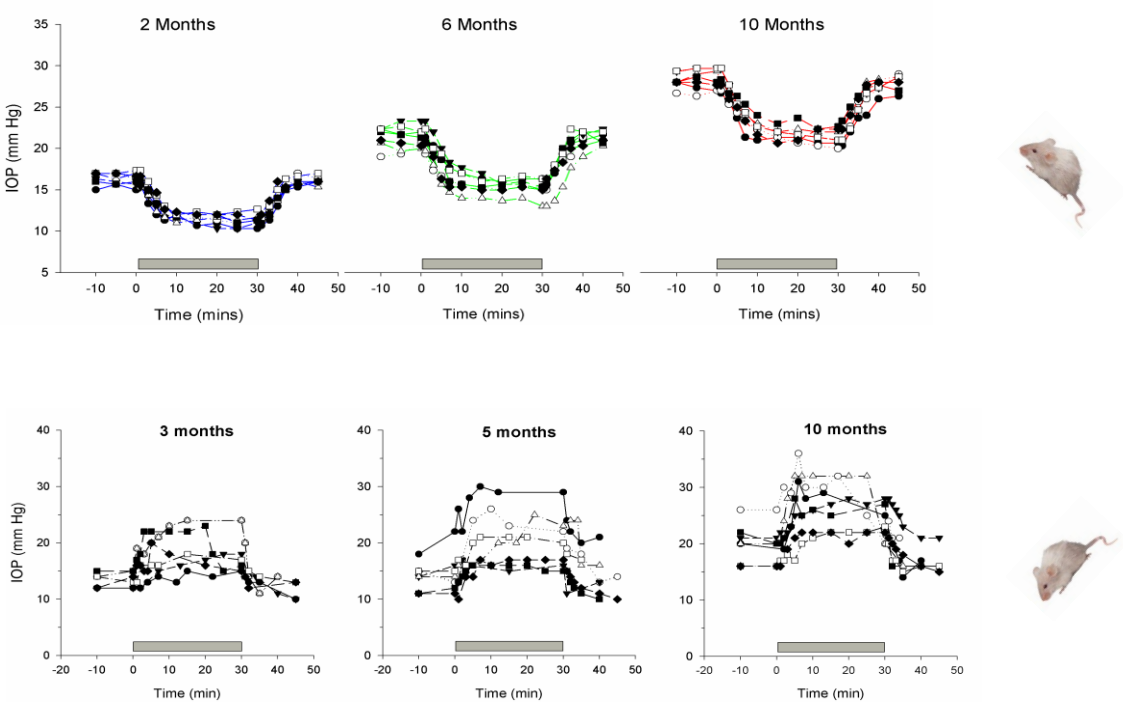

Figure 10. Upon tilting, IOP progressively changes following an exponential time course with a time constant of 4-5 minutes and remains stable at a new level. (n= 21 eyes) (Nagaraju, M., M. Saleh, Vittorio Porciatti, IOVS, 2007, 48 (10): 4573-9)

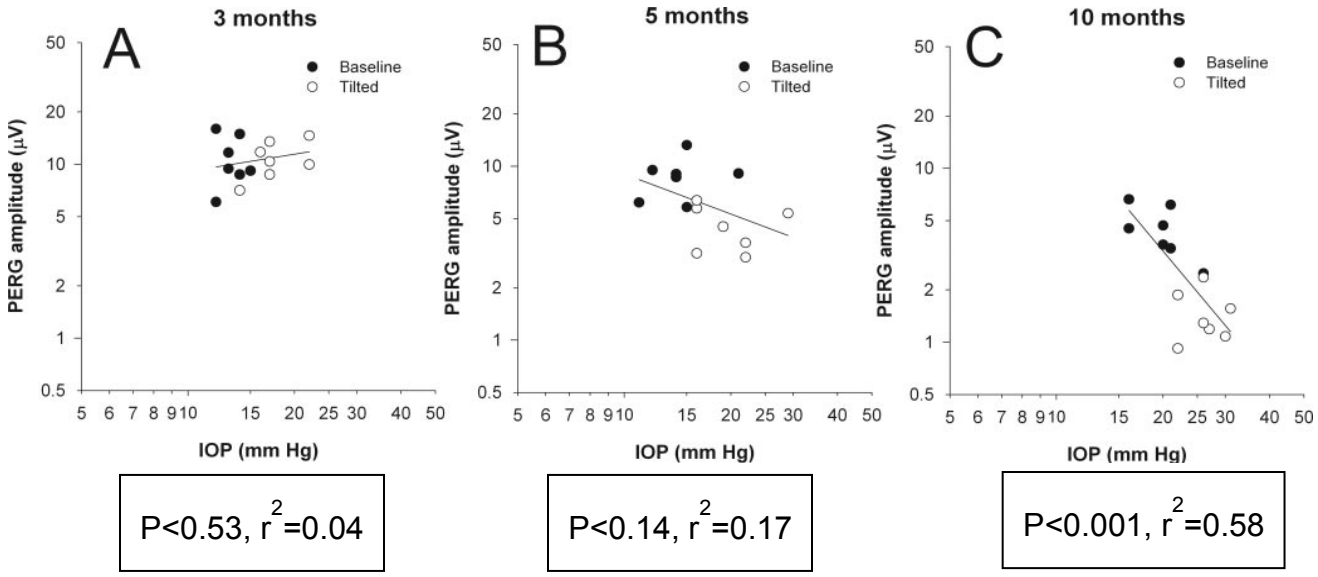

Figure.11. Acute induced IOP elevation by head-down tilt in D2 mice. Filled circle represents baseline data of IOP and PERG and open circle represents the head-down tilting data. The correlation between PERG amplitude and IOP increases with age of mice (3 month old: $r^2 = 0.04$, P=0.53; 5 month-old: $r^2 = 0.17$, P=0.14; 10 month-old: $r^2 = 0.58$, P<0.001). (Nagaraju, M., M. Saleh, Vittorio Porciatti, IOVS, 2007, 48 (10): 4573-9)

www.manaraa.com

2.5 Acute induced IOP reduction by head-up body-tilt and RGC function

The time course of IOP changes for -60° of tilt was determined in D2 mice aged 2 to12 months (2-month-old, n = 7; 6-month-old, n = 7, 10-month-old, n = 7, 12-month-old, n = 7) (Figure 12). Note in Figure 12 that baseline IOP values differed among age groups. Upon -60° tilting, IOP progressively diminished and tended to plateau at a lower level in all age groups. Upon horizontal repositioning, IOP recovered to baseline conditions with an approximately mirror-symmetric time course. For both head-up and horizontal repositioning the time constant of the IOP change (time required to reach 63% of its plateau value) was of the order of 5 to 6 minutes. Baseline IOPs (average of three consecutive measures over 10 minutes) and tilted IOPs (average of 4 consecutive measures 10 to 25 minutes after tilt) for each age group are reported in Table 2.

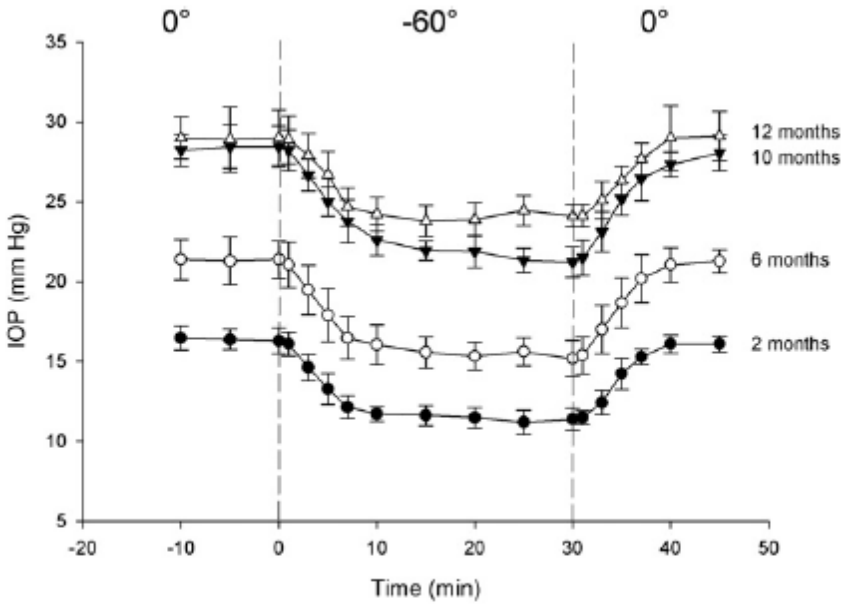

Figure.12. Acute induced IOP reduction (mean ± SD) by head-up tilt in D2 mice. (-60° for 30 minutes followed by horizontal repositioning) in groups of D2 mice with different ages. Different symbols represent different age groups. (n= 45 mice) (Porciatti, V. and M. Nagaraju, Experimental Eye Research, 2010, 90(3): 452-460.)

www.manaraa.com

Age (months)/ mean IOP (mmHg)	Baseline	SD	Tilted	SD	Delta
2 months	16.4	0.8	11.1	0.7	-5.3
6 months	21.0	1.4	15.4	0.8	-5.6
10 months	28.1	0.9	22.0	0.6	-6.1
12 months	29.0	1.7	24.1	1.0	-4.9

Table2. Intraocular pressure under either baseline or -60° head-up conditions for groups of DBA/2J mice at different ages.

Approximately one week after IOP measurements, PERGs and FERGs were recorded before, during, and after head-up (-60°) body tilt from the right eyes of D2 mice of different ages (2 to 3-month-old, n = 7; 6-month-old, n = 7; 10-month-old, n = 6; 12-month-old, n = 6).

Tilted PERGs and FERGs were recorded in the 10 to 25 minutes time window after onset of tilt. Recovery PERGs/FERGS were recorded in the 10 to 25 minutes time window after horizontal repositioning. To provide a summary characterization of PERG and FERG changes across conditions, grand-average waveforms were calculated together with their SEM and displayed in the Figure 13. In 2-month-old D2 (A), the baseline average PERG amplitude was about of 9 μV and did not change upon head-up tilt. In 10-month-old D2 (B) as well as in 12-month-old D2 (C) the average baseline PERG amplitude (maximum-to-minimum voltage in the waveform) was about 2 μV. Upon

www.manaraa.com

head-up tilt, the average PERG amplitude substantially increased in both 10 month and 12-month-old D2, and then returned to the baseline magnitude upon horizontal repositioning. In 10-month-old D2 (D) the baseline FERG had peak-to-trough amplitude larger than 60 μV, which did not change upon head-up body tilt. Comparable FERG waveforms were obtained at all ages (not shown). (Porciatti and Nagaraju 2010)

www.manaraa.com

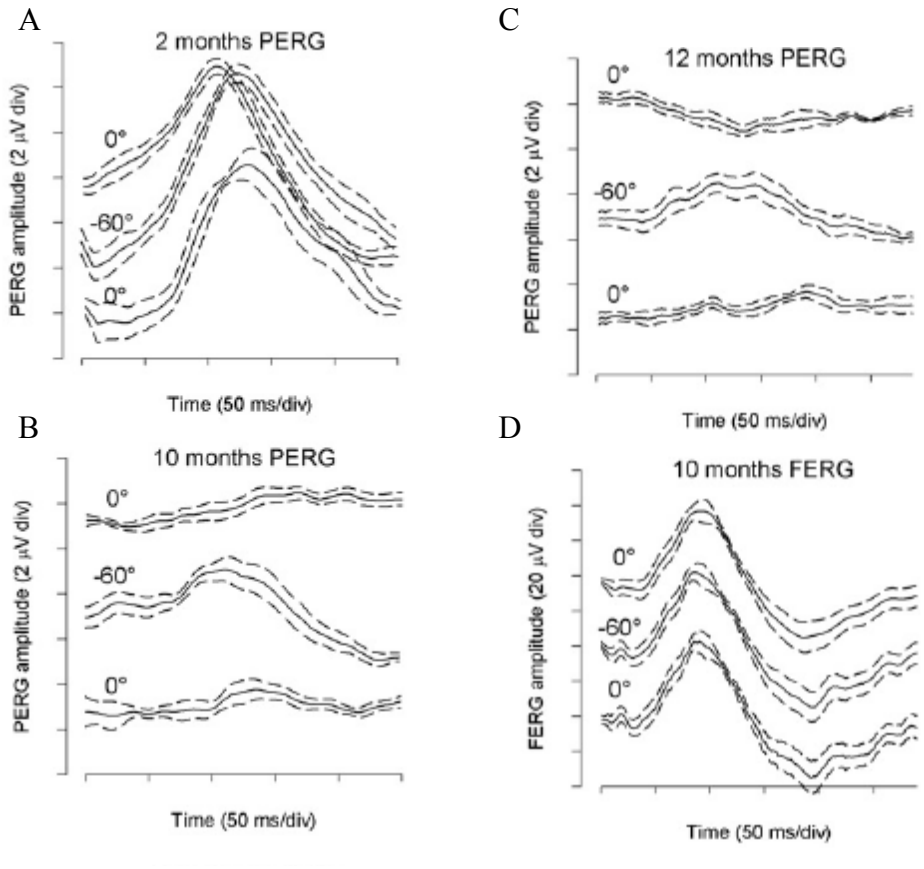

Figure 13. Effect of -60° head-up body tilt on PERG and FERG of DBA/2J mice at different ages. Note that at 2 months of age (A), the PERG is not affected by head-up tilt, whereas at 10 and 12 months of age (B and C) an initially reduced PERG signal improves after tilt and returns to baseline range after horizontal repositioning. Also note that in 10-month-old mice (D) a normal baseline FERG signal is not affected by body tilt. Comparable FERG responses are obtained in all age groups (2, 6, 10, 12 months). (n= 45 mice)(Porciatti, V. and M. Nagaraju, Experimental Eye Research, 2010, 90(3): 452-460.)

www.manaraa.com

2.6 Missing information of systematical study with new design tool.

In order to systemically record RGC function during body-tilt (IOP modulation), we need to design a better tool combined body-tilt and PERG measurement. The current pattern stimulation by CRT monitor is heavy and cannot easily tilt-up and tilt-down during mouse body tilt. We need to find light weight pattern stimulation and also need to find a non-invasive method instead of histology to measure the whole eye size and retinal nerve fiber thickness with age in D2 compared with B6. Thus, we will describe the tool we have currently in next chapter and design a tool we need for measuring RGC function during IOP modulation in the chapter 4.

www.manaraa.com

Chapter 3. Existing Research Tools

3.1 How to measure the relevant variable of the glaucoma mouse model

3.1.1 Intraocular pressure (IOP) by a rebound tonometer

Tonometers originally designed for large animal eyes have been adapted for the small murine eye (Reitsamer, Kiel et al. 2004) and new tonometers have been developed specifically for the mouse.(Pease, Hammond et al. 2006; Wang 2006) IOP was measured with an induction/impact tonometer design specifically for both mouse and rat (Tonolab Colonial Medical Supply, Franconia, NH).(Danias, Kontiola et al. 2003) The tonometer was fixed in a vertical position to a support stand by means of clamps. (Figure 14)

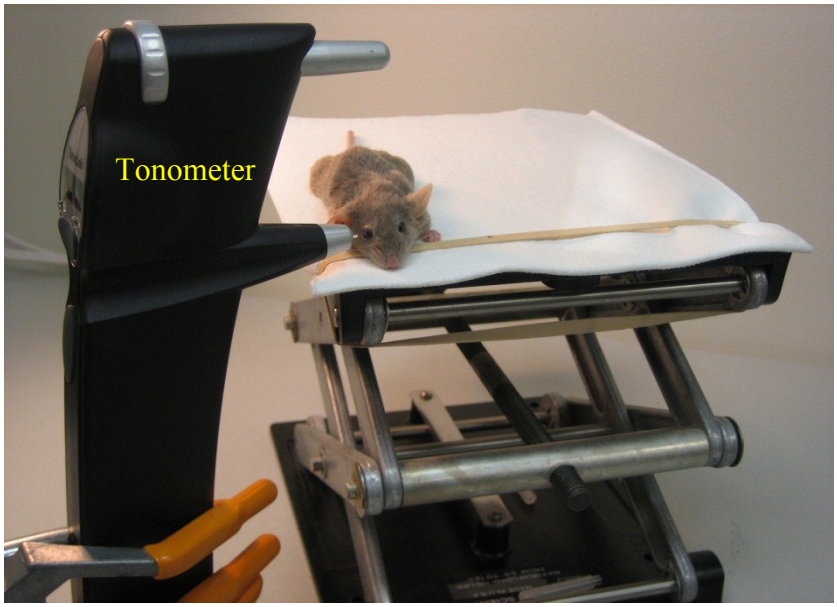

Figure.14. IOP measurement by a Tonolab rebound tonometer.

Anesthetized mice were placed on an adjustable stand and the tail restrained with adhesive tape. The probe tip was aligned with the optical axis of the eye at 1-2 mm distance by using a magnifier lamp. Five consecutive IOP readings were averaged.

www.manaraa.com

Importantly, the impact of the Tonolab probe on the cornea is minimal, such as local corneal anesthesia is not necessary.(Wang 2006) In a previous longitudinal study over one year (Saleh, Nagaraju et al. 2007) , we did not find obvious corneal damage at biomicroscopic examination. IOP readings obtained with Tonolab have been proven to be accurate and reproducible (coefficient variation less than 30%).

In different mouse strains including DBA/2J, (Wang 2006) the TonoLab rebound tonometer generated IOP readings that correlated very well with the IOP measured by the pressure transducer. In the mouse model, the regression lines had a mean slope of 0.99 ± 0.05 (n = 3), and a mean Y-intercept of 0.8 ± 1.4.

3.1.2 Ocular dimension by time domain OCT

We measured the ocular dimension with ages in D2 compared with B6 by time-domain OCT. Axial length (AL) was measured from the anterior corneal surface to the retinal pigment epithelium. (Figure.28A) The principle of OCT is based on low coherence interferometry. The optical setup consists of an interferometer, typically Michelson type, with a low coherence, broad bandwidth light source. The light coming from the light source is split into two arms, a sample arm (containing the item of interest) and a reference arm that usually contains a mirror. The combination of reflected light from the sample arm and light from the reference arm produce an interference pattern, only if the optical path length difference between the two arms lies within the coherence length of the light source. (Figure.15)

www.manaraa.com

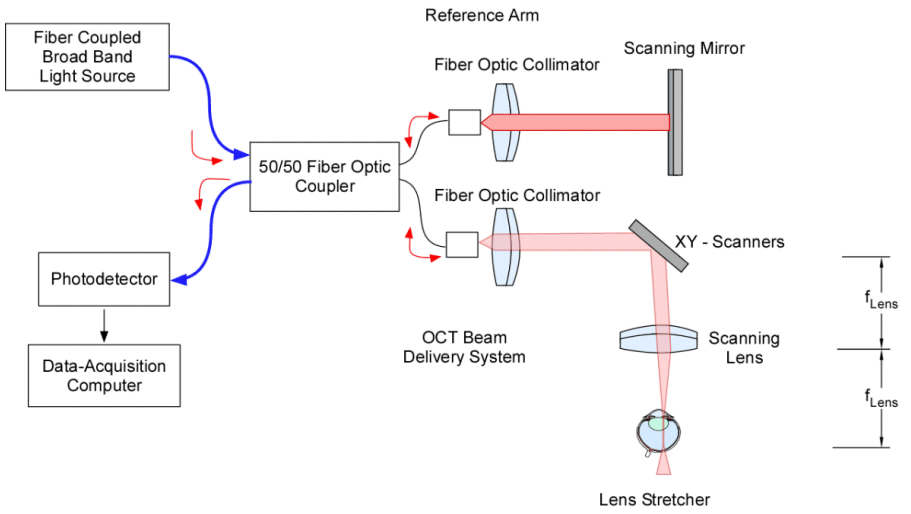

Figure.15. The principle of time-domain OCT system based on low coherence interferometery.

A custom time-domain OCT system was designed for cross-sectional imaging of the whole mouse eye, including precise alignment of the mouse eye with the imaging system (Uhlhorn, Borja et al. 2008; Manns, Kocaoglu et al. 2009) It uses a superluminescent diode with a center wavelength of 825 nm, a bandwidth of 25 nm, and a maximum output power of 6mW (SLD-38-HP, Superlum, Cork, Ireland). The reference arm of the OCT interferometer is a linear delay line using a corner cube retroreflector. The system has an axial scan length of 7.1 mm in the ocular tissue and produces axial a-scan interferograms at a rate of 20A-lines/s with a resolution 12 μm in the air. The OCT beam spot diameter at the focus was 60 μm. Images were recorded with 5000 points per A-line and 500 A-lines per frame at a rate of 20 A-lines/s. Image acquisition speed was limited by the scanning speed of the linear delay line and the long scanning distance of this delay line. The total image acquisition time was on the order of 25 seconds per B-scan image. This

www.manaraa.com

system allows for non-contact imaging of anesthetized mice. The mouse is placed on a 6 axis positioner consisting of 2 goniometers, a rotation stage and 3 linear translation stages and was held in a heated cylindrical holder. (Figure.16) In all experiments, the cornea was irrigated at regular intervals using a cannula filled with Balanced Salt Solution (BSS, Alcon, Ft Worth, TX) to avoid dehydration and loss of transparency. Any fluid accumulated on the ocular surface was gently removed with a microsponge before each image acquisition. The absence of the fluid layer was confirmed on the OCT images. Image distortions due to refraction were corrected in order to obtain reliable biometric data about the morphology of the refracting interfaces such as the depth of ocular components, surface curvature. The program detects the ocular surface boundaries and performs a conic section fit to calculate the radius of curvature and asphericity of each surface. The program also uses a ray-tracing algorithm to correct image distortions due to refraction. Typical examples showing the uncorrected and corrected conic section fits of ocular boundaries are shown in Figure 28B. A semi-automated customized edge detection algorithm was used (Ruggeri, Kocaoglu et al. 2010) to segment the images and measure anterior corneal shape, posterior corneal shape, corneal thickness, anterior chamber depth, lens thickness, vitreous depth, retinal thickness and axial eye length. Optical distances were converted to geometrical distances using published values of the refractive indices of the mouse ocular cornea (n=1.403), lens (n=1.666), aqueous (n=1.335) and vitreous (n=1.334).(Remtulla and Hallett 1985) A refractive index n=1.38 was assumed for the retina. We also quantify anterior and posterior corneal curvature by the semi-automated edge detection program. The test-retest variation of measurement on ocular thickness in the same mouse is less than 1%.

www.manaraa.com

Figure.16. The beam delivery system of OCT and the heated cylindrical holder mounted on 6-axis positioner. (Uhlhorn SR, Borja D, Manns F, Parel JM. Vision Research 2008; 48:2732-2738)

3.1.3 RGC function by PERG

The PERG is a particular kind of ERG in response to contrast-reversal of patterned stimuli that reflects cone-driven non-linearities in the inner retina.(Porciatti 2007) RGC activity is necessary for PERG generation, since RGC loss after optic nerve transection abolishes the response (Maffei and Fiorentini 1981; Porciatti, Pizzorusso et al. 1996); PERG generation also depends on the ability of anatomically present RGCs to generate action potentials, since the PERG signal is altered after intravitreal TTX injections in non-transected animals.(Trimarchi, Biral et al. 1990; Viswanathan, Frishman et al. 2000)

www.manaraa.com

The conventional cone-driven flash-ERG, which originates in the outer retina, is not affected by these procedures.

A vast PERG literature developed in the last 20 years (Riggs, Schick et al. 1964; Maffei and Fiorentini 1981; Riggs 1986; Regan 1989). In 2000, ISCEV proposed basic guidelines for the clinical application of the PERG(Bach, Hawlina et al. 2000). The pattern stimulus consists of black–white elements of equal areas that its luminance increases and decreases in time (flicker) at a given frequency (Hz). Schematic drawing of stimulus modulation and retinal activity during either pattern reversal (A) or uniform flicker (B) represent how the PERG response generates. (Fig. 17) For both conditions, stimulus elements alternate (time 0, 1) between two conditions of different luminance (darker, lighter). Alternation of a patterned stimulus (A) generates local flicker ERGs, which are 180° out of phase, so that their summed activity is canceled at the corneal recording electrode. However, pattern elements generate lateral inhibition via horizontal cells. Differential center-surround activation of the RGC dendritic field occurs for either period of the pattern reversal. Local RGC responses are in-phase and sum at the electrode. Alternation of a uniform field (B) generates local flicker ERGs, which are in-phase sum at the electrode. Different from pattern-reversal, uniform field flicker generates little differential center-surround activation of the RGC receptive field. Thus, uniform field flicker ERG is dominated by outer retina activity, whereas the PERG is dominated by inner retina activity. Outer retina activity is necessary for the PERG generation but it is not apparent in the PERG waveform because of cancellation at the electrode.(Porciatti 2007)

www.manaraa.com

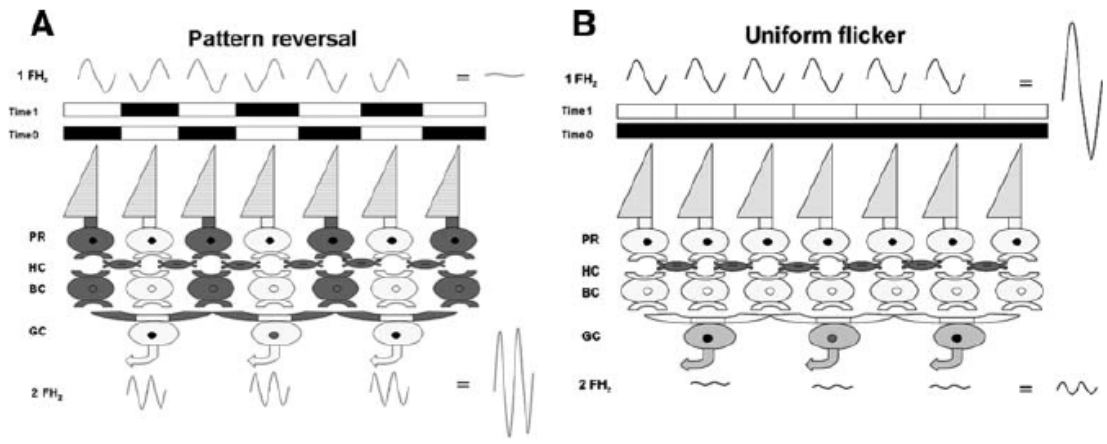

Figure.17. Schematic diagram of retinal activity during either pattern reversal (A) or uniform flicker stimulation (B).(Porciatti 2007)

An optimized protocol for mouse PERG recording has been recently described.(Porciatti, Saleh et al. 2007) In brief, mice are weighted and anesthetized with intraperitoneal injections (0.5-0.7 ml/Kg) of a mixture of Ketamine, 42.8 mg/ml and Xylazine, 8.6 mg/ml. Mice are gently restrained using a mouth bite bar and a nose holder that allows unobstructed vision, and kept at a constant body temperature of 37.8°C using a feedback controlled heating pad (TCAT-2LV, Physitemp Instruments, Inc. Clifton, NJ). Under these conditions the eyes of mice are naturally wide open and in a stable position, with pupils pointing laterally and upward. The recording electrode is a thin (0.25 mm diameter) silver wire configured to a semi-circular loop of 2 mm radius, which is gently placed on the extrapupillary corneal surface by means of a micromanipulator in such a way as to encircle the undilated pupil without interfering with vision as shown in figure 18. Reference and ground electrodes are small stainless steel needles inserted in the skin of the back of the head and the back of the body, respectively. Instillations of BSS drops every 30 min are sufficient to maintain the cornea and lens in excellent condition for many hours.

www.manaraa.com

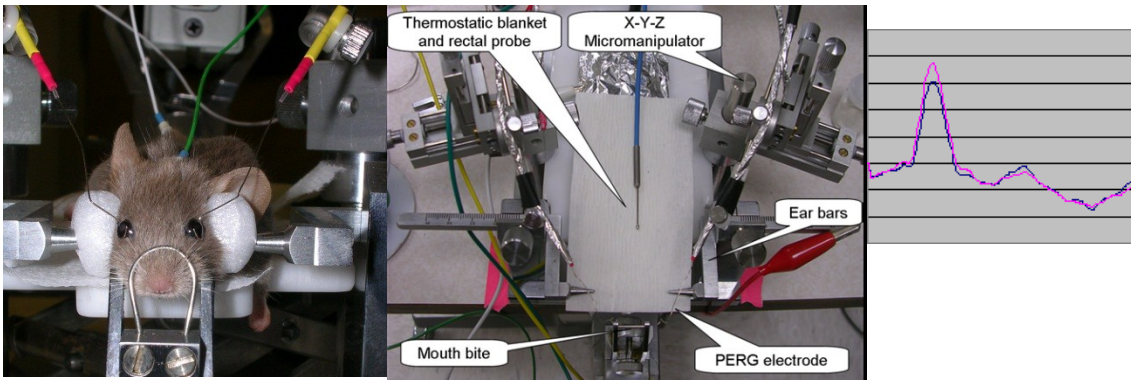

Figure.18. Experimental set up for PERG recording and an example of PERG waveform on the right side.

Pattern stimuli consist of horizontal bars of variable spatial frequencies and contrast that alternate at different temporal frequency generated by a programmable graphic card (VSG- Cambridge Research Systems, Rochester, UK) on a CRT display (Sony Multiscan 500). Stimuli are displayed on a CRT monitor whose center is aligned with the projection of the pupil and presented from a short distance (typically 15 cm) to stimulate a large retinal area (69.4° x 63.4°) centered on the optic disk. Eyes are not refracted for the viewing distance, because the mouse eye has a large depth of focus due to the pinhole pupil. Pattern has fixed mean luminance of 50 cd/m^2. The luminance of the CRT display was gamma-corrected using a photometer (OptiCal OP200-E, Cambridge Research Systems, Rochester, UK). Contrast is defined as C = (Lmax − Lmin) / (Lmax + Lmin), where Lmax = luminance of the bright stripes and Lmin = luminance of the dark stripes. (Michelson 1995) Retinal signals are amplified (10,000-fold) and band-pass filtered (1–30 Hz). Three consecutive responses of 600 contrast reversals each are recorded. The responses are superimposed to check for consistency and then averaged (1800 sweeps).

www.manaraa.com

The waveform of averaged PERGs to high-contrast (1.0) gratings of low spatial frequency (0.05 cycles/deg) consist of a major positive peak at around 90-120 ms (defined as P100) followed by a slower negative wave with a broad trough at around 200-300 ms (defined as N250, examples in Figure 17). All procedures were performed in compliance with the Association for Research in Vision and Ophthalmology (ARVO) statement for use of animals in ophthalmic and vision research. The experimental protocol was approved by the Animal Care and Use Committee of the University of Miami.

3.1.4 Retinal verve fiber layer (RNFL) thickness by spectral domain OCT

A high-resolution SD-OCT system was built for in vivo imaging of mice retina.(Ruggeri, Wehbe et al. 2007) OCT fundus images similar to those acquired with a scanning laser ophthalmoscope (SLO) were constructed from the measured OCT data, which provided precise spatial registration of the OCT cross-sectional images on the fundus. Later, we use commercial Bioptigen SD-OCT system to measure RNFL thickness. A 3D segmentation algorithm was developed by Marco Ruggeri using MATLAB software (figure 32 B. C) for calculation of the RNFL thickness. RNFL thicknesses on OCT images were also compared by histological examination with previous published references.(Saleh, Nagaraju et al. 2007) The results of retinal thickness are similar in histology compared with using SD-OCT. (Figure. 19)

www.manaraa.com

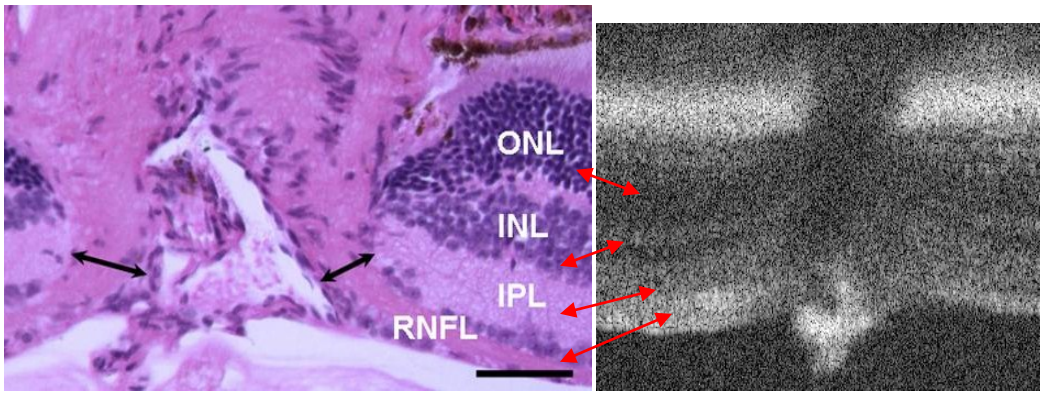

Figure.19. Comparison of a histologic cross-section (H&E staining) of C57BL/6 mouse retina with corresponding OCT cross-sectional image. All retinal layers can be recognized in the OCT image. RNFL: retinal nerve fiber layer; IPL: inner plexiform layer; INL: inner nuclear layer; ONL: outer nuclear layer.

www.manaraa.com

Chapter 4. Development Of New Research Tools

4.1 Introduction of new design tool for retinal function measurement

As the discussion in previous chapter, we had a tool to measure the inner retinal function for one eye at one time. However, it was cumbersome to do body-tilt with CRT pattern stimulation during PERG recording. And we also need to record both eyes simultaneously because the anesthesia level in mice can change with time during PERG recording. The PERG acquisition time should be short, so we can make sure three times of PERG recordings are under the same physiological condition.

Thus, we are in need of a new design system to measure both eyes simultaneously and independently, and also the new PERG recording system should be combined with the pattern stimuli during body-tilt for IOP modulation.

4.2 Research tool design

Task 1: Development of a PERG measurement system for glaucoma model mice

Purpose: A new hardware including for acquisition system, LED pattern stimuli, and body-tilt.

Specification:

1. Acquisition system (Commercial system): Amplifier gain: 10000, low-pass: 30 Hz, high-pass: 1 Hz.

2. Pattern stimulation (Custom made):

Weight: very light in order to combined with goniometer for body-tilt.

Temporal frequency: 1 Hz (2 Hz reversals/ second), 6 bar contains 3 dark bars and 3 light bars.

www.manaraa.com

Distance between stimuli and mouse corneal: 10 cm to stimulate a large retinal area (69.4° x 63.4°) as previous PERG recording system.

3. Body-tilt (Custom made): Between head-down (-60°) and head-up (60°).

Description:

The two channels amplifier and digital signal processing (DSP) box are from IHS Company, the hardware is controlled by IHS SMARTEP-CAM continuous acquisition software program. The low pass filter, high pass filter, notch filter are included in the amplifier system. The digital signal processing (DSP) box controlled by software sends the Transistor-Transistor Logic (TTL) signal in order to trigger the circuit of LED pattern stimulation for both eyes. (Figure 20.)

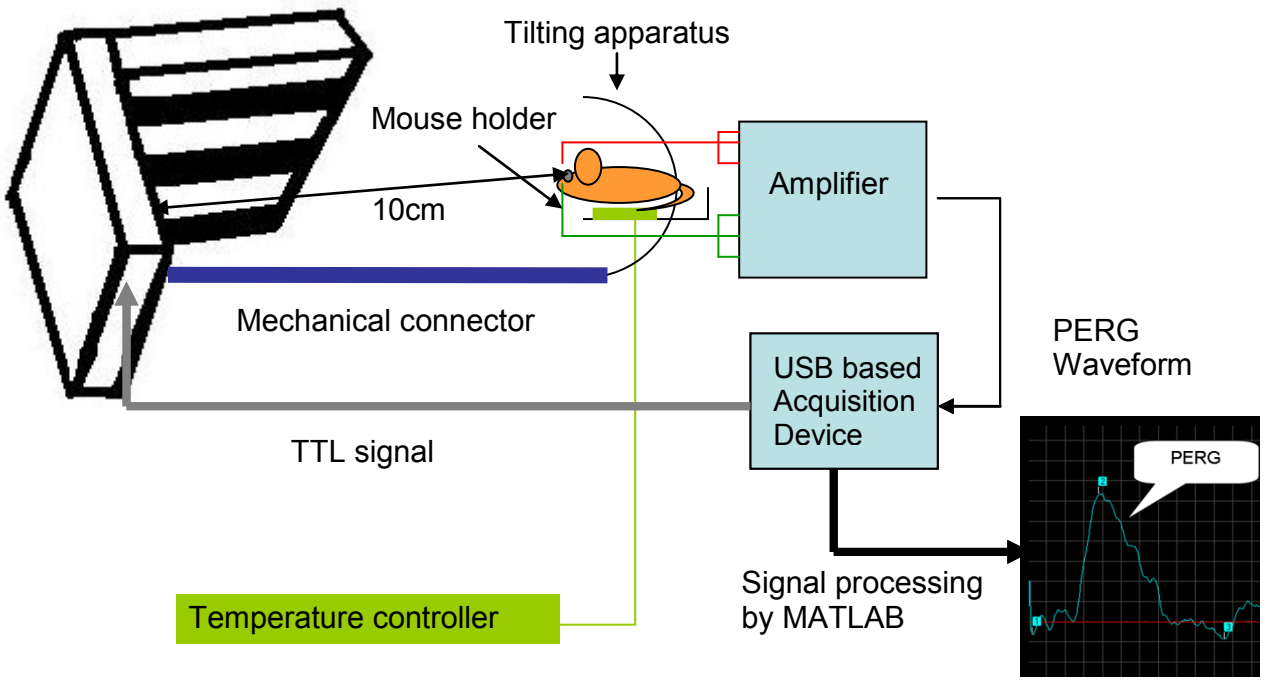

Figure.20. Schematic of entire PERG set up, including goniometric mouse holder, binocular pattern stimulus, and acquisition system.

www.manaraa.com

Evaluation:

The new PERG recording system is allowing body-tilt (IOP modulation) during PERG measurement.

Task 2: PERG acquisition software design

Purpose:

This software in figure 21 is designed to record two channels PERG measurements simultaneously and continuously, and the signal are acquired by using MATLAB program (IHS commercial program) for customizing the ERG signal parameter.

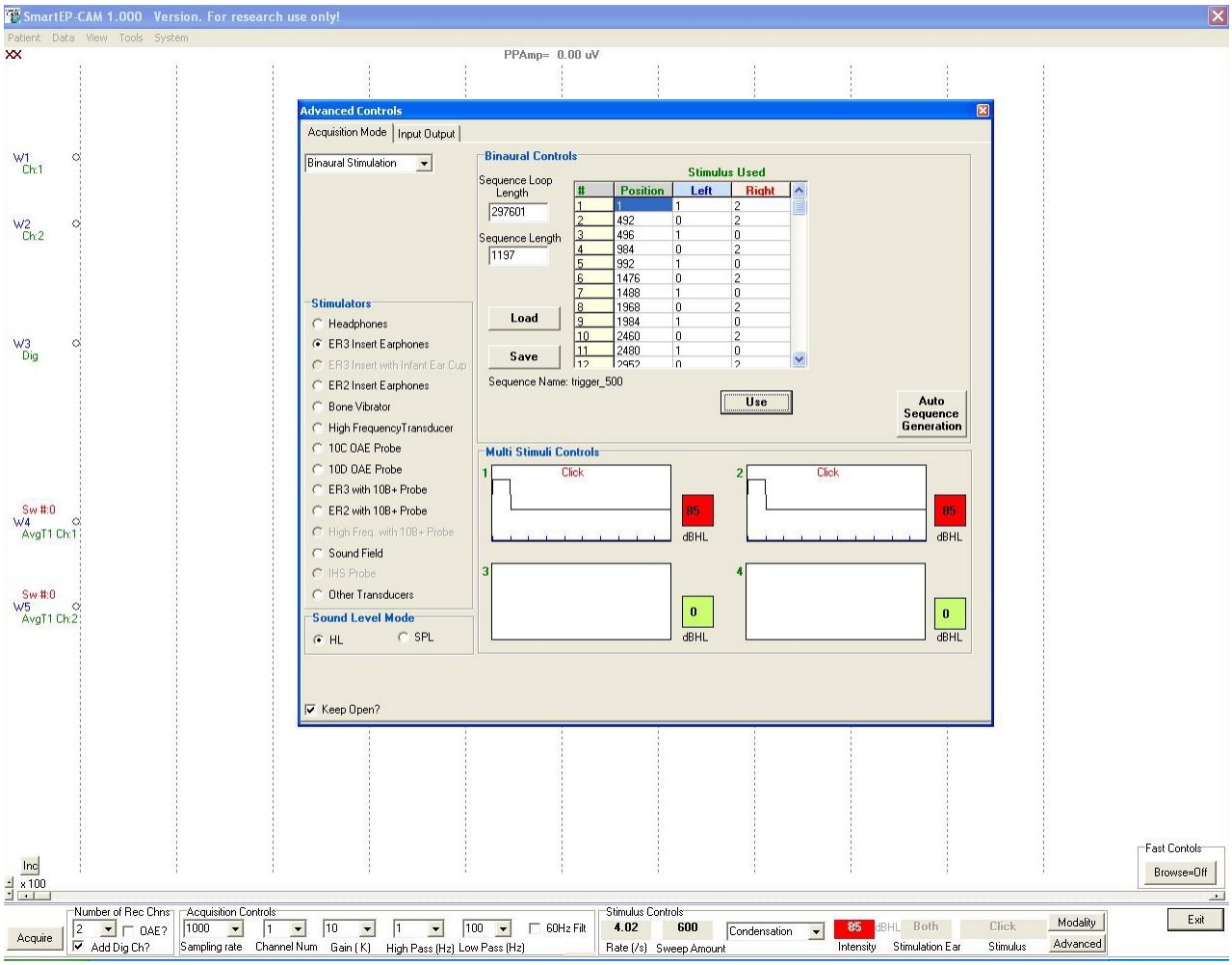

Figure 21. The front panel is designed for PERG acquisition in both eyes independently and simultaneously.

www.manaraa.com

Specification:

1. Sweep length: 496 ms for channel 1 and 492 ms for channel 2.

2. Triggering sequences design by MATLAB to fit the sweep length.

3. Cross-talk elimination: average of 372 sweeps PERG responses in each channel.

4. PERG signal Test-retest variability: <30%

Description:

We had tried to measure simultaneously both PERG in both eyes by two visual stimulations in order to reduce the recording time, and also to prevent the adverse affects of prolonged anesthesia on the development of cataract. To our surprise, we found out both PERG waveforms were virtually identical in the two eyes, thus indicating interocular cross-talk of the PERG signal. Note the FERG signal does not display interocular cross-talk under binocular stimulation. Thus, we designed two independent trigger signals for the two pattern LED display, resulting in unsynchronized stimulation frequency that allowed acquisition of PERG signal independently in the two eyes, thus overcoming the problem of interocular cross-talk. Stimulus 1 sends the TTL signal at every 496 ms and stimulus 2 sends the TTL signal at every 492 ms. There is 4 ms difference between PERG in both eyes for the average of 372 sweeps of PERG. These specific sweep lengths and the number of average are based on the following method. The mathematics theory that enables the simultaneous recording of PERGs in both eyes is as following. (Jorge E Bohórquez 2010)

Assume we have two types of stimuli (s1 and s2) presented simultaneously to each eye of a mouse using two different stimulation sequences (h1 and h2) having their own sweeps

www.manaraa.com

length (n1 and n2 samples). Assume an acquisition sampling period of length T. Figure 22 shows the stimulus delivery proposed method:

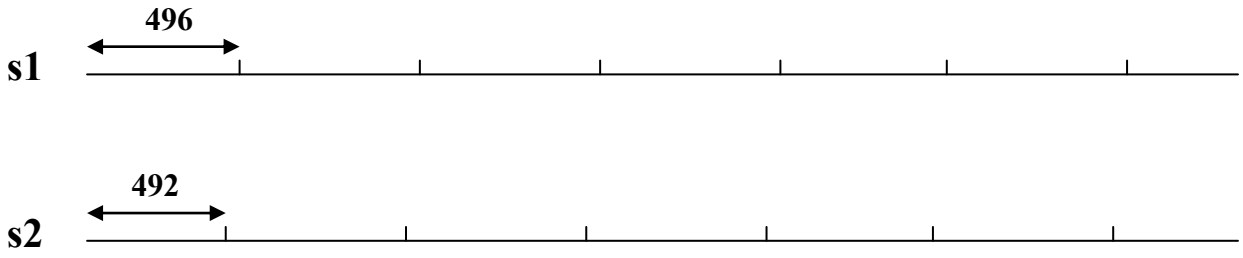

Figure 22. Delivery method for two simultaneous sequences. (Stimulus 1 for left eye and stimulus 2 for right eye.)

To recover the responses of two sweeps averages, PERGs from both eyes have its own length and represent by the variable x (t).

$$y_1(nT) = \frac{1}{K1}\sum_{k=1}^{K1} x_{\,1}\big((n+kn_1)T\big), n = 1,2,\dots,n_1$$

$$y_2(nT) = \frac{1}{K2}\sum_{k=1}^{K2} x_{\,2}\big((n+kn_2)T\big), n = 1,2,\dots,n_2$$

In absence of noise, the recorded signal is the superposition of the responses for each sequence:

$$x(nT) = x_1(nT) + x_2(nT)$$

In this model, $x_1(t)$ is periodic with period n_1T and $x_2(t)$ is periodic with period n_2T.

$$y_1(nT) = x_1(nT) + \frac{1}{K1}\sum_{k=1}^{K1} x_2\big((n+kn_1)T\big), n = 1,2,\dots,n_1$$

- (equation 1)

$$y_2(nT) = x_2(nT) + \frac{1}{K2}\sum_{k=1}^{K2} x_1\big((n+kn_2)T\big), n = 1,2,\dots,n_2$$

- (equation 2)

www.manaraa.com

In equation 1 and 2, we can identify the most right terms as the sequence of cross-talk terms. They must be minimized to obtain good individual signal estimations.

The cross talk from stimuli s2 into the recovered signal y1 is:

$$R_{21}(nT) = \frac{1}{K1}\sum_{k=1}^{K1} x_2\big((n+kn_1)T\big)$$

- (equation 3)

Using the fact that the signal $x_2(t)$ is periodic and ignoring its DC component, it can be expressed in terms of its Fourier series:

$$x_2(t) = \sum_{i=1}^{\infty} a_i \cdot \cos(\omega_i t + \varphi_i)\,, \qquad \omega_i = \frac{2\pi i}{n_2 T}$$

Substituting $x_2(t)$ into the equation 3, we found:

$$R_{21}(nT) = \frac{1}{K1}\sum_{k=1}^{K1}\sum_{i=1}^{\infty} a_i \cdot \cos(\omega_i(n+kn_1)T + \varphi_i)$$

Above equation can be arranged to obtain:

$$R_{21}(nT) = \sum_{i=1}^{\infty} a_i \cdot \frac{1}{K1}\sum_{k=1}^{K1} \cos(\omega_i(n+kn_1)T + \varphi_i)$$

$$R_{21}(nT) = \sum_{i=1}^{\infty} a_i \cdot R_i \cdot cos(\omega_i nT + \theta i\,)$$

By calculation from the above, we get the interference term R_i is :

$$R_i = \frac{1}{K_1}\sqrt{\frac{1-\cos(\omega_i K_1 n_1 T)}{1-\cos(\omega_i n_1 T)}}$$

- (equation 4)

Substituting the angular frequency into equation (4):

www.manaraa.com

$$R_i = \frac{1}{K_1}\sqrt{\frac{1-\cos(2\pi i K_1 \frac{n_1}{n_2})}{1-\cos(2\pi i \frac{n_1}{n_2})}}$$

- (equation 5)

The term R_i is independent of the sampling period, it is a property associated to the sequence lengths and the sweep number K_1. A similar development can be done for the interference from the sequence 1 into the recovered signal $x_2(t)$ to obtain:

$$R_j = \frac{1}{K_2}\sqrt{\frac{1-\cos(2\pi j K_2 \frac{n_2}{n_1})}{1-\cos(2\pi j \frac{n_2}{n_1})}}$$

- (equation 6)

Where j corresponds to the harmonic number of the periodic signal $x_1(t)$ and K_2 is the number of sweeps average for the sequence s2. The corresponding physical frequency to the R_j croos-talk term is:

$$\omega_j = \frac{2\pi j}{n_1 T}$$

In summary, equation 5 and 6 show the cross-talk effect of the response $x_2(t)$ on the estimation of $x_1(t)$ as a linear combination of the harmonics of $x_2(t)$ shaped by a transfer function depending on the number of sweeps and the ratio between the sweep length.

The optimal sweep numbers: for a given two sequence lengths (n_1 and n_2), the cross-talk term R_i has a minimum when $\cos(2\pi i K_1 \frac{n_1}{n_2}) \approx 1$. This implies that the cosine argument is an even multiple of pi. $2\pi i K_1 \frac{n_1}{n_2} \approx 2m\pi \rightarrow i K_1 \frac{n_1}{n_2} \approx m, m \in Z$. This equation shows that if K1 is chosen to minimize the cross-talk of the first harmonic (i=1), it will also

www.manaraa.com

work for higher harmonics. To continue the analyses, assume i=1 and let us find the integer number of sweeps that obeys the following equation:

$$K_1 \approx \left(\frac{n_1}{n_2}\right) m$$

Let us assume $n_1 > n_2$, their ratio can be expressed as $\frac{n_1}{n_2} = 1 - \alpha$.

Let assume $\frac{1}{\alpha}$ is an integer m, then sweep number $K_1 \approx \left(\frac{1}{\alpha}\right)$-1

By this math, we can get the relationship between sweep length ($n_{1,}n_{2,}$) and sweep number ($K_{1,}$)

So, we can decide the sweep numbers of two eyes PERGs and appropriate sweep number to eliminate the cross-talk of PERG.

In the future, we also try to disclose the origin of intraocular cross-talk phenomena of PERG signal.

Evaluation:

We stimulate one eye only and to check if there is cross-talk effect in the non-stimulated eye. The result shows there is no cross-talk. (Figure 48.) PERG signal to noise ratio is 10 as previous system and the test-retest variability is less than 30 %.

Task 3: Development of LED pattern stimulation

Purpose: To design pattern stimuli to stimulate a large retinal area similar to previous CRT stimulation.

Specification:

1. Stimulated retinal area: 56.3° (=arc tangent (15/10)) x 63.4° (=arc tangent (20/10)).

2. Mean luminance: 500 cd/m^2.

www.manaraa.com

3. Contrast: C ~1 = (Lmax − Lmin) / (Lmax + Lmin), where Lmax = luminance of the bright stripes and Lmin = luminance of the dark stripes.

Description:

The dimension of the LED tablet is half the size of the original CRT monitor as shown in figure 23. The viewing distance is 10 cm compared to 20 cm for the CRT to normalize the visual angle. The LED tablet size is 15 cm by 20 cm, corresponding to stimulated retina area of 56.3° (=arc tangent (15/10)) by 63.4° (=arc tangent (20/10)). Each pattern bar size is 2.5 cm and distance between stimulation and mouse eye is 10 cm, covering 14° (=arc tangent (2.5/10)) of retina. This size is similar to the receptive field size of retinal ganglion cells in the mouse (Porciatti 2007). The LED has an emitting angle at 120°. In order to have uniform luminance, we arrange the LED as shown in figure 24 and we also put the light shaping diffuser (LSD) on the top. LSD can be custom-tailored to meet brightness, uniformity, and viewing angle requirements for our PERG application. In order to get better contrast, we put alumina reflective strip between LED bars. The height of LED tablet was calculated by MATLAB in order to get highest and uniform luminance. (Figure 25) It is shown that we get the most inform luminance on the top of LED tablet when we have 4 cm high of reflective strip. The contrast-reversal rates (temporal frequency) of two pattern stimulations were generated unsynchronized by MATLAB software.

www.manaraa.com

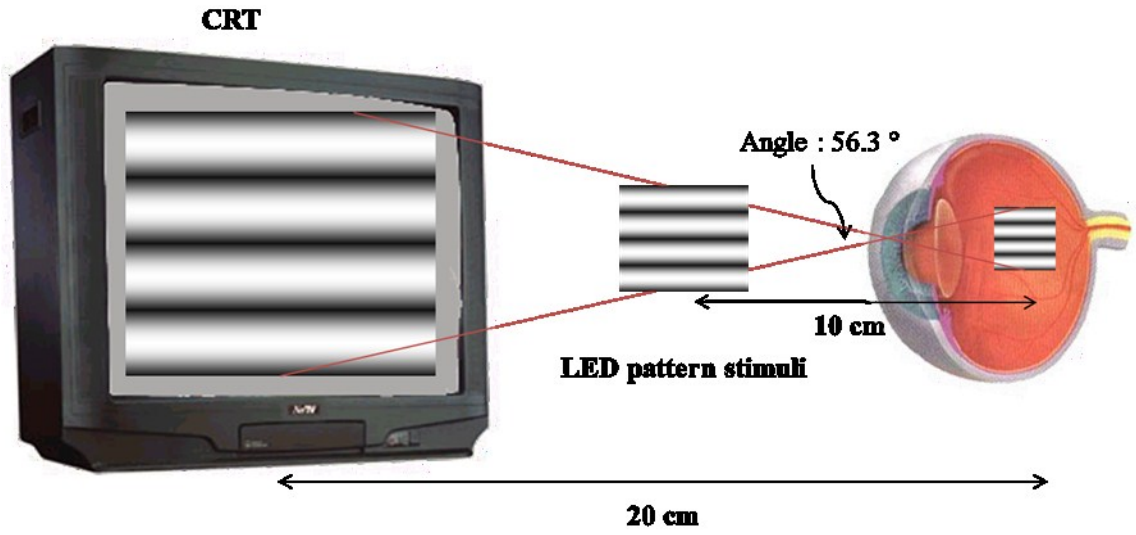

Figure 23. Same stimulated retinal area by CRT and LED pattern stimulation.

www.manaraa.com

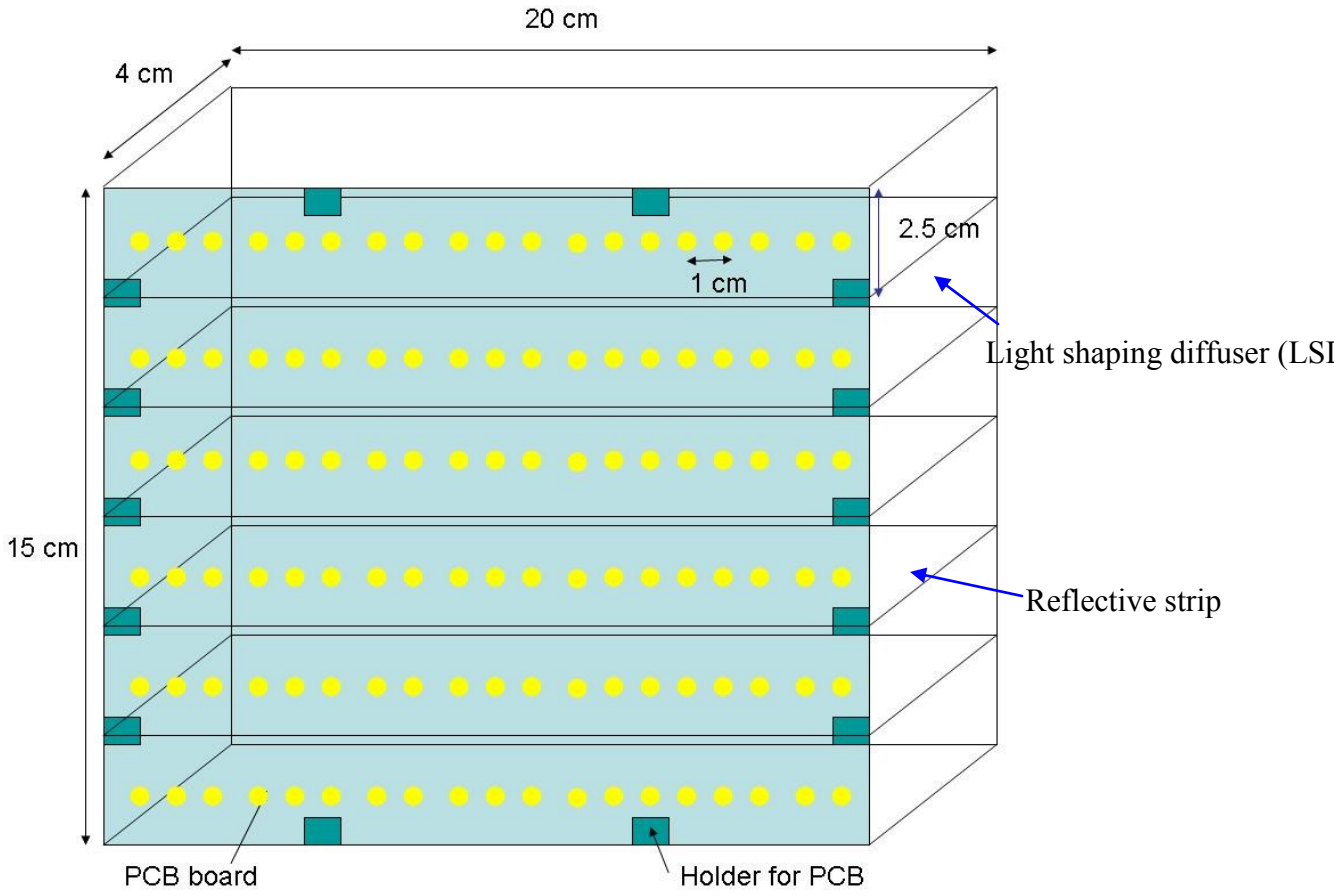

Figure.24. LED arrangement of pattern stimulation.

www.manaraa.com

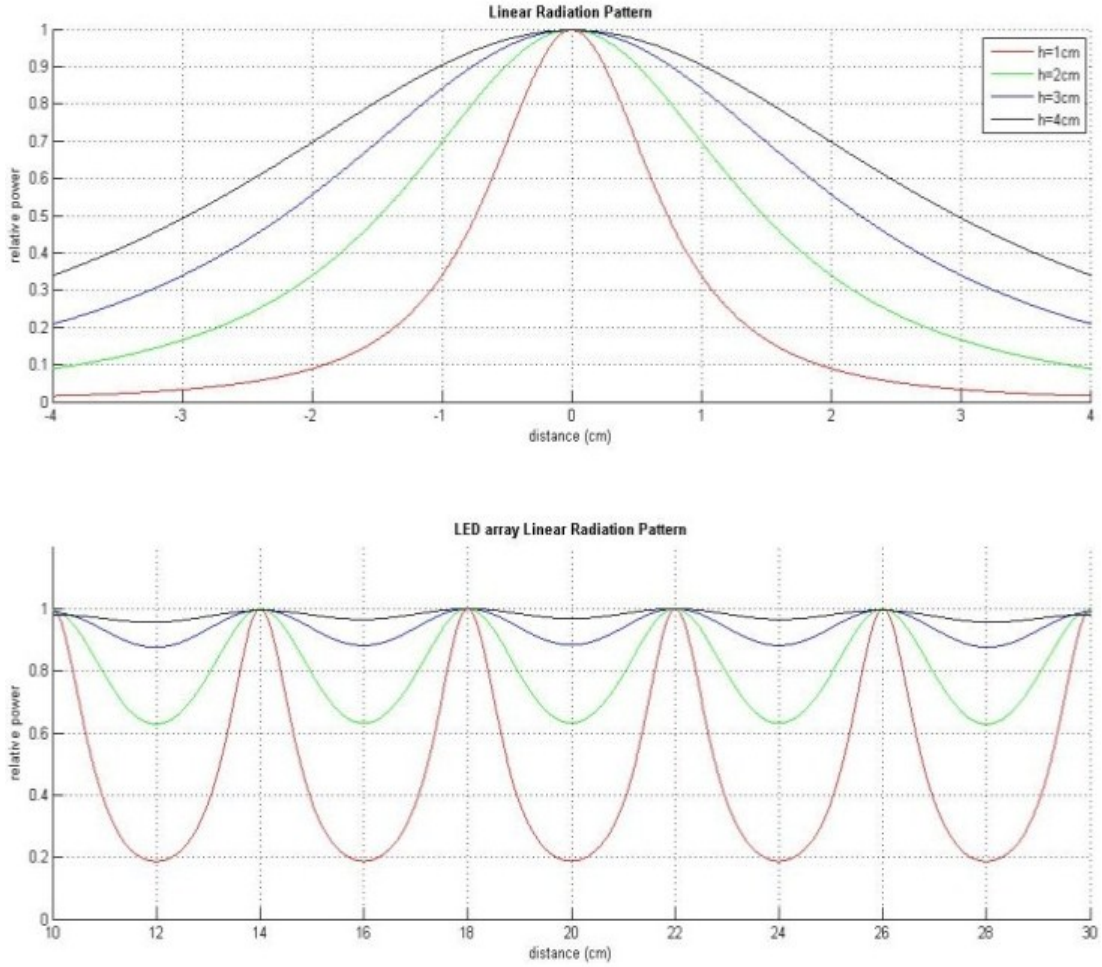

Figure.25. MATLAB simulation of luminance on the top of LED tablet with different height of reflective strip. (H = 1(red line), 2(green line), 3(blue line), 4(black line) cm)

Evaluation:

The contrast of LED pattern stimulation is same as CRT monitor (100%). The luminance is 10 times as CRT monitor. The PERG response was measured in the same mouse by CRT pattern stimulation and LED pattern stimulation. The result is shown in figure 39.

www.manaraa.com

Task 4: Development of a goniometric holder for mouse body-tilt allowing both IOP measurement and PERG recording.

Purpose: To make sure the stimulated retinal area is always the same location and the angle of body-tilt for IOP modulation.

Specification:

1. Light weight: mechanical connector between LED tablet and goniometer.

2. Connection: Without obstruction of pattern stimulation.

Description:

We designed a mechanical connector between LED tablets and body-tilt apparatus. Optimization included means to stabilize the mouse body together with the temperature controller for any position of body posture to ensure constant electrode position for PERG acquisition. (Figure.26, 27)

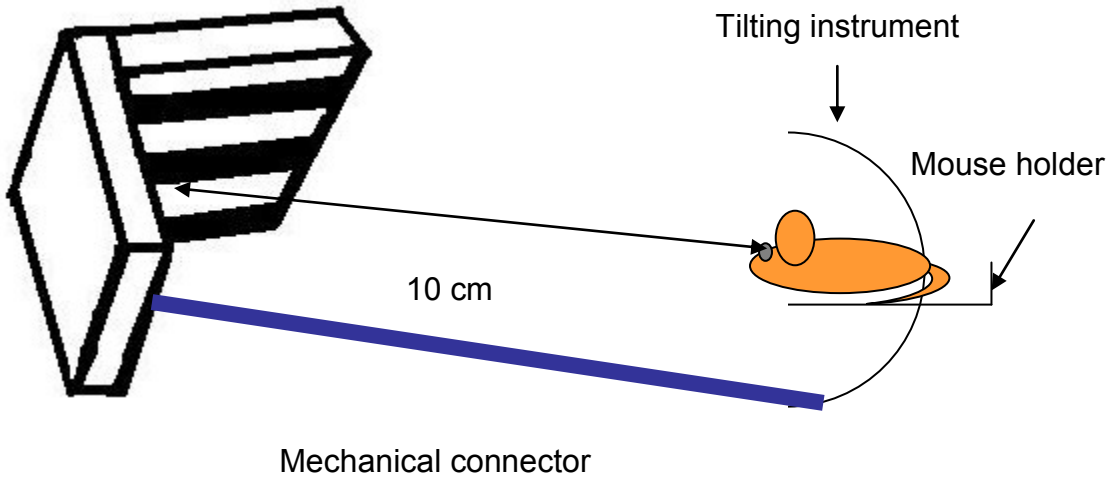

Figure.26. Pattern stimulation with tilting apparatus; the center is aligned with the projection of the pupil and presented from a short distance (10 cm) to stimulate a large retinal area (50°-60°) centered to the optic disk.

www.manaraa.com

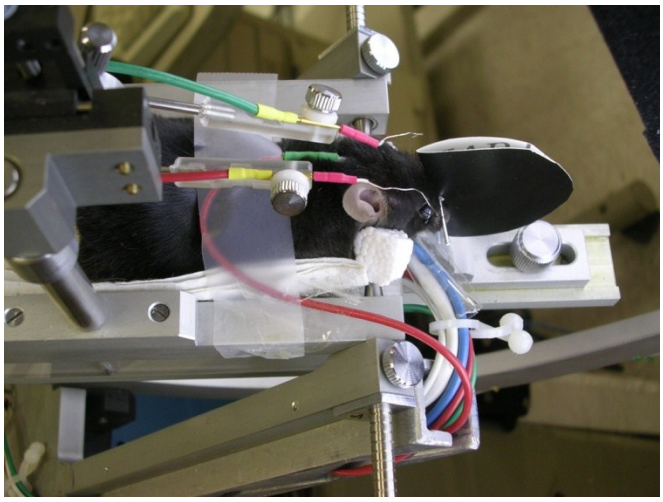

(A)

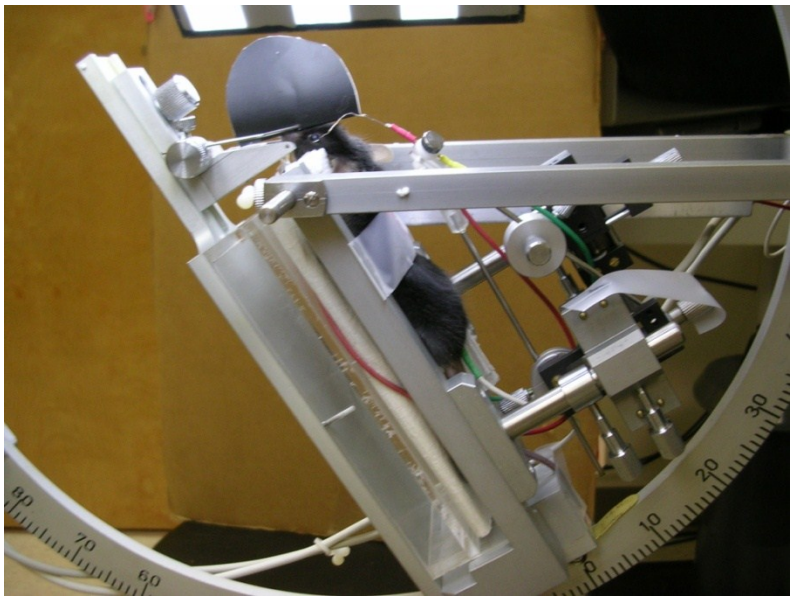

(B)

Figure 27. The custom-made body-tilt apparatus with PERG recording system. (A) Closed view of PERG recording in both eyes. (B) 60 deg head-up position.

Task 5: 10 Hz LED luminance flicker.

Purpose: Luminance flicker stimulation (~10 Hz) of the photoreceptors is known to increase retinal blood flow. This increase of the blood flow should meet the enhanced metabolic need of the neural retina under a physiological stimulus. (Hammer, Vilser et al.

www.manaraa.com

2011) We apply this knowledge to generate the metabolic challenge to retina in different strains of mice to investigate if there is effect on retinal function.

Specification:

1. Flicker frequency: 10 Hz (induced metabolic change in retina), 100 Hz (control-beyond temporal resolution of mouse cone ERG)

2. LED Flicker need to be light weight and small object in order to superimpose with pattern stimulation without obstruction of pattern stimulation.

Description:

We used the Arduino Duemilanove (2009) microcontroller board. "Duemilanove" means 2009 in Italian and is named after the year of its release. It has 14 digital input/output pins (of which 6 can be used as PWM outputs), 6 analog inputs, a 16 MHz crystal oscillator, a USB connection, a power jack, and a reset button. It contains everything needed to support the microcontroller; simply connect it to a computer with a USB cable or power it with an AC-to-DC adapter or battery to get started. The Arduino Duemilanove can be programmed with the Arduino software (downloadable on the Arduino website). I programmed with this software in order to trigger the five LED board at 10 Hz and 100 Hz. During PERG recording, we applied 10 Hz flicker to induce the metabolism change in retina and applied 100 Hz flicker as control recording for under the same luminance.

Evaluation:

PERG amplitudes and latencies were compared between with 10 Hz flicker and 100 Hz flicker in different strains of mice at the same age. The latency of PERG represents how fast the retinal ganglion cell response to the pattern stimulation. When flicker increases

www.manaraa.com

the demand of metabolic need of retina, the latency of PERG in different strain mice may be different.

www.manaraa.com

Chapter 5. Results

5.1 Age-related changes of the eye structure (TD-OCT images) in D2 mice and other genetic strains.

Figure 28 shows an example of B6 TD-OCT image with uncorrected and corrected ocular boundaries. Axial length (AL) was measured from the anterior corneal surface to the top of retinal pigment epithelium, and corresponded to the summed thicknesses of all eye components: Corneal thickness (CT), anterior chamber depth (ACD), lens thickness (LT), vitreous chamber depth (VCD), retinal thickness (RT): AL = CT+ACD+LT+VCD+RT (details in Figure 28).

Figure 29 shows representative examples of whole-eye OCT recorded in D2 and B6 mice at different ages. The images clearly show the boundaries that are not obscured by the iris, including the cornea, anterior iris, anterior chamber, lens, vitreous, and retina.

Axial length, AC depth, and lens thickness increase significantly ($P<0.001$) between 2.5 and 20 months of age in both D2 and B6 mice.(Figure 29) (Chou, Borja et al. 2009) Age-related changes are well fit by linear regressions on log-log coordinates (R^2 range: 0.65 to 0.9). However, the increase in axial length is larger in D2 (~21%) compared to B6 (~9%) mice. The increase in axial length is associated with increase in AC depth (D2:~10%; B6; ~1.5%) and increase in lens thickness (D2: ~7%; B6: ~9%). Corneal thickness is similar in D2 and B6 mice and does not significantly change with age; there is corneal deposit in old D2. Figure 30 provides summary scattergrams of changes in mean size of all ocular components as a function of increasing age. Actual sizes at specific ages for each eye component are reported in Tables 3 and 4 together with significance of age-related

www.manaraa.com

changes (one-way ANOVA). Overall comparisons between D2 and B6 were tested with two-way ANOVA. Main effects tested were, Strain (size differs between D2 vs. B6), Age (size changes with age), and interaction between strain and age (age-related changes are different between D2 and B6). We also put our data comparing with previous publication with eye size and cornea radius of curvature changes in table 4 and 5.

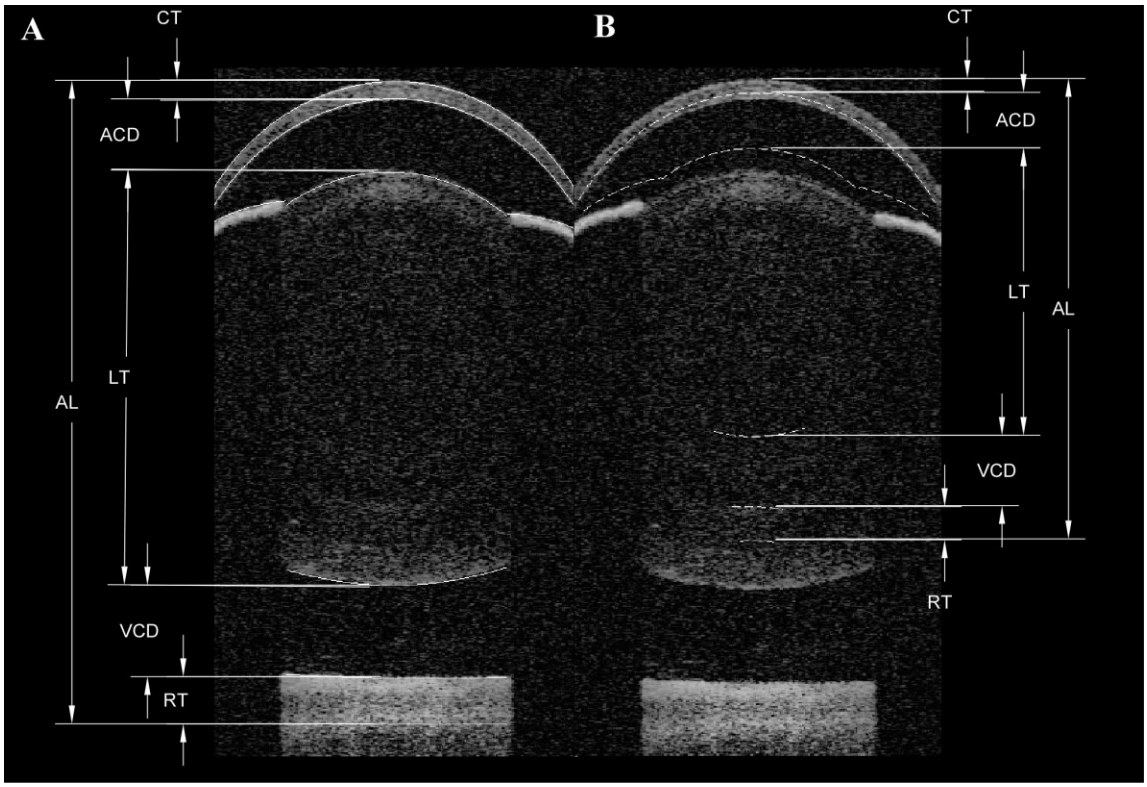

Figure.28. Representative in vivo OCT image of the whole of a C57BL/6J mouse.
The cornea, anterior chamber, iris and portions of the lens, vitreous and retina that are not blocked by the iris can be clearly visualized. Panel A indicates how eye components were measured. CT: corneal thickness; ACD: anterior chamber depth; LT: lens thickness; VCD: vitreous chamber depth; RT: retinal thickness; AL: axial length. AL=CT+ACD+LT+VCD+RT. The images show the distance measurements after segmentation with automated edge detection before (A) and after (B) correction for image refractive distortion. (Manns, F., O. P. Kocaoglu, et al. ,IOVS, 2009. 50(5):5670.)

www.manaraa.com

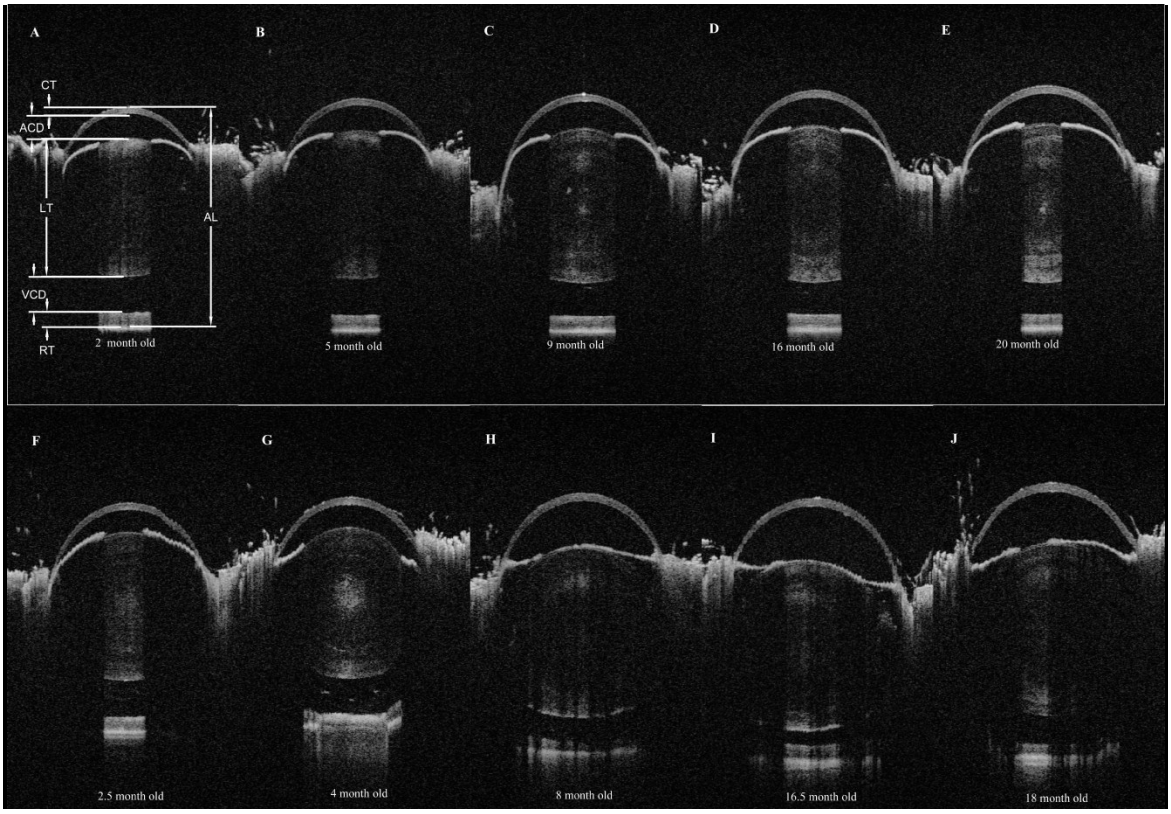

Figure 29.Upper panels: Representative examples of whole-eye OCT images recorded in C57BL/6J mice aged 2 months (A), 5 months (B), 9 months (C), 16 months (D), and 20 months (E). Lower panels: Corresponding representative examples for DBA/2J mice aged 2.5 months (F), 4 months (G), 8 months (H), 16.5 months (I), and 18 months (J). Note irregularities of the iris signal due to depigmentation in older mice (H, I, J) that cause image discontinuity in the lens and retina. (Chou T-H, Borja D, Kocaoglu OP, Uhlhorn SR, Manns F and Porciatti V. IOVS, 2011)

www.manaraa.com

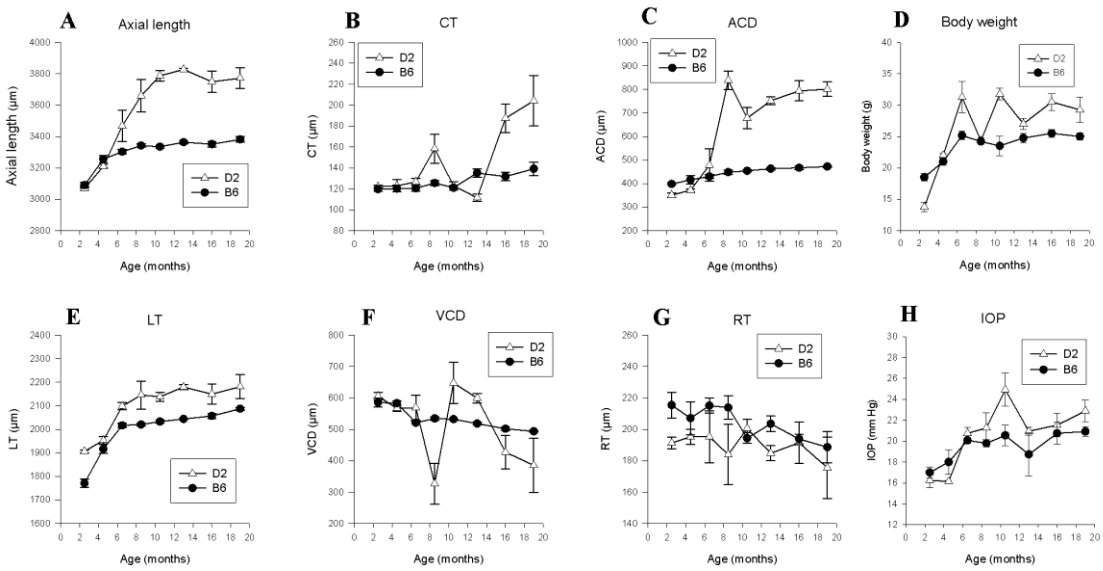

Figure.30. Changes of axial ocular components with age in DBA/2J (n=32) and C57BL/6J mice (n= 36). (A) axial length (AL) (B) corneal thickness (CT), (C) anterior chamber depth (ACD), (E) lens thickness(LT), (F) vitreous chamber depth(VCD), (G) retinal thickness (RT), measured by time-domain OCT. (D) Body weight, (H) IOP, measured by Tonolab tonometer. For each age group, symbols represent the mean ± SE. (Chou T-H, Borja D, Kocaoglu OP, Uhlhorn SR, Manns F and Porciatti V. IOVS, 2011)

www.manaraa.com

D2 age	N	CT	ACD	LT	VCD	RT	AL
2 – 3	4	122 ± 9	351 ± 27	1906 ± 29	606 ± 37	191 ± 13	3069 ± 43
4 – 5	4	123 ± 9	372 ± 27	1953 ± 29	567 ± 37	195 ± 11	3209 ± 43
6 – 7	4	127 ± 9	478 ± 27	2098 ± 29	569 ± 37	195 ± 11	3467 ± 43
8 – 9	4	158 ± 7	837 ± 27	2146 ± 23	327 ± 31	184 ± 9	3660 ± 43
10 – 11	4	123 ± 9	678 ± 27	2138 ± 29	648 ± 37	201 ± 11	3787 ± 43
12 – 14	4	111 ± 9	752 ± 27	2180 ± 29	600 ± 37	185 ± 11	3827 ± 43
15 – 17	4	188 ± 9	794 ± 27	2150 ± 29	427 ± 37	191 ± 11	3749 ± 43
18 – 20	4	204 ± 9	801 ± 27	2181 ± 33	385 ± 43	175 ± 13	3771 ± 50
B6 Age	**N**	**CT**	**ACD**	**LT**	**VCD**	**RT**	**AL**
2 – 3	6	120 ± 7	398 ± 22	1771 ± 23	586 ± 31	215 ± 9	3089 ± 45
4 – 5	3	120 ± 10	416 ± 27	1917 ± 33	583 ± 43	207 ± 13	3256 ± 37
6 – 7	6	121 ± 7	430 ± 22	2016 ± 23	521 ± 31	215 ± 9	3303 ± 36
8 – 9	5	126 ± 8	448 ± 24	2020 ± 26	534 ± 33	214 ± 10	3342 ± 23
10 – 11	4	121 ± 9	454 ± 27	2033 ± 29	532 ± 37	194 ± 11	3335 ± 24
12 – 14	4	135 ± 9	463 ± 27	2044 ± 29	518 ± 37	203 ± 11	3363 ± 19
15 – 17	4	132 ± 9	467 ± 27	2057 ± 29	502 ± 37	194 ± 11	3353 ± 30
18 – 20	3	139 ± 10	472 ± 31	2087 ± 33	494 ± 43	189 ± 13	3388 ± 31

Table 3. Dimensions of eye components in D2 and B6 mice aged 2-20 months (means in µm ± SD).

www.manaraa.com

B6, Age 2 – 3 months	**Method**	**CT**	**ACD**	**LT**	**VCD**	**RT**	**AL**
Present results	OCT	120 (SD 7)	398 (SD 22)	1771 (SD 23)	586 (SD 31)	215 (SD 9)	3089 (SD 45)
Schaeffel et al., 2004 (100 days old)	Frozen tissue	85	293	2049	572	223	3340
Remtulla and Hallett, 1985 (98 to 203 days old)	Frozen tissue	93 (SE 4)	452 (SE 8)	203 (SE 2)	558 (SE 20)	237 (SE 13)	3372
Zhou et al., 2008 (29 days old)	OCT	90.8 (SD 4.6)	311.7 (SD 18.1)	1558.7 (SD 18)	707.4 (SD 21.4)	186.9 (SD 15.1)	3003.3 (SD 44.1)
Puk et al., 2006 (11 week-old)	OCT	72.47 to 130.87	473 to 581	1999 to 2149			3430 to 3622
Zhou et al., 2008 (67 days old)	OCT	114 (SD 7)	370 (SD 13)	1734 (SD 29)	651 (SD 24)	187 (SD 16)	3233 (SD 30)
Tkatchenko, 2010 (67 days old)	MRI		381 (SD 3)	1940 (SD 24)	908 (SD 36)		3246 (SD 3)
Cone et al, 2010 (6 to 12 week-old)	Fresh tissue						3430 to 3680 (SD 100)
Wang et al., 2010 (8 week-old)	OCT	113 (SD 4.6)	413.3 (SD 7.4)	1783.4(SD 15.5)	643.3 (SD 14.8)	205.2 (SD 13.7)	3158.2 (SD 21.6)
B6, Age 6 -7months	**Method**	**CT**	**ACD**	**LT**	**VCD**	**RT**	**AL**
Present results	OCT	121 (SD 7)	430 (SD 22)	2016 (SD 23)	521 (SD 31)	215 (SD 9)	3303 (SD 36)
Remtulla and Hallett, 1985 (98 to 203 days)	Frozen section	93 (SE 4)	452 (SE 8)	2032 (SE 21)	558 (SE 20)	237 (SE 13)	3372
D2, Age 2 - 3months	**Method**	**CT**	**ACD**	**LT**	**VCD**	**RT**	**AL**
Present results	OCT	122 (SD 9)	351 (SD 27)	1906 (SD 29)	606 (SD 37)	191 (SD 13)	3069 (SD 43)
Cone et al, 2010 (6 to 12 week-old)	Fresh tissue						3350 to 3500 (SD 80-100)
D2, Age 12 - 14months	Method	CT	ACD	LT	VCD	RT	AL
Present results	OCT	111 (SD 9)	752 (SD 27)	2180 (SD 29)	600 (SD 37)	185 (SD 11)	3827 (SD 43)
Cone et al, 2010 (50 week-old)	Fresh tissue						3830 (SD 230)

Table 4. Comparison of ocular dimensions in B6 and D2 mice of different age.
Legend. CT: corneal thickness; ACD: anterior chamber depth; LT: lens thickness; VCD: vitreous chamber depth; RT: retinal thickness; AL: axial length; SE: standard error; SD: standard deviation. Data represent the means in µm.

www.manaraa.com

B6, Age 2 - 3months	**Method**	**Entire Cornea**	**Anterior Cornea**	**Posterior Cornea**
Present results	curve-fitting		1301 (SD 76)	1338 (SD 81)
F. Schaeffel et al., 2004 (100 days old)	frozen section		1414 (SD 19)	1415 (SD 44)
	Infrared photokeratometry		1493 (SD 80)	
Zhou et al., 2008 (67 days old)	Topcon keratometer	1503 (SD 13)		
Tkatchenko, 2010 (67 days old)	Calculated from AC depth/width	1483 (SD 16)		
B6, Age 6 - 7months	**Method**	**Entire Cornea**	**Anterior Cornea**	**Posterior Cornea**
Present results	curve-fitting		1474 (SD 40)	1460 (SD 37)
Remtulla and Hallett, 1985 (5 month old)	curve-fitting		1457 (SE 85)	1404 (SE 74)

Table 5. Comparison of corneal radius of curvature in B6 mice of different ages.
Legend. SD: standard deviation; SE: standard error. Data represent the means in μm.

Discussion:

Eye size grows differently in D2 and B6 with age. IOP may play a role in exaggerated eye size growth in D2 compared with B6. Please read more discussion in section 6.3.

5.2 Age-related changes of the RNFL thickness (SD-OCT images) in D2 mice and other genetic strains.

The RNFL thickness measurement is located away from optic nerve end point of 200, 400, 600 μm in three age groups D2 mice by spectral-domain OCT. (Figure 31) We can tell that RNFL thickness decreased with age and also decreased with the location away from the optic nerve end point. We first measured the RNFL thickness by SD-OCT in Ophthalmic Biophysics Lab.

www.manaraa.com

Later, we measured the inner retinal thickness and whole retinal thickness in D2 mice at 3 and 6 month of age as shown in table 6. (SD-OCT, Bioptigen Inc.) The representative example of retinal image in 3 month old D2 is shown Figure 32 A (cross-section view) and B, C (top view).

A hollow cylinder of tissue (outer radius 0.65 mm, inner radius 0.2 mm) centered on the optic disk was analyzed. Mean thicknesses were calculated on 100 b-scans spanning the retinal tissue using custom semi-automatic software. We can tell that there is significant ($P < 0.05$) reduction of total retinal reduction in D2 with age in table 6. We also measure the inner retinal (retinal nerve fiber layer and inner plexiform layer) thickness and retinal thickness in D2 compared with B6 of ages by SD-OCT (Figure 33).

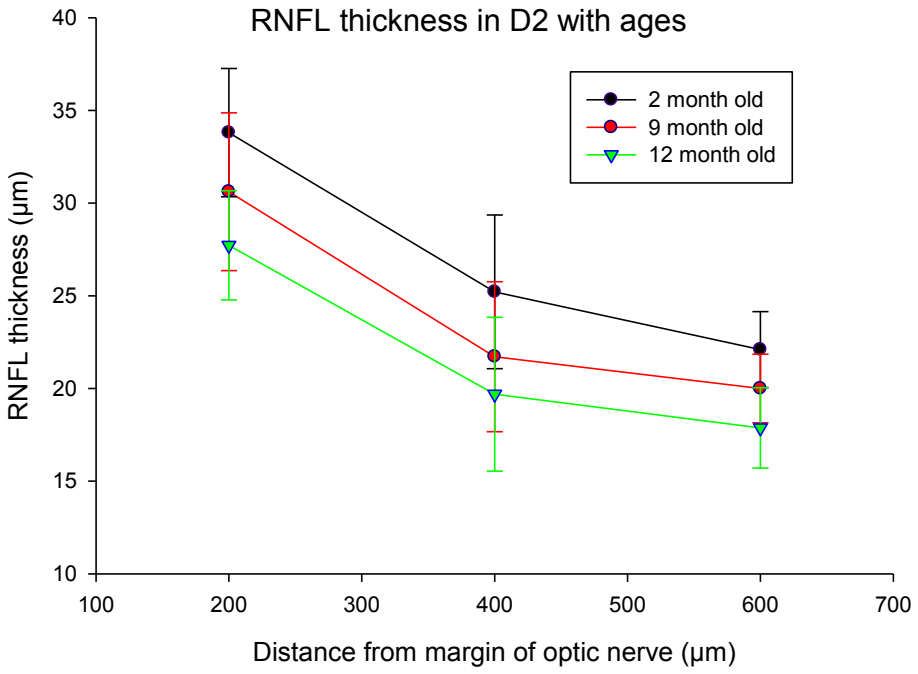

Figure.31. RNFL thickness measurement closed to optic nerve head in three age groups D2 mice by spectral-domain OCT in Marco's lab.

www.manaraa.com

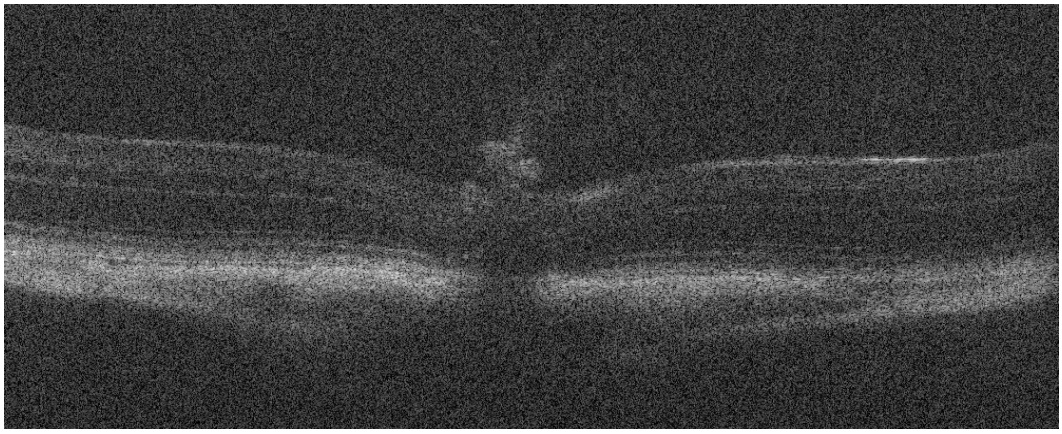

Figure 32 (A) Representative of 3 month old D2 retinal image by Bioptigen SD-OCT.

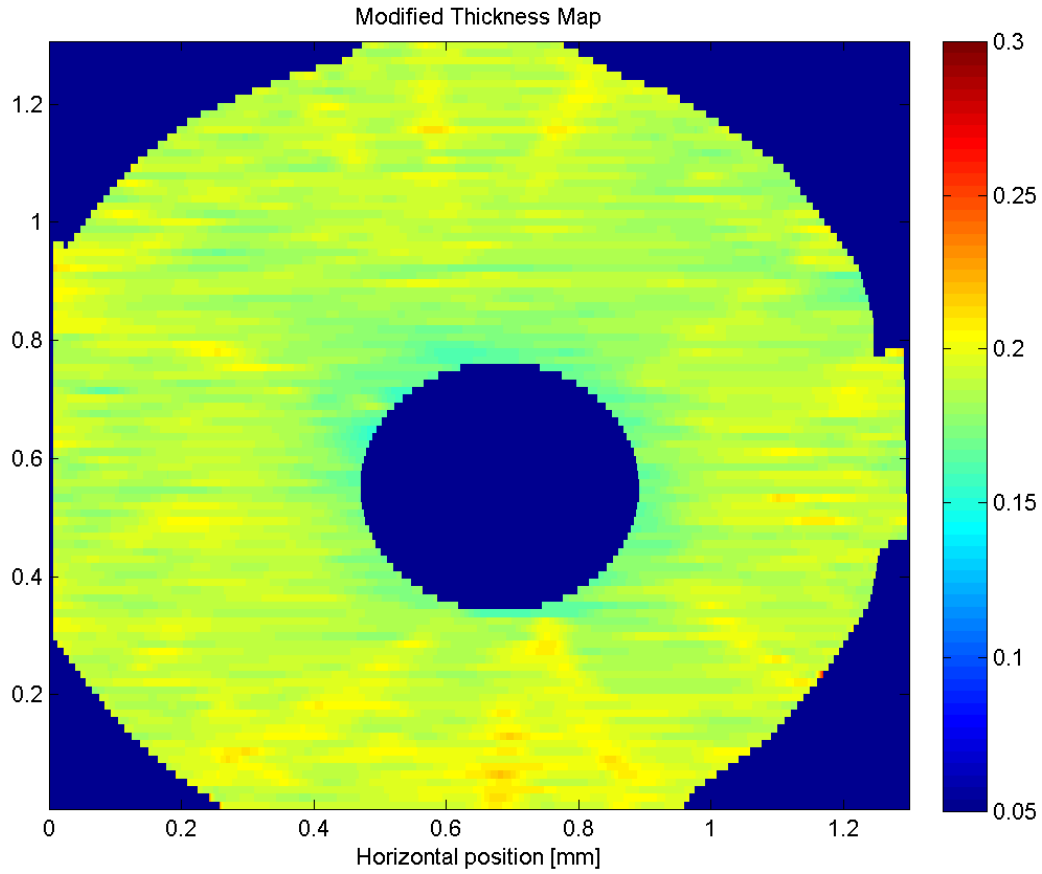

Figure 32 (B) Representative of 2D retinal thickness map in 3 month old D2. Unit: mm. Note that the removed center area is optic nerve area. The retinal thickness in retina is not uniform as you can see they are in different color.

www.manaraa.com

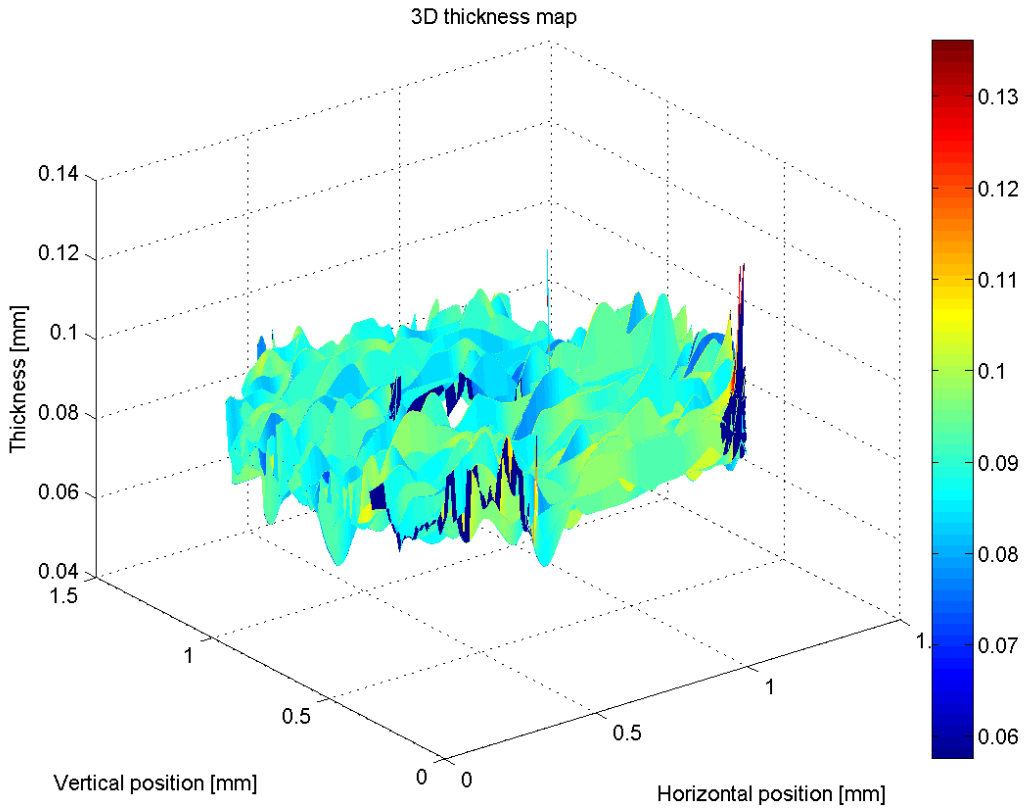

Figure 32 (C) Representative of 3D retinal thickness map in 3 month old D2. Unit: mm. Note that the removed center area is optic nerve area.

www.manaraa.com

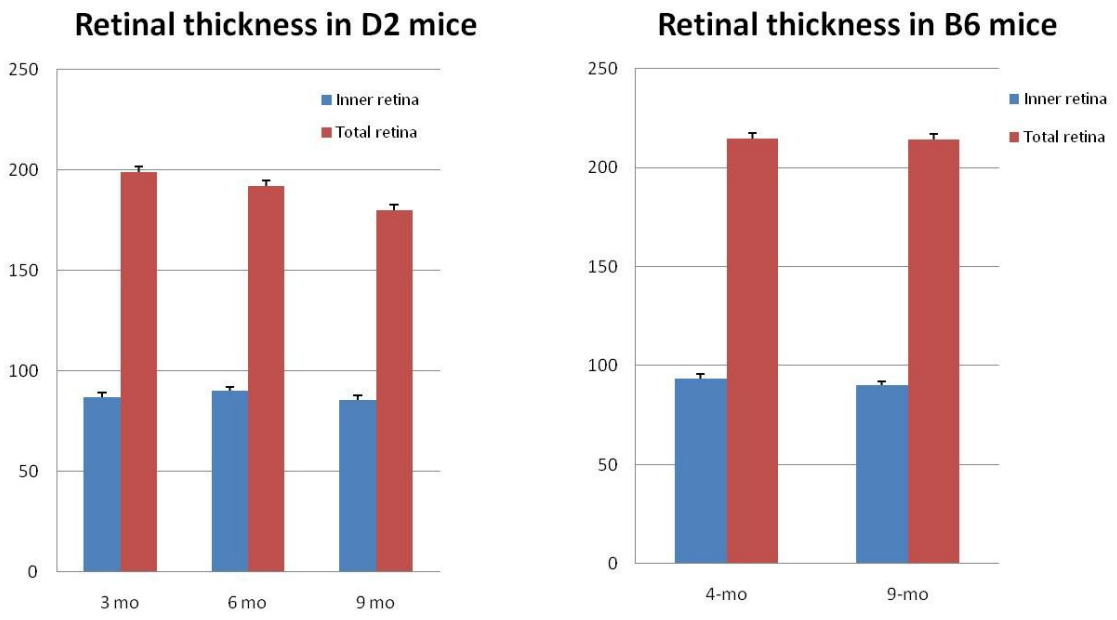

Figure 33. The retinal thickness in D2 compared with B6 of ages by SD-OCT.

Age (months)	Inner retina	Total retina	Outer retina	Inner/Outer
3	87.08 (SE 2.19)	198.83 (SE 2.75)	111.75 (SE 3.75)	0.44
6	90 (SE 0.43)	191.82 (SE 1.41)	101.82 (SE 1.31)	0.47
t-test	0.27	0.03	0.01	0.04

Table 6. Comparison of inner, outer, and total retinal thickness in D2 mice at 3 and 6 month old. Data represent the means in μm. SE: standard error.

Discussion: The retinal thickness decrease with age in D2 and does not change with age in B6. There should be some structure loss in D2 retina, and we believe the major factor of the retinal reduction is from the decrease of RNFL (ganglion cell layer) in D2 of old age.

www.manaraa.com

5.3 Comparison of IOP, RNFL, eye size between D2 and B6 mice

In section 1.3 (figure1), we provided a schematic drawing of the postnatal changes of IOP, eye size, and RNFL in D2 compared with B6. I summarize the measurement data of IOP (A), axial length (B), and retinal thickness by TD-OCT (C) and by SD-OCT (D) in D2 compared with B6. (Figure.34)

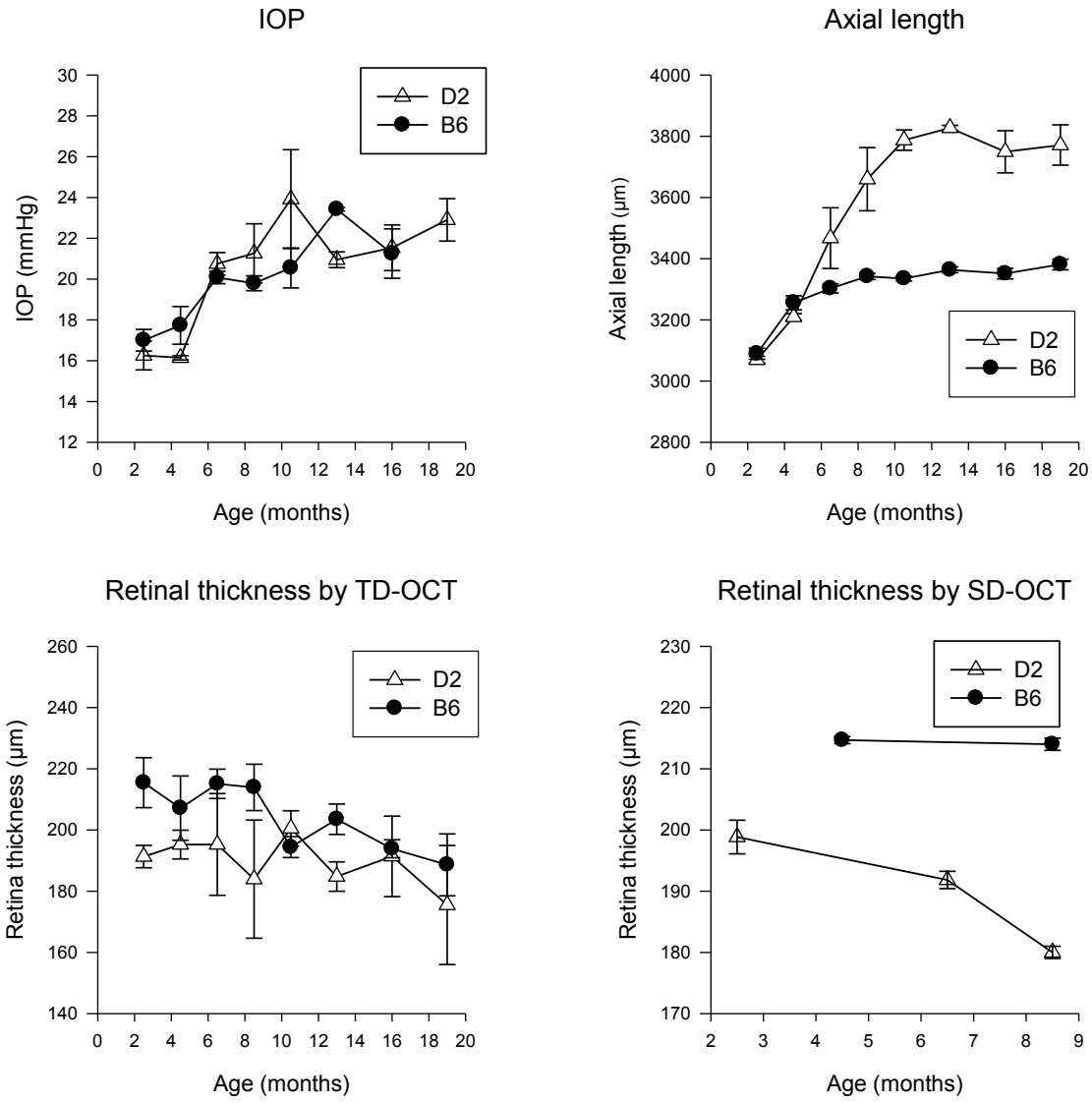

Figure 34. IOP, axial length, retinal thickness changes in D2 (n= 32 mice) compared with B6 (n= 36 mice). The data represent the mean ± SEM.

www.manaraa.com

Discussion: The reduction of retinal thickness in D2 compared with B6 may be due to both the IOP increase and eye size growth with age. The IOP causes the eye size exaggerated growth and make the retinal thickness thinner in D2. Please read more discussion in section 6.3.

5.4 Comparison of IOP between different body-tilt apparatus in D2 mice.

Previous results on IOP elevation associated with head-down body posture (Nagaraju, Saleh et al. 2007) by prototype body-tilt apparatus are shown in figure 8. I investigated sequential IOP changes using the goniometric body-tilt apparatus in D2 mice aged 5- 6 months (Figure 35 B, untreated group).

Discussion:

With this new apparatus, body posture can be easily changed between 60 degree head-down and 60 degree head-up systematically, while PERG can also be recorded simultaneously from both eyes by means of LED pattern stimulation (Figure 24). This approach can help understand the RGC function change during IOP modulation.

www.manaraa.com

5.5 Susceptibility of retinal ganglion cell function to IOP provocation in DBA/2J glaucoma.

D2 mice aged 5- 6 months (n=6) were anesthetized with ketamine-xylazine. IOP (Tonolab) and PERG amplitude were sequentially (10-15 minutes apart) measured in 5 conditions: horizontal (H1); 60 deg head-down (HD); horizontal (H2); 60 deg head-up (HU); horizontal (H3). PERG amplitude differences between HU and HD conditions were considered as posture-dependent changes [PDC= (HU-HD)/ mean (H1, H2)]. As shown in figure 35, the PERG amplitude with sequential body-tilt is shown in D2 in figure 35(A). Modulation of IOP with positive and negative body-tilt induced significant changes of PERG amplitude (PDC=0.69±0.24, P< 0.01). The experiment was repeated in 5- 6 month-old D2 after treatment with Timolol maleate, which reduced baseline IOP from 21.3 ±4.6 mm Hg to13.6 ± 2.6 mm Hg.

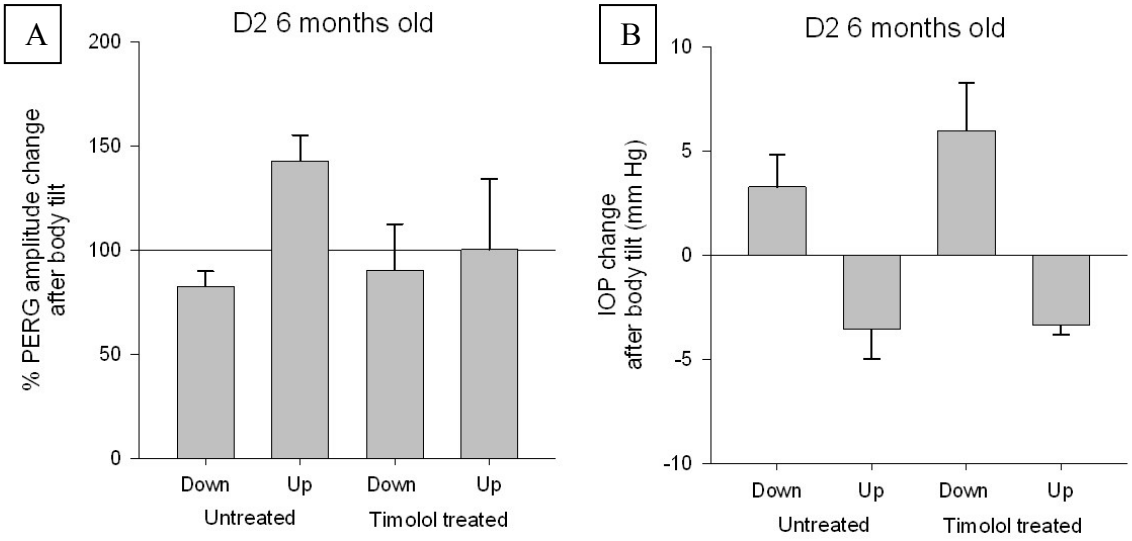

Figure.35. Posture-dependent PERG amplitude (left panel) and IOP (right panel) changes in 6 month-old D2 mice with and without timolol treatment. For each position group, symbols represent the mean ± SEM. (n=7 mice) (Nagaraju, M., M. Saleh, Vittorio Porciatti, IOVS, 2007, 48 (10): 4573-9)

www.manaraa.com

Discussion: After timolol treatment, body tilt no longer induced PERG changes (PDC=0.09±0.29, P>0.05). Results suggest that IOP-dependent modifiability of RGC function depend on baseline IOP (Chou, Lee et al. 2010). RGC function is reversible by IOP modulation. I summarize the relationship between RGC function and RGC structure with ages in D2. (Figure 36.)

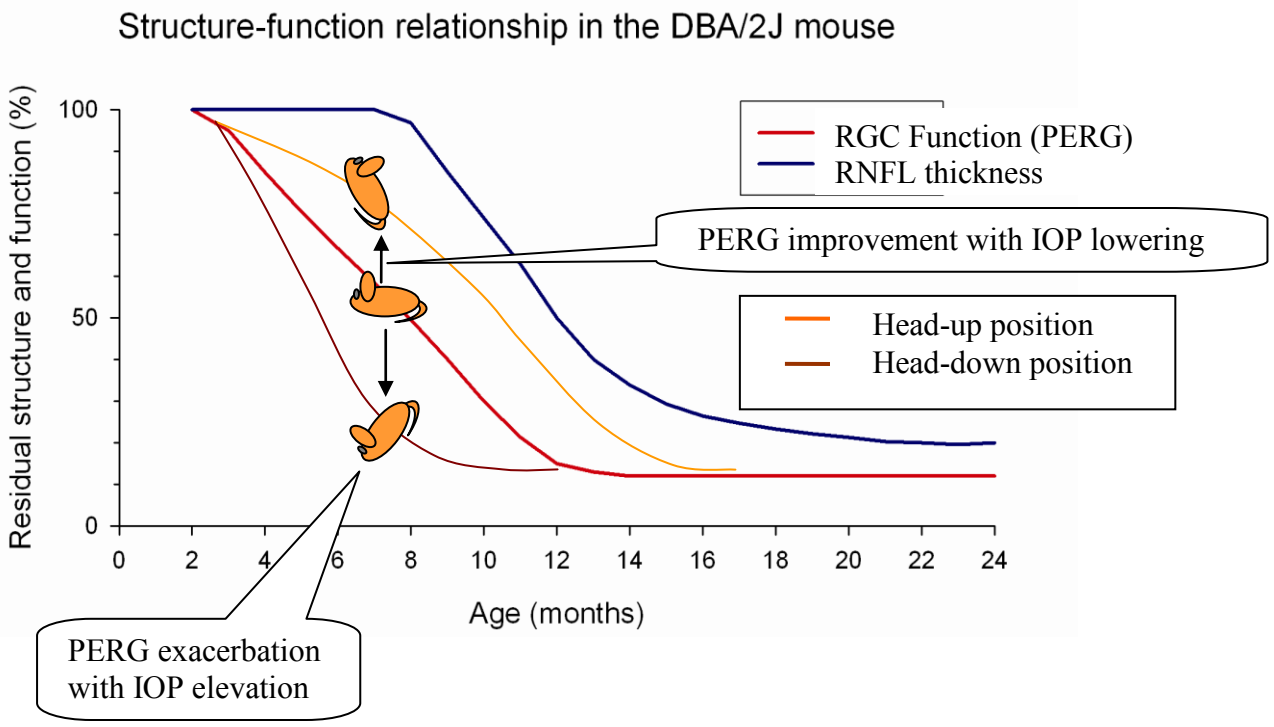

Figure.36. RGC dysfunctions and RNFL thickness decreases with age in D2 mice, PERG can be improved by body-tilt in a time window when RGC dysfunction is reversible by IOP changing.

www.manaraa.com

5.6 Different visual signal processing in the inner retina of B6, D2, and D2-Gpnmb+.

To characterize differences in retinal ganglion cell (RGC) function in mouse strains relevant to disease models, young (2-4 months of age) B6, D2, and D2-Gpnmb+ mice (n=6 for each group) were tested with the PERG in response to different contrasts and spatial frequencies. (Porciatti, Chou et al. 2010)

B6 vs D2 in contrast transfer function (figure 37 (A, C)):

There was a statistically significant strain × contrast level interaction in normalized PERG amplitude means (P=0.041, repeated measures analysis of variance; figure 37 (A)). Post-hoc t-tests revealed no significant differences between strains for contrast levels 0.2 through 0.6; however, there were significant differences between strains for contrast levels 0.8 (p=0.050) and 0.9 (P=0.029). Latency become significantly greater with decreasing contrast in B6 mice than in D2 mice (P=0.015, figure 37 (C)) while no interaction was observed (P=0.25). In summary, the form of PERG amplitude contrast function significantly differed between B6 and D2 strains at high-contrasts. PERG latency significantly differed between B6 and D2 strains but the form of the latency transfer function was similar.

D2 vs D2-Gpnmb+ in contrast transfer function (figure 37 (B, D)):

There was a statistically significant strain × contrast level interaction in normalized PERG amplitude means (P=0.031, repeated measures analysis of variance; see figure 37 (B)). Post-hoc t-tests revealed differences that were significant at contrast levels 0.2 (P=0.031), 0.3 (P=0.004), and 0.8 (P=0.015). There was a highly significant strain × contrast level interaction in normalized PERG latency means (P=0.001, repeated

www.manaraa.com

measures analysis of variance; see figure 37 (D)). Post-hoc t-tests on PERG latency could have been performed; however, orthogonal polynomial decomposition revealed that the interaction was due to differences in the slopes of the linear relation of PERG response to contrast between the two strains of mice (P=0.001). In summary, the form of PERG amplitude contrast function significantly differed between D2 and D2-Gpnmb+ strains at both low and high-contrasts. PERG latency significantly differed between the two strains but the form of the latency transfer function was similar.

B6 vs D2 in spatial transfer function (figure 38 (A, C)):

PERG amplitude: there was no statistically significant difference between strains (P=0.26) and strain × spatial frequency interaction (P=0.75, figure 39 (A)). PERG latency: there was no statistically significant difference between strains (P=0.37) and strain × spatial frequency interaction (P=0.55, figure 38 (C)). In summary, there were no significant differences in the form of both amplitude and latency spatial functions between B6 and D2 strains.

D2 vs D2-Gpnmb+ in spatial transfer function (figure 38 (B, D)):

There was a statistically significant difference in PERG amplitude strain × spatial frequency interaction (P=0.011, figure 38 (B)). Post-hoc t-tests revealed significant strain differences at 0.2 cycles/deg (P=0.032) and at 0.4 cycles/deg (P=0.028). There was a statistically significant difference in PERG latency between strains (p=0.001) but no strain × spatial frequency interaction (p=0.89, figure 38 (D)). In summary, there was a significant difference in the form of amplitude function between D2 and D2-Gpnmb+ for intermediate spatial frequencies. PERG latency significantly differed between the two strains but the form of the latency transfer function was similar.

www.manaraa.com

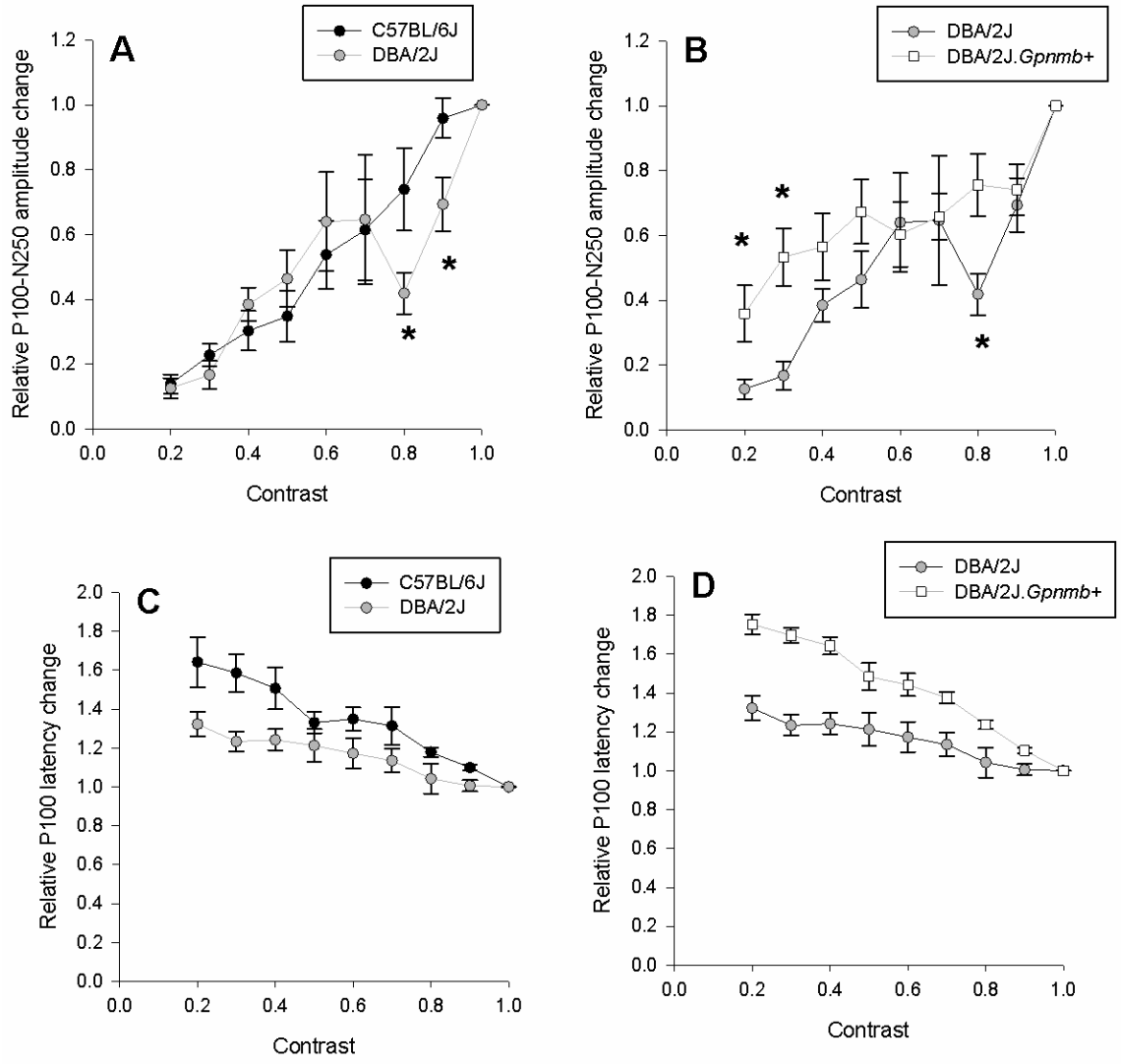

Figure 37. Contrast transfer functions of PERG amplitude (A,B) and PERG latency (C,D) for different mouse strains. All responses have been obtained at a fixed spatial frequency of 0.05 cycles/degree and temporal frequency of 1 Hz. In all panels, symbols represent the mean ±SEM (n=6 mice for each strain). Amplitude and latency changes have been expressed in relative units compared to the maximal PERG in response to gratings of 0.05 cycles/degree and contrast of 1.0 reversing at 1 Hz. (n= 6 in each strain) (Vittorio Porciatti, Tsung-Han Chou, Molecular vision. 2010, 31; 16: 2939-47.)

www.manaraa.com

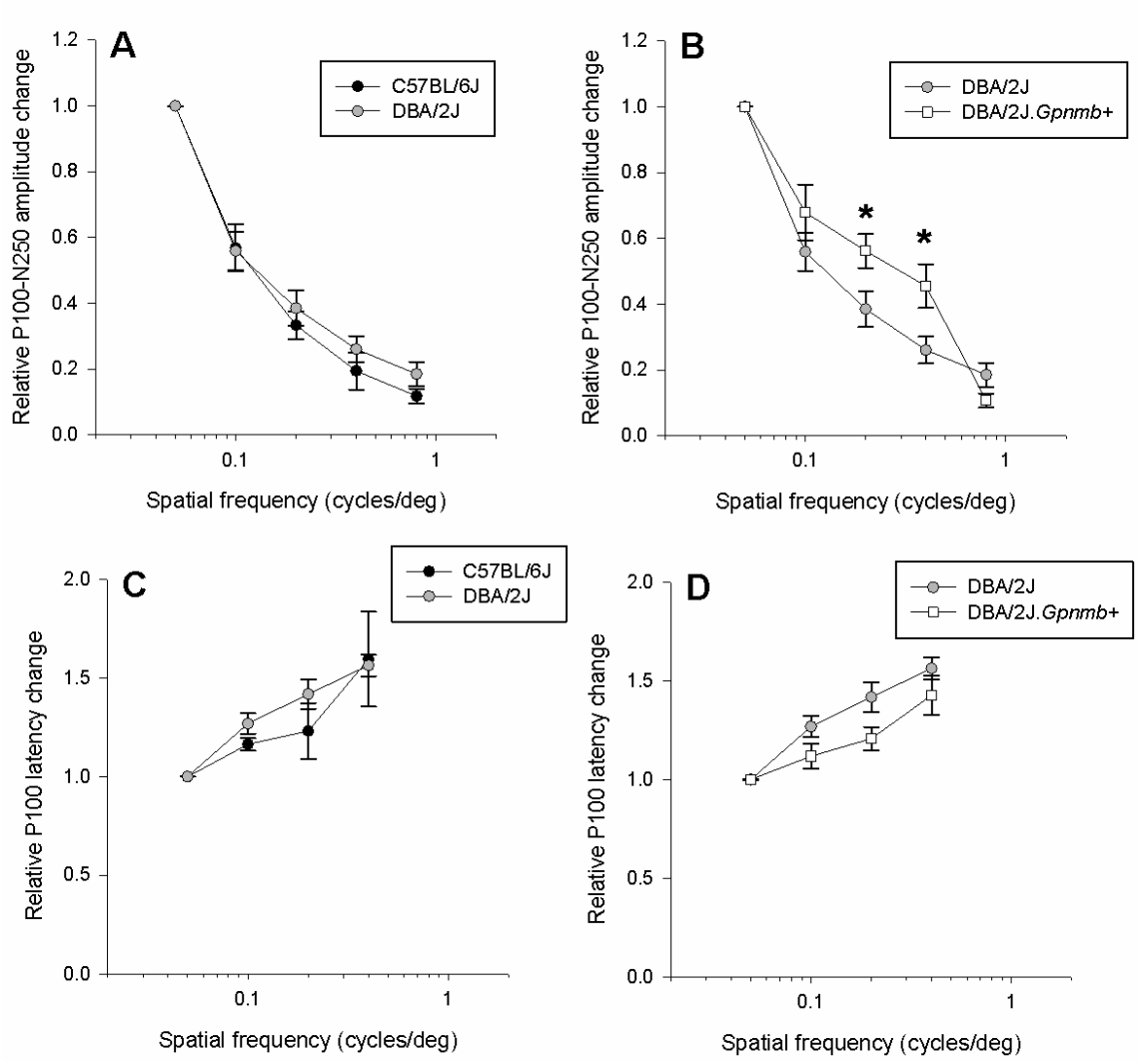

Figure 38. Spatial transfer functions of PERG amplitude (A, B) and PERG latency (C, D) for different mouse strains. All responses have been obtained at a fixed temporal frequency of 1 Hz and contrast of 1.0. In all panels, symbols represent the mean ±SEM. Amplitude and latency changes have been have been expressed in relative units compared to the maximal PERG in response to gratings of 0.05 cycles/degree and contrast of 1.0 reversing at 1 Hz. . (n= 6 in each strain) (Vittorio Porciatti, Tsung-Han Chou, Molecular vision. 2010, 31; 16: 2939-47.)

Discussion: Differences in contrast transfer functions of amplitude and latencies can be understood in terms of different mechanisms of contrast gain control in the PERG generators (Shapley and Victor 1978). PERG analysis shows that B6, D2, and D2-Gpnmb+ mice have comparable thresholds for contrast and spatial frequency.

www.manaraa.com

Suprathreshold spatial contrast processing, however, has different characteristics in these mouse strains, implying different synaptic circuitry in the inner retina. Please read more discussion in section 6.4.

5.7 Comparison of PERG stimulated by CRT monitor and LED pattern stimulation.

The LED stimulus subtended the same retinal area and had the same contrast as the CRT monitor, however its luminance was higher (500 cd/m^2 vs 50 cd/m^2). Figure 39 shows differences in PERG waveform between LED and CRT displays in B6 mice. The averaged amplitude of PERG was ~1.5 times with LED stimuli than CRT stimuli, but the latencies were similar for both pattern stimuli. Thus, response obtained with different stimuli can be compared after normalization. In future research, it will be more advantageous to use the LED pattern stimulus because i) yields response of larger amplitude (and signal to noise ratio), and allows to adjust the luminance by changing current, ii) will allow coupling to the goniometric holder, iii) it allows independent stimulation and analysis of PERGs recorded simultaneously from each eye.

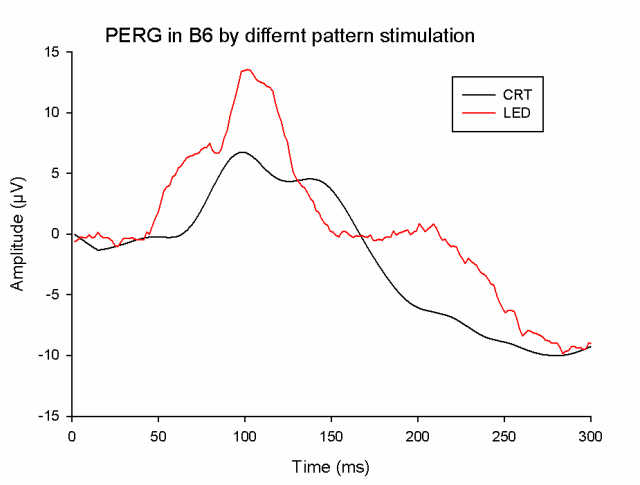

Figure.39. Representative in PERG of a C57BL/6J mouse stimulated by CRT and LED pattern stimulation.

www.manaraa.com

5.8 Adaptive changes in the PERG induced by flickering light in D2 compared with B6 and D2-Gpnmb+ mice.

PERGs were recorded in 32 mice 2-3 months old (C57BL/6J, n=9; DBA/2J, n=10; DBA/2J-Gpnmb+, n=13) with superimposed flicker at either 10 Hz (test) or 100 Hz (control - beyond temporal resolution of mouse cone ERG). Flicker-induced PERG amplitude/latency changes were calculated as differences between test and control. PERG stimuli were horizontal gratings of 0.05 cycles/degree and 100% contrast. Flicker stimuli were bright white LED, and were asynchronous with the PERG stimulus, in order not to generate any recordable flicker ERG. Baseline PERG amplitudes were similar in the three strains. Superimposition of 10 Hz flicker induced increases of PERG latency in all strains (B6, 15.4 ms (SE 2.7); D2, 22.3 ms (SE 3.8); DBA/2J.Gpnmb+, 5.9 ms (SE 3.1)). Strain differences in latency were significant (ANOVA, P=0.006). Flicker induced amplitude changes were unremarkable and not different among strains (ANOVA, P=0.25). PERG amplitude changes and latency changes are shown in figure 40.

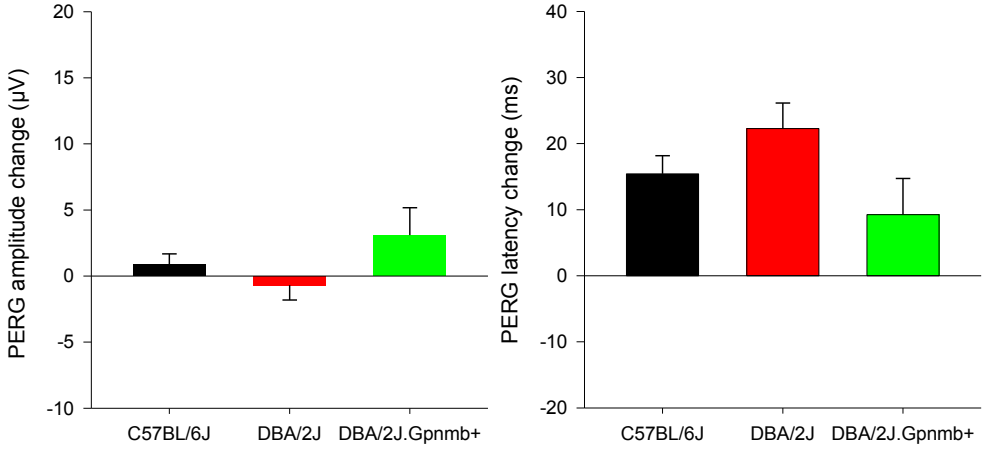

Figure 40. PERG amplitude and latency changes after 10 Hz flicker in B6 (n=9), D2 (n=10), and D2.wt (n= 16) mice. The data represent the mean ± SEM. (Vittorio Porciatti, Tsung-Han Chou, ARVO, 2011)

www.manaraa.com

Discussion: The flicker induces the metabolic challenge in retina. Our results indicate that these metabolic changes are associated with increased PERG latency at constant PERG amplitude. PERG latency changes are relatively greater in pre-glaucomatous DBA/2J mice, possibly indicating altered neurovascular/neurometabolic response in a strain prone to glaucoma.

5.9 Disclose the PERG cross-talk in mouse model.

PERGs and FERGs were recorded simultaneously from each eye in 18 mice (C57BL/6J, n=10; DBA/2J, n=4; DBA/1J, n=4) using corneal silver loops referenced to a subcutaneous needle on the back of the head. PERG stimuli were horizontal gratings of 0.05 cycles/degree and 100% contrast. Photopic FERG stimuli were strobe flashes superimposed on and adapting background. Pattern stimuli were delivered either monocularly (with the non-stimulated eye occluded) or binocularly as shown in Figure 41. In some experiments, TTX was injected in one eye and saline in the contralateral eye. (Figure 43)

Monocular PERGs were recordable from both the stimulated and the non-stimulated eye with similar amplitudes. (Figure 42) Under binocular stimulation, the PERG amplitude was 1.7 times (SE 0.18) larger than the monocular amplitude ($p<0.01$). TTX injected in the stimulated eye abolished the PERG in both eyes, whereas TTX injected in the non-stimulated eye had no effect on PERG of both eyes. (Figure 44) Monocular FERGs were recordable from the stimulated eye only. Binocular and monocular FERGs had the same amplitudes.

www.manaraa.com

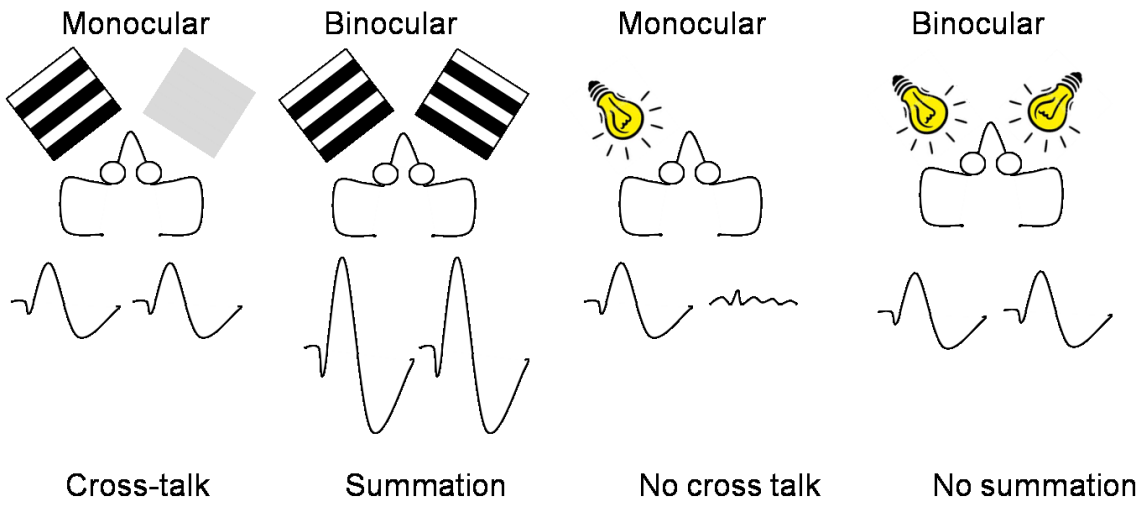

Figure.41. Representative in PERG and FERG of a C57BL/6J mouse stimulated by monocular or binocular pattern and flash stimulation.

www.manaraa.com

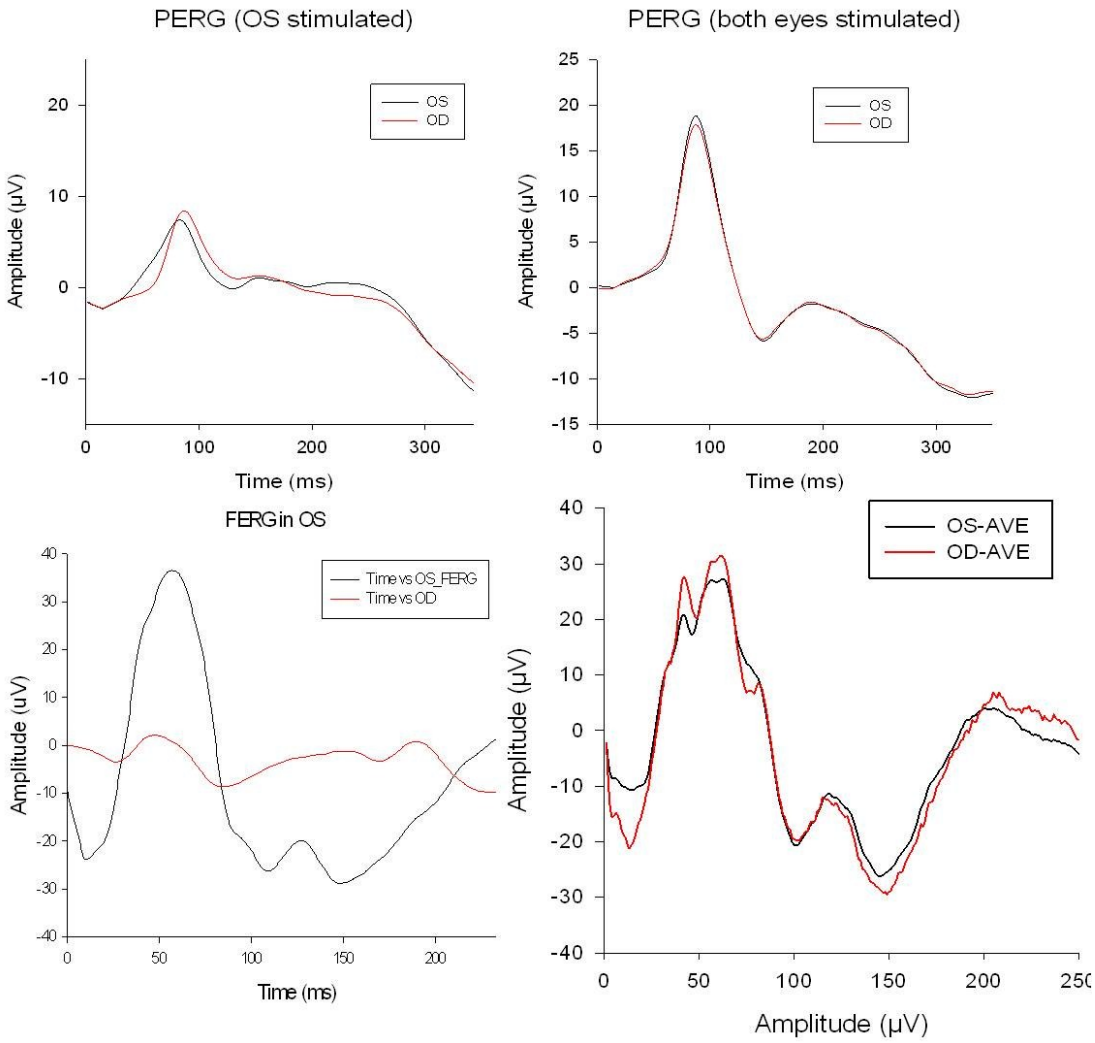

Figure.42. Data of PERG and FERG of a C57BL/6J mouse stimulated by monocular or binocular pattern and flash stimulation.

www.manaraa.com

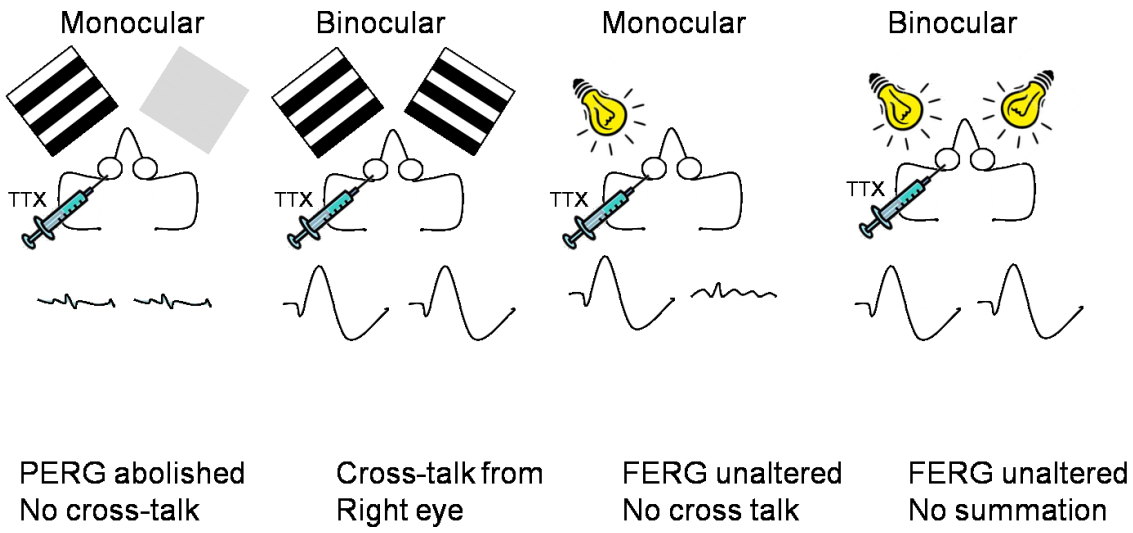

Figure.43. Representative in PERG and FERG of a C57BL/6J mouse with TTX injected in left eye stimulated by monocular or binocular pattern and flash stimulation.

www.manaraa.com

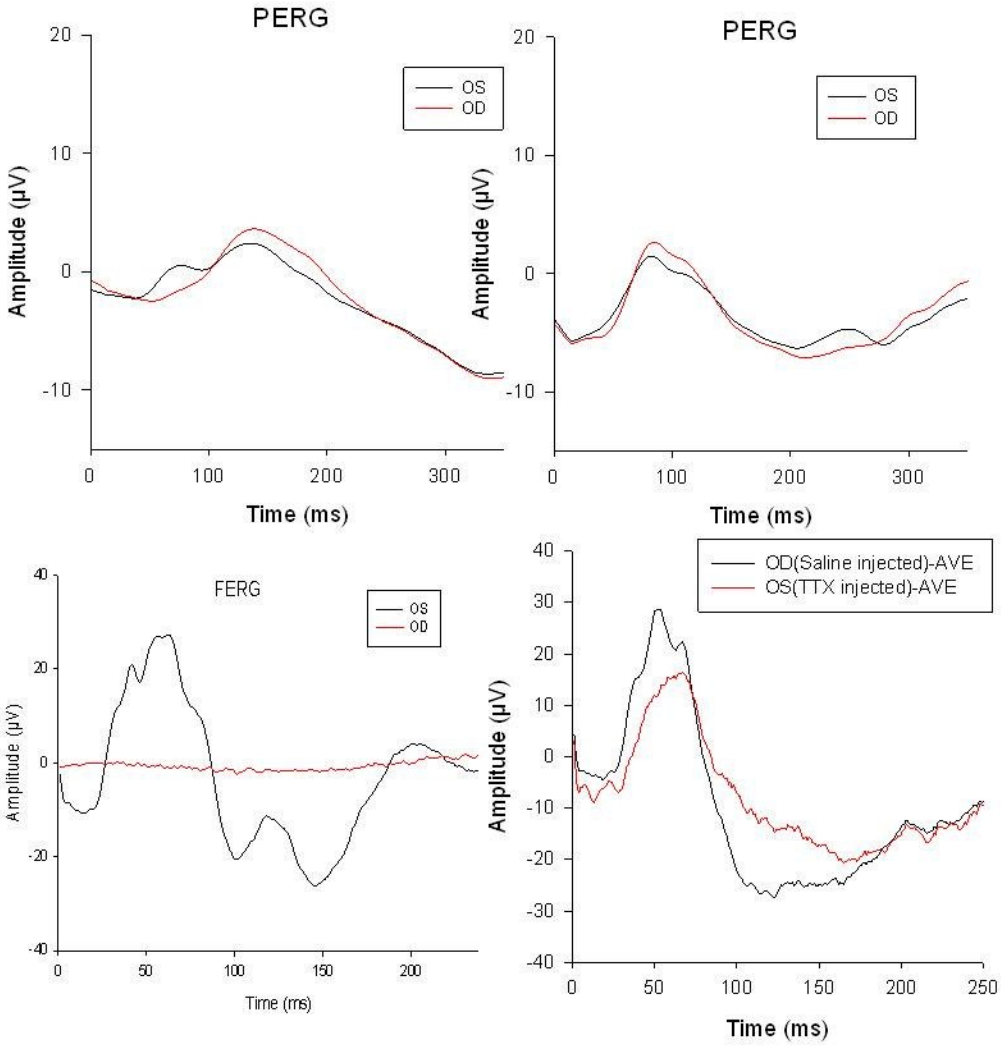

Figure.44. Data of PERG and FERG of a C57BL/6J mouse with TTX injected in left eye stimulated by monocular or binocular pattern and flash stimulation.

Discussion: We summarize and normalize the PERG amplitude in monocular and binocular pattern stimulation in figure 45. We found the cross-talk effect doubles the PERG amplitude during binocular pattern stimulation. We propose a PERG dipole mode that can fit with this data compared the FERG dipole mode. (Figure 46) The blue circle represents the eye ball and the red line represents the iso-potential line of dipole. The

www.manaraa.com

FERG dipole is parallel to optic axis but the PERG dipole is perpendicular to optic axis. This model is well fit with the PERG and FERG data we have.

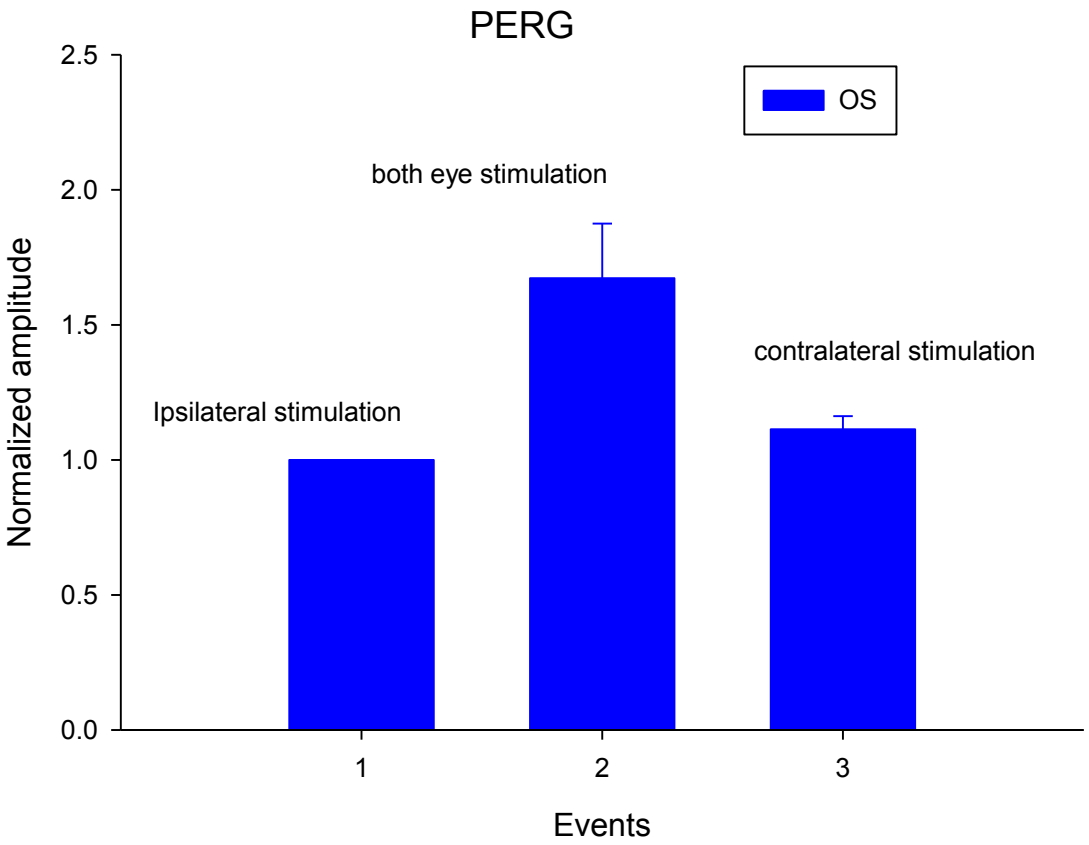

Figure.45. Summary data of PERG of three strains of mice (D1, D2 and B6 mice) stimulated by monocular or binocular pattern stimulation. (n=14)

www.manaraa.com

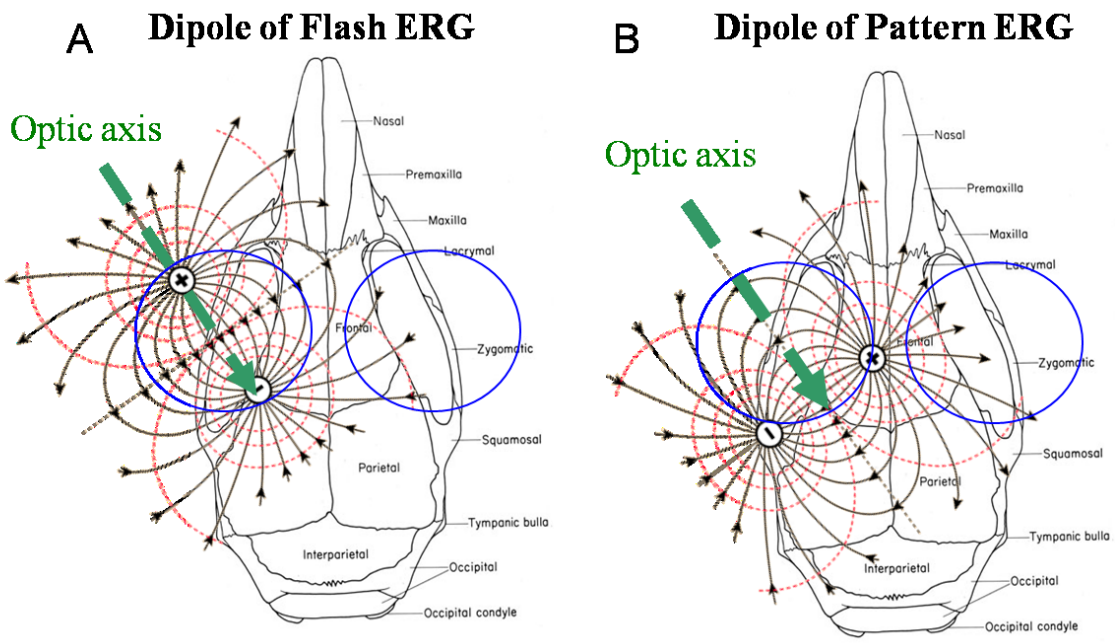

Figure.46. The dipole of FERG (A) and the dipole of PERG (B). The blue circle represent the eye ball and the red line represent the iso-potential line of dipole.

5.10 PERG cross-talk elimination by means of de-synchronized LED pattern stimuli and acquisition/analysis of de-convolved retinal signals.

After we apply the two specific sweep numbers and send triggering signal to each LED tablet, the right eye was covered and the left eye was stimulated, the outcome is shown in figure 47. The cross-talk is eliminated, so there is no PERG signal in un-stimulated right eye.

www.manaraa.com

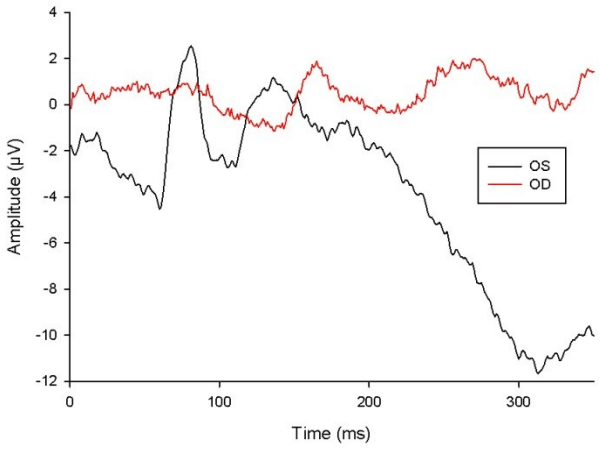

Figure.47. Representative in PERG in left eye of a C57BL/6J mouse stimulated by LED pattern stimulation and covered by black tap in the right eye.

www.manaraa.com

Chapter 6. Discussion

6.1 The natural history of structural-functional changes in D2 mice.

Previous publications of our group have been shown that young (2–3 month-old) DBA/2J mice have normal IOP, normal PERG, and normal histological appearance of RGCs and optic nerves. Glaucoma damage in the optic nerve is apparent in about 50% of eyes by 10–11 months of age, and in about 90% of eyes by 18 months.(Nagaraju, Saleh et al. 2007) At 8 months of age, when the PERG amplitude has lost about 50% of its baseline value (2 month-old) level,(Saleh, Nagaraju et al. 2007) the optic nerves are histologically intact. Between10 and 11 months of age, when only 50% of the optic nerves show signs of degeneration, the PERG amplitude is at or close to the noise level (about 85% smaller than the baseline level) in 100% of mice.(Nagaraju, Saleh et al. 2007) The light-adapted flash-ERG displays only minor changes,(Libby, Porciatti et al. 2006; Nagaraju, Saleh et al. 2007), and the outer retina is histologically intact.(Jakobs, Libby et al. 2005) (Howell, Libby et al. 2007) Altogether, these results suggest that in DBA/2J mice inner retina dysfunction precedes anatomical axon loss. On average, the IOP increases from 15 mm Hg to 20 mm Hg between 2 and 6 months, after 6 months the IOP displays a steeper increase and tends to level off by 11 months at a value of about 30 mm Hg.(Nagaraju, Saleh et al. 2007)

This physiopatyhological sequence does not seem limited to the D2 glaucoma model. Recently, our group has shown in a mouse model of multiple sclerosis that RGC undergo a long stage of progressive dysfunction preceding death and associate with motor impairment (Ding, Algecirs et al. 2010).

www.manaraa.com

Evaluation of PERG changes in response to artificial IOP modulation may represent a powerful tool to noninvasively assess RGC susceptibility to IOP insult in genetically distinct mouse models of glaucoma.(Nagaraju, Saleh et al. 2007)

6.2 The relationship between intraocular pressure (IOP) and loss of retinal ganglion cells.

In glaucoma, IOP represents the most important risk factor. Still, the role of IOP on RGC dysfunction is not well understood. I addressed this issue by modulating IOP with changes of body posture and concurrently recording the PERG, a surrogate measure of RGC function. Previous results of our group (Nagaraju, Saleh et al. 2007) have shown the head-down/head-up body tilt induces systematic positive/negative changes of about ± 5 mm Hg, respectively, which are rather independent of age and strain. Posture-induced IOP elevation is closely related to increase of the episcleral venous pressure (EVP) as experimentally demonstrated in human(Krieglstein, Waller et al. 1978; Friberg, Sanborn et al. 1987) as well as mouse.(Aihara, Lindsey et al. 2003) Previous data of our group showed that the time constant of IOP elevation is about 5 minutes.(Nagaraju, Saleh et al. 2007) The gradual rise of IOP probably reflects the dynamic interaction between the rate of aqueous humor formation and the establishment of a new equilibrium IOP to compensate for the increase in afterload to aqueous outflow.

The study shows that head-down posture induces IOP elevation associated with reversible, age-dependent reductions of PERG amplitude in DBA/2J mice. In mice of all ages, posture-induced IOP elevation did not cause FERG changes, thereby excluding a generalized retinal effect and indicating that PERG changes reflect inner retina

www.manaraa.com

dysfunction. Altogether, these results indicate that IOP initiates or amplifies pathogenetic processes of RGCs resulting in progressive reduction of electrical responsiveness. An abnormal PERG signal in older mice may be improved with either mannitol or head-up-induced IOP lowering. These results suggest that reduction of RGC electrical responsiveness in older D2 mice is at least in part reversible by lowering IOP. The implication of this is that RGC undergo a stage of IOP-dependent reversible dysfunction before irreversible cell death.

Susceptibility of RGC to IOP fluctuation may depend on the baseline IOP. As shown in sections 2.4 and 2.5. The same IOP fluctuation (induced by head-down/head-up posture) that causes PERG changes in 6 months old D2 mice, is no longer effective in the same mice after IOP-lowering treatment with Timolol maleate.

6.3 The relationship between eye size, IOP and loss of retinal ganglion cells.

In this study we used a custom-build, whole-eye OCT system to longitudinally investigate postnatal changes of eye size in the well known DBA/2J (D2) mouse model of glaucoma, which is characterized by spontaneous, long standing IOP elevation. We focused on the changes of axial distances in D2 mice and compared them with corresponding changes measured in the C57BL/6J (B6) mouse, a common control strain. We also tried to better understand the role of IOP elevation on eye size in D2 mice. Altogether, the present results show clear, progressive postnatal changes of all eye components in both B6 and D2 mice between 2 and 20 months of age. While the axial length was similar in the two strains in the age range 2-5 months, it increased relatively more in D2 than in B6 after 6 months of age and plateaued after 10-11 months. As it is

www.manaraa.com

known that in D2 mice IOP becomes elevated after 6 months of age and remains elevated thereafter, it is conceivable that exaggerated eye growth may be related to IOP elevation/exposure. Another finding in support of the view that IOP plays a role in abnormal eye growth in D2 mice is the exaggerated growth of the anterior chamber depth compared to axial length. At about 8 months of age, there is a sharp growth of the anterior chamber depth which is associated to corresponding reduction of the vitreous chamber depth. We interpret this finding as related to the fact that at 8 months the IOP is known to substantially increase in D2 mice.(Libby, Anderson et al. 2005; Zhou, Li et al. 2005; Scholz, Buder et al. 2008) This may result in a pressure gradient between the AC and VC that tends to dislocate the lens posteriorly. At later ages of 10 months, the pressure gradient between AC and VC may be no longer present, so that the lens tends to be pulled back in the original, although unstable, position. Assuming that IOP is the primary cause of abnormal eye growth, it should be taken into account that the time course of IOP changes may not precisely match that of axial length changes due to the unknown role of compliance of eye tissues to eye pressure. In addition, there may be genetic factors that influence the rate/duration of eye growth.(Zhou and Williams 1999) In summary, our data support the idea that elevated IOP plays a role in the exaggerated growth of eye size in D2 mice compared to B6. However, a precise relationship between IOP and eye size cannot be firmly established because of a high degree of covariance between age, axial length and IOP as well as the unknown role of tissue compliance on the mutual relationships among these variables.

www.manaraa.com

The values of the radius of curvature of B6 mice and its increase with age are consistent with previous results obtained using frozen sections (Remtulla and Hallett 1985) and keratometry (Schmucker and Schaeffel 2004; Zhou, Shen et al. 2008)Measurements from histological sections seem to provide larger values(Smith, Korb et al. 2002), probably due to histological preparation artifacts. Here we find that there are only small differences between the anterior and posterior corneal radii of B6 mice. This result is expected since the mouse cornea is thin and approximately uniform in thickness. Young D2 mice have a flatter cornea than B6 mice, whereas at older ages the reverse seems to be true. The larger variability in the anterior corneal curvature of D2 mice compared to B6 seems due to the fact that the D2 cornea may becomes irregular in shape. In older D2 mice, the cornea becomes steeper (radius of curvature becomes smaller). The steepening occurs approximately in the same age range as the increase in corneal thickness, plateau in the axial eye length, increase of anterior chamber depth, and decrease of the vitreous chamber depth. Corneal steepening associated with increased axial length in older D2 mice suggests development of myopia. All these concurrent phenomena may be associated with changes of the IOP. Overall, the results show that there are baseline differences between D2 and B6 mice as well as differences in the age-dependence of the corneal shape.

6.4 Genetic background differences between B6, D2, D2-Gpnmb+.

An important component of glaucoma studies is the choice of suitable non-glaucomatous controls. C57BL/6J (B6) is the most common control strains. Our DBA/2J (D2) model has two mutated genes, tyrosinase-related protein 1 (Tyrp1) and glycoprotein non-

www.manaraa.com

metastatic melanoma protein B (Gpnmb), causing iris disease and intraocular pressure (IOP) elevation. The DBA/2J.Gpnmb(+) strain is the wild type for the Gpnmb mutation and does not develop IOP elevation and glaucoma. We systematically investigated the baseline characteristics of RGC function in these three strains. Our results show that the PERGs of B6, D2, and D2-Gpnmb+ displayed many similarities but some notable differences. The waveform of PERG obtained under conditions that maximize the signal (spatial frequency 0.05 cycles/deg, max contrast 1.0) (Porciatti, Saleh et al. 2007) differed between B6 and D2 strains. Namely, in D2 strains the PERG had a substantially longer latency (about 20 ms) compared to B6. No obvious differences in amplitude and latency between D2 and D2-Gpnmb+ strains were observable. The major difference among the three mouse strains was the way PERG amplitude and latency changed as a function of spatial contrast (contrast transfer function). In B6 mice, the contrast transfer function of PERG amplitude was linear, whereas in D2 there was a clear notch in PERG amplitude at 0.8 contrast. In addition, the slope of latency increase associated with decreasing contrast was shallower in D2 compared to B6. The amplitude notch at 0.8 contrast occurring in D2 mice was not present in D2-Gpnmb+ mice, which had a more robust response at lower contrasts. In addition, the slope of latency increase associated with decreasing contrast was shallower in D2 compared to D2-Gpnmb+ mice. Amplitude notches at high contrast have been reported before for the VEP, (Nakayama and Mackeben 1982; Nakayama and Mackeben 1982; Strasburger, Scheidler et al. 1988) but their origin is still matter of speculation. One possibility is that the notch originates from interaction between different underlying neural generators that respond with different latency, resulting in amplitude cancellation. Overall, differences in contrast transfer

www.manaraa.com

functions of amplitude and latencies can be understood in terms of different mechanisms of contrast gain control in the PERG generators (Shapley and Victor 1978). The spatial frequency function of PERG amplitude (obtained at max contrast) was similar in B6 and D2 mice but displayed subtle differences between D2 and D2-Gpnmb+. The spatial frequency threshold (acuity) was about 0.8 cycles/degree in all strains. RGC population in DBA/2J mice is reported to be significantly larger (63,351 ±1208) than that of C57BL/6J (54,630 ±874) (Williams, Strom et al. 1996). This may have a counterpart in a different inner retina circuitry between B6 and D2 mice resulting in different spatial contrast functions. Differences in the PERG spatial contrast function between D2 and D2-Gpnmb+ mice, however, are likely to result from factors other than RGC number.

In summary, PERG analysis shows that B6, D2, and D2-Gpnmb+ mice have comparable thresholds for contrast and spatial frequency. Suprathreshold spatial contrast processing, however, has different characteristics in these mouse strains, implying different synaptic circuitry in the inner retina. It remains to be established whether these differences have a counterpart in susceptibility to RGC to insult of disease.

6.5 PERG cross-talk elimination by means of de-synchronized LED pattern stimuli and acquisition/analysis of de-convolved retinal signals.

There is tremendous need for simultaneously and independently PERG measurement in both eyes in order to compare the experimental and control eyes of the same mouse under the same general conditions (primarily the level of anesthesia). As interocular PERG cross-talk prevented ordinary binocular recording, we designed two independent trigger signals for the two pattern LED display. This resulted in unsynchronized stimulation

www.manaraa.com

frequency that allowed acquisition of PERG signal independently in the two eyes, thus overcoming the problem of inter-ocular cross-talk. I published and described the phenomena of cross-talk during PERG both eyes recording and tried to disclose why this phenomenon happened in the mouse model. (Chou, et al., ARVO 2011) PERG and FERG generate different bioelectric fields in the mouse. The FERG signal does not propagate to the non-stimulated eye as expected, whereas the PERG displays obvious cross-talk, including summation under binocular stimulation. Results were relevant for better understanding of PERG generators and had technical implications for binocular recordings. I combined this PERG recording method with goniometry for body-tilt (induced IOP changes) and LED flicker (induced metabolic needs) in order to probe the susceptibility of RGC dysfunction. This tool can help other scientist to investigate the PERG differentness in different strains of mice under retinal metabolic challenge.

www.manaraa.com

Chapter 7. Conclusion

We have developed a better and more powerful tool for non-invasive and serial monitoring of the RGC function in-vivo with PERG. We are able to record PERG in both eyes simultaneously and independently by eliminating the cross-talk. The development of LED pattern stimulation makes PERG measurable during mouse body-tilt. We have applied this technology to a well established mouse model of glaucoma and also monitored age-related changes in eye size, IOP and RGC loss either by histology in-vitro or by spectral domain OCT.(Ruggeri, Wehbe et al. 2007) We were able to describe the time course of all the relevant variables by the custom-made and commercial tool. Posture-induced IOP elevation/lowering by means of customized goniometric holder provided key information on susceptibility of retinal ganglion cells to IOP insult. We characterized the dynamics of IOP changes in response to change with body posture and age in D2 mice. Induced IOP changes have an age-dependent impact on RGC function of D2 mice.(Nagaraju, Saleh et al. 2007) The PERG signal is susceptible to head-down body tilt in D2 mice 5- 6 month old but not in D2 mice 2-3 month old. Susceptibility of PERG signal in D2 mice 5- 6 months old is abolished after IOP-lowering treatment with Timolol maleate, suggesting that treatment improves RGC resistance to IOP insult. This might provide a neurophysiological explanation for the protective role of IOP-lowering treatment on age-related RGC loss in D2 mice (Matsuhara, 2006, Schuettauf, 2002). The head-down approach might provide a means to predict the benefits of IOP-lowering or other neuroprotective treatments based on modifiability of PERG signal. RGCs rescue and glaucoma prevention might be achieved by reversing RGC dysfunction before cell death.

www.manaraa.com

Altogether, the combination of these measures represents a powerful tool for glaucoma research using mouse models and has important implications for human glaucoma. A further step would be to establish whether chronic IOP-lowering treatment alters the time course of PERG reduction in parallel with that of RGC death. Such a determination would represent strong proof that PERG alteration represents an early predictor of impending cell death.

www.manaraa.com

References

Aihara, M., J. D. Lindsey, et al. (2003). "Episcleral venous pressure of mouse eye and effect of body position." Current Eye Research **27**(6): 355-362.

Anderson, M. G., R. T. Libby, et al. (2005). "High-dose radiation with bone marrow transfer prevents neurodegeneration in an inherited glaucoma." Proceedings of the National Academy of Sciences of the United States of America **102**(12): 4566-4571.

Anderson, M. G., R. S. Smith, et al. (2002). "Mutations in genes encoding melanosomal proteins cause pigmentary glaucoma in DBA/2J mice." Nature Genetics **30**(1): 81-85.

Bach, M., M. Hawlina, et al. (2000). "Standard for pattern electroretinography. International Society for Clinical Electrophysiology of Vision." Documenta Ophthalmologica **101**(1): 11-18.

Bill, A. and G. O. Sperber (1990). "Aspects of oxygen and glucose consumption in the retina: effects of high intraocular pressure and light." Graefes Arch Clin Exp Ophthalmol **228**(2): 124-127.

Bill, A. and G. O. Sperber (1990). "Control of retinal and choroidal blood flow." Eye (Lond) **4 (Pt 2)**: 319-325.

Brown, A. S. (2005). "In vivo assessment of postnatal murine ocular development by ultrasound biomicroscopy (vol 30, pg 45, 2005)." Current Eye Research **30**(5): 415-415.

Calkins, D. J., P. J. Horner, et al. (2008). "Manganese-enhanced MRI of the DBA/2J mouse model of hereditary glaucoma." Investigative Ophthalmology & Visual Science **49**(11): 5083-5088.

Chang, B., R. S. Smith, et al. (1999). "Interacting loci cause severe iris atrophy and glaucoma in DBA/2J mice." Nature Genetics **21**(4): 405-409.

Chou, T.-H., D. Borja, et al. (2009). "Postnatal growth of eye size in DBA/2J mice compared with C57BL/6J mice: In-vivo analysis with OCT." Investigative Ophthalmology & Visual Science **50**(5): 2776-.

Chou, T.-H., W. Lee, et al. (2010). "Susceptibility of retinal ganglion cell function to acute IOP modulation in DBA/2J glaucoma." ARVO Meeting Abstracts **51**(5): 5484.

Danias (2004). "Quantitative analysis of retinal ganglion cell (RGC) loss in aging DBA/2NNia glaucomatous mice: Comparison with RGC loss in aging C57/BL6

www.manaraa.com

mice (vol 44, pg 5151, 2003)." Investigative Ophthalmology & Visual Science **45**(3): 806-806.

Danias, J., A. I. Kontiola, et al. (2003). "Method for the noninvasive measurement of intraocular pressure in mice." Investigative Ophthalmology & Visual Science **44**(3): 1138-1141.

Ding, D., M. Algecirs, et al. (2010). "Retinal Deimination and Functional Status in a Mice Model of Multiple Sclerosis." ARVO Meeting Abstracts **51**(5): 5995.

Falsini, B., C. E. Riva, et al. (2002). "Flicker-evoked changes in human optic nerve blood flow: relationship with retinal neural activity." Investigative Ophthalmology & Visual Science **43**(7): 2309-2316.

Falsini, B., C. E. Riva, et al. (2002). "Relationship of blood flow changes of the human optic nerve with neural retinal activity: a new approach to the study of neuro-ophthalmic disorders." Klin Monbl Augenheilkd **219**(4): 296-298.

Filippopoulos, T., J. Danias, et al. (2006). "Topographic and morphologic analyses of retinal ganglion cell loss in old DBA/2NNia mice." Investigative Ophthalmology & Visual Science **47**(5): 1968-1974.

Friberg, T. R., G. Sanborn, et al. (1987). "Intraocular and episcleral venous pressure increase during inverted posture." American Journal of Ophthalmology **103**(4): 523-526.

Hammer, M., W. Vilser, et al. (2011). "Retinal venous oxygen saturation increases by flicker light stimulation." Investigative Ophthalmology & Visual Science **52**(1): 274-277.

Hernandez, M. R. (2000). "The optic nerve head in glaucoma: Role of astrocytes in tissue remodeling." Progress in Retinal and Eye Research **19**(3): 297-321.

Howell, G. R., R. T. Libby, et al. (2008). "Mouse genetic models: an ideal system for understanding glaucomatous neurodegeneration and neuroprotection." Prog Brain Res **173**: 303-321.

Howell, G. R., R. T. Libby, et al. (2007). "Absence of glaucoma in DBA/2J mice homozygous for wild-type versions of Gpnmb and Tyrp1." Bmc Genetics **8**: -.

Jakobs, T. C., R. T. Libby, et al. (2005). "Retinal ganglion cell degeneration is topological but not cell type specific in DBA/2J mice." Journal of Cell Biology **171**(2): 313-325.

www.manaraa.com

John, S. W. M. (2005). "Mechanistic insights into glaucoma provided by experimental genetics - The Cogan lecture." Investigative Ophthalmology & Visual Science **46**(8): 2650-2661.

Jorge E Bohórquez, Ö. Özdmar. (2010). "Multiple 80Hz AM-ASSRs and transient responses: Two-tone interaction explored by deconvolution." the American Auditory Society Annual Meeting.

Kass, M. A., D. K. Heuer, et al. (2002). "The Ocular Hypertension Treatment Study - A randomized trial determines that topical ocular hypotensive medication delays or prevents the onset of primary open-angle glaucoma." Archives of Ophthalmology **120**(6): 701-713.

Krieglstein, G. K., W. K. Waller, et al. (1978). "The vascular basis of the positional influence of the intraocular pressure." Albrecht Von Graefes Arch Klin Exp Ophthalmol **206**(2): 99-106.

Libby, R. T., M. G. Anderson, et al. (2005). "Inherited glaucoma in DBA/2J mice: Pertinent disease features for studying the neurodegeneration." Visual Neuroscience **22**(5): 637-648.

Libby, R. T., V. Porciatti, et al. (2006). "PERG analysis detects physiological dysfunction prior to ganglion cell loss in the DBA/2J mouse glaucoma model." Investigative Ophthalmology & Visual Science **47**(5): 4005-.

Maffei, L. and A. Fiorentini (1981). "Electroretinographic responses to alternating gratings before and after section of the optic-nerve." Science **211**(4485): 953-955.

Manns, F., O. P. Kocaoglu, et al. (2009). "Two-dimensional biometry of the whole mouse eye using optical coherence tomography." Investigative Ophthalmology & Visual Science **50**(5): 5670-.

Michelson, A. A. (1995). Studies in Optics. New York, Dover Publications.

Nagaraju, M., M. Saleh, et al. (2007). "IOP-dependent retinal ganglion cell dysfunction in glaucomatous DBA/2J mice." Investigative Ophthalmology & Visual Science **48**(10): 4573-4579.

Nagaraju, M., M. Saleh, et al. (2007). "Postural changes of IOP and pattern ERG in DBA/2J mice." Investigative Ophthalmology & Visual Science **48**(5): 211-.

Nakayama, K. and M. Mackeben (1982). "Steady state visual evoked potentials in the alert primate." Vision Research **22**(10): 1261-1271.

Nakayama, K. and M. Mackeben (1982). "Steady state visual evoked potentials in the alert primate." Vision Res **22**(10): 1261-1271.

www.manaraa.com

Pease, M. E., J. C. Hammond, et al. (2006). "Manometric calibration and comparison of TonoLab and TonoPen tonometers in rats with experimental glaucoma and in normal mice." Journal of Glaucoma **15**(6): 512-519.

Porciatti, V. (2007). "The mouse pattern electroretinogram." Documenta Ophthalmologica **115**(3): 145-153.

Porciatti, V., T. H. Chou, et al. (2010). "C57BL/6J, DBA/2J, and DBA/2J.Gpnmb mice have different visual signal processing in the inner retina." Molecular Vision **16**: 2939-2947.

Porciatti, V. and M. Nagaraju (2010). "Head-up tilt lowers IOP and improves RGC dysfunction in glaucomatous DBA/2J mice." Experimental Eye Research **90**(3): 452-460.

Porciatti, V., M. Nagaraju, et al. (2008). "Dynamics of IOP changes with head-up and head-down tilt in DBA/2J mice." Investigative Ophthalmology & Visual Science **49**(5): 1047-.

Porciatti, V., T. Pizzorusso, et al. (1996). "The visual response of retinal ganglion cells is not altered by optic nerve transection in transgenic mice overexpressing Bcl-2." Proceedings of the National Academy of Sciences of the United States of America **93**(25): 14955-14959.

Porciatti, V., M. Saleh, et al. (2007). "The pattern electroretinogram as a tool to monitor progressive retinal ganglion cell dysfunction in the DBA/2J mouse model of glaucoma." Investigative Ophthalmology & Visual Science **48**(2): 745-751.

Porciatti, V., M. Saleh, et al. (2007). "The pattern electroretinogram as a tool to monitor progressive retinal ganglion cell dysfunction in the DBA/2J mouse model of glaucoma." Investigative Ophthalmology & Visual Science **48**(2): 745-751.

Puk, O., C. Dalke, et al. (2006). "Variations of eye size parameters among different strains of mice." Mammalian Genome **17**(8): 851-857.

Quigley, H. A. (1996). "Number of people with glaucoma worldwide." British Journal of Ophthalmology **80**(5): 389-393.

Quigley, H. A., R. M. Hohman, et al. (1983). "Morphologic changes in the Lamina Cribrosa correlated with neural loss in open-angle glaucoma." American Journal of Ophthalmology **95**(5): 673-691.

Regan, D., Ed. (1989). Human Brain Electrophysiology: Evoked Potentials and Evoked Magnetic Fields in Science and Medicine New York, Elsevier Science Ltd

www.manaraa.com

Reitsamer, H. A., J. W. Kiel, et al. (2004). "Tonopen measurement of intraocular pressure in mice." Experimental Eye Research **78**(4): 799-804.

Remtulla, S. and P. E. Hallett (1985). "A schematic eye for the mouse, and comparisons with the rat." Vision Research **25**(1): 21-31.

Richard S. Smith, S. W. M. J., Patsy M. Nishina, John P. Sundberg, Ed. (2002). Systematic Evaluation of the Mouse Eye: Anatomy, Pathology, and Biomethods Boca Ranton, CRC Press LLC.

Riggs, L. A. (1986). "Electroretinography." Vision Research **26**(9): 1443-&.

Riggs, L. A., A. M. L. Schick, et al. (1964). "Electrical responses of human eye to moving stimulus patterns." Science **144**(361): 567-&.

Riva, C. E., E. Logean, et al. (2005). "Visually evoked hemodynamical response and assessment of neurovascular coupling in the optic nerve and retina." Progress in Retinal and Eye Research **24**(2): 183-215.

Ruggeri, M., O. P. Kocaoglu, et al. (2010). "In vivo quantitative analysis of ocular biometric parameters in the C57BL/6J mouse." Investigative Ophthalmology & Visual Science **51**(5): 6363-.

Ruggeri, M., H. Wehbe, et al. (2007). "In vivo three-dimensional high-resolution imaging of rodent retina with spectral-domain optical coherence tomography." Investigative Ophthalmology & Visual Science **48**(4): 1808-1814.

Saleh, M., M. Nagaraju, et al. (2007). "Longitudinal evaluation of retinal ganglion cell function and IOP in the DBA/2J mouse model of glaucoma." Investigative Ophthalmology & Visual Science **48**(10): 4564-4572.

Saleh, M., M. Nagaraju, et al. (2007). "The natural history of retinal ganglion cell dysfunction and its relationship with IOP in DBA2/J mice." Investigative Ophthalmology & Visual Science **48**(5): 210-.

Schlamp, C. L., Y. Li, et al. (2006). "Progressive ganglion cell loss and optic nerve degeneration in DBA/2J mice is variable and asymmetric." Bmc Neuroscience **7**: -.

Schmucker, C. and F. Schaeffel (2004). "A paraxial schematic eye model for the growing C57BL/6 mouse." Vision Research **44**(16): 1857-1867.

Scholz, M., T. Buder, et al. (2008). "Dependency of intraocular pressure elevation and glaucomatous changes in DBA/2J and DBA/2J-Rj mice." Investigative Ophthalmology & Visual Science **49**(2): 613-621.

www.manaraa.com

Shapley, R. M. and J. D. Victor (1978). "The effect of contrast on the transfer properties of cat retinal ganglion cells." J Physiol **285**: 275-298.

Smith, R. S., D. Korb, et al. (2002). "A goniolens for clinical monitoring of the mouse iridocorneal angle and optic nerve." Molecular Vision **8**(4): 26-31.

Strasburger, H., W. Scheidler, et al. (1988). "Amplitude and phase characteristics of the steady-state visual evoked potential." Appl Opt **27**(6): 1069-1088.

Thylefors, B. and A. D. Negrel (1994). "The global impact of glaucoma." Bulletin of the World Health Organization **72**(3): 323-326.

Trimarchi, C., G. Biral, et al. (1990). "The flash-electroretinogram and pattern-electroretinogram generators in the cat - a pharmacological approach." Clinical Vision Sciences **6**(1): 19-24.

Uhlhorn, S. R., D. Borja, et al. (2008). "Refractive index measurement of the isolated crystalline lens using optical coherence tomography." Vision Research **48**(27): 2732-2738.

Viswanathan, S., L. J. Frishman, et al. (2000). "The uniform field and pattern ERG in macaques with experimental glaucoma: Removal of spiking activity." Investigative Ophthalmology & Visual Science **41**(9): 2797-2810.

Wang (2006). "Noninvasive measurement of rodent intraocular pressure with a rebound tonometer (vol 46, pg 4617, 2005)." Investigative Ophthalmology & Visual Science **47**(4): 1268-1268.

Williams, R. W., R. C. Strom, et al. (1996). "Genetic and environmental control of variation in retinal ganglion cell number in mice." J Neurosci **16**(22): 7193-7205.

Yanoff M., D. J. S., Ed. (2004). Mechanisms of glaucoma. Ophthalmology 2nd edition. Mosby, St. Louis.

Zhou, G. and R. W. Williams (1999). "Eye1 and Eye2: Gene loci that modulate eye size, lens weight, and retinal area in the mouse." Investigative Ophthalmology & Visual Science **40**(5): 817-825.

Zhou, X. H., F. Li, et al. (2005). "Involvement of inflammation, degradation, and apoptosis in a mouse model of glaucoma." Journal of Biological Chemistry **280**(35): 31240-31248.

Zhou, X. T., M. X. Shen, et al. (2008). "The development of the refractive status and ocular growth in C57BL/6 mice." Investigative Ophthalmology & Visual Science **49**(12): 5208-5214.

www.manaraa.com